ORNL-3527
UC-4 – Chemistry
TID-4500 (41st ed.)

ENGINEERING DEVELOPMENT OF A FOAM COLUMN FOR COUNTERCURRENT SURFACE-LIQUID EXTRACTION OF SURFACE-ACTIVE SOLUTES

P. A. Haas

OAK RIDGE NATIONAL LABORATORY
operated by
UNION CARBIDE CORPORATION
for the
U.S. ATOMIC ENERGY COMMISSION

DISCLAIMER

Printed in USA. Price $6.00. Available from the Clearinghouse for Federal Scientific and Technical Information, National Bureau of Standards, U.S. Department of Commerce, Springfield, Virginia

ORNL-3527

Contract No. W-7405-eng-26

CHEMICAL TECHNOLOGY DIVISION

ENGINEERING DEVELOPMENT OF A FOAM COLUMN FOR COUNTERCURRENT SURFACE-LIQUID EXTRACTION OF SURFACE-ACTIVE SOLUTES

P. A. Haas

This report was prepared as a thesis and submitted to the Graduate Council of The University of Tennessee in partial fulfillment of the requirements for the degree of Doctor of Philosophy in the Department of Chemical Engineering.

JUNE 1965

OAK RIDGE NATIONAL LABORATORY
Oak Ridge, Tennessee
operated by
UNION CARBIDE CORPORATION
for the
U.S. ATOMIC ENERGY COMMISSION

ACKNOWLEDGMENT

This study was started as part of a Chemical Engineering Research Program of the Chemical Technology Division, Oak Ridge National Laboratory. The author wishes to thank F. L. Culler, Jr., Division Director, and M. E. Whatley, Section Chief, whose support made this work possible.

The advice and suggestions of Dr. H. F. Johnson of the University of Tennessee and of Dr. Ernest Schonfeld, the principal investigator of the chemistry of foam-liquid systems at the Oak Ridge National Laboratory, are acknowledged and appreciated. The assistance of several Oak Ridge National Laboratory technicians, particularly that of D. A. McWhirter, merits acknowledgment.

ABSTRACT

The foam separation process uses differences in surface activity to effect the separation of components of a solution. Engineering problems were solved and methods developed for the design and operation of countercurrent liquid-foam columns. Six- and 24-in.-ID columns were operated to measure contacting efficiency, foam densities, foam drainage, and foam condensation. The experimental results agree with a model for countercurrent liquid-foam flow based on capillary flow through the Plateau borders between foam bubbles. Data for the drainage of the liquid from the foam flowing vertically or horizontally also agree with the same model. The heights of transfer units based on the liquid phase (HTU_x) were about 1 cm for the best conditions of uniform foams of 0.56- to 1.0-mm bubble diameter, liquid flows of 100 gal/sq ft-hr or less, and uniform liquid feed distribution with low inlet velocities. The ability of gas spargers to give uniform foam bubbles was important; spinnerets with 50- or 80-μ-diam holes as used by the rayon industry were superior to porous metal or fritted glass. There was little variation in HTU_x values for countercurrent column lengths of 10 to 28 cm. The major effects of liquid and foam flow rates and of liquid feed distributors on HTU_x values were due to their influence on the extent of channeling. The foams were condensed by means of orifices, air-operated sonic whistles, screen-lined centrifugal foam breakers, or cyclones. The removal of radioactive strontium to decontaminate Oak Ridge National Laboratory low-level waste was shown to be practical if preceded by a precipitation step (head-end step) to decrease the calcium and magnesium concentrations.

TABLE OF CONTENTS

LIST OF TABLES

LIST OF FIGURES

CHAPTER I

INTRODUCTION

The fact that solute concentrations near the surface of a solution differ from those in the interior has long been recognized and studied. This concentration difference may be used to separate surface-active solutes (21). The attainment of a large area of surface per volume of liquid is possible in foams generated by introducing small bubbles of gas into a solution, thereby increasing the surface and consequently the number of molecules at the overall surface. A foam-liquid column may be used to obtain the advantages of countercurrent mass transfer between the surface of a foam flowing up the column and the liquid flowing down the column. Operations analogous to stripping, enrichment, or scrubbing in liquid-liquid solvent extraction may be obtained, depending on whether the liquid flowing countercurrent to the foam is chiefly the feed solution, a reflux of condensed foam, or a wash solution.

Studies of the chemistry of foams and of solutions of surface-active solutes is a current program of the Chemical Technology Division, Oak Ridge National Laboratory. The emphasis is on solutions and surface-active complexes applicable to the removal of radioactive elements from low-level radioactive waste. For example, if the small amounts of strontium and cesium could be preferentially removed in order to remove the Sr^{90} and Cs^{137} radioactivity, the remaining

radioactivity would be below the maximum permissible concentrations for water and would therefore not interfere with the disposal of this waste.

The purpose of this study was to solve the engineering problems and to develop methods for the design and operation of countercurrent liquid-foam columns. This information, along with a knowledge of the chemistry of and complexing agents applicable to a particular system, would permit the selection of optimum foam separation conditions for a given system and evaluation of the practicality of the separation. The experimental studies of unusual operations necessary for the operation of a foam column included: (a) generation of a uniform, stable foam; (b) countercurrent continuous contacting of foam with a liquid; and (c) drainage and breaking of the foam to give a concentrated liquid product. Also, analytical and mathematical studies were necessary to adapt conventional separation-process theory to foam separation. The objective was to obtain mathematical expressions for column performance which could be verified experimentally and which could be used to calculate the performance of untested systems, and the objective was met.

In this thesis, the physical chemistry and physical characteristics of foams are reviewed; then, analytical and mathematical studies are presented and applied to correlation of experimental results. Finally, the application of foam separation to low-level waste generated at the Oak Ridge National Laboratory is considered.

CHAPTER II

PHYSICAL CHEMISTRY OF FOAM-LIQUID SYSTEMS

The literature on the physical chemistry of gas-liquid interfaces contains a variety of information useful to the development of foam separation. Equilibrium data has been correlated both by use of the thermodynamically rigorous Gibbs equation and by adsorption isotherms. Experimental data on rates of adsorption have been compared with the results predicted by diffusion or by kinetic models for adsorption isotherms. This chapter presents a generalized discussion of these subjects as applicable to foam separation.

II-I The Gibbs Equation

A rigorous model for the thermodynamics of solution-gas interfaces was originally developed by Gibbs (16); amplified and more readable developments of Gibbs' model are presented by Guggenheim and Adams (18) or Adamson (1). The model considers a gas and a liquid phase in equilibrium with each other, with uniform temperature and pressure. The physical interface does not have a sharply defined boundary; instead, the density and concentrations vary over a region. The gas and liquid bulk phases will each be completely homogeneous away from this region in which the interface exists.

The model considers a column of cross section area A, with the axis of the column perpendicular to the interface and bounded by surfaces sufficiently far from the interface such that homogeneous,

bulk-phase concentrations are attained. The value for the thickness, σ, is limited only by the requirement that it include all the variations across the interface. General energy summations may be made for this region (σ) and for the α and β phases as if they had persisted

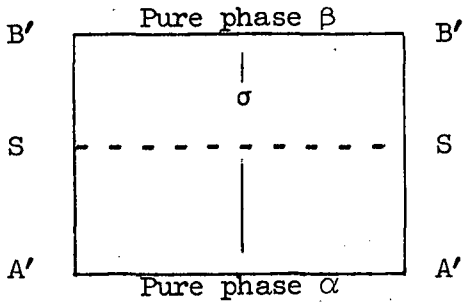

Schematic diagram for Gibbs' model of an interface.

unchanged up to the interface. Using the common thermodynamic notation and the interfacial tension γ for the cross section, A:

$$E^{\sigma} = TS^{\sigma} - PV^{\sigma} + \gamma A + \Sigma \mu_i n_i^{\sigma} , \tag{1}$$

$$E^{\alpha} = TS^{\alpha} - PV^{\alpha} + \Sigma \mu_i n_i^{\alpha} , \tag{2}$$

$$E^{\beta} = TS^{\beta} - PV^{\beta} + \Sigma \mu_i n_i^{\beta} . \tag{3}$$

Subtracting and noting that $V^{\sigma} = V^{\alpha} + V^{\beta}$:

$$(E^{\sigma} - E^{\alpha} - E^{\beta}) = T(S^{\sigma} - S^{\alpha} - S^{\beta}) + \gamma A + \Sigma \mu_i (n_i^{\sigma} - n_i^{\alpha} - n_i^{\beta}) , \tag{4}$$

$$E^{S} = TS^{S} + \gamma A + \Sigma \mu_i n_i^{S} , \tag{5}$$

where the superscript S refers to the excess quantity associated with the existence of the surface. These quantities are not defined until an interface is defined to fix the quantities in equations (2), (3), or (4). Equation (5) may be differentiated to give:

$$dE^S = TdS^S + S^S dT + \gamma dA + Ad\gamma + \Sigma\mu_i dn_i^S + \Sigma n_i^S d\mu_i \quad . \qquad (6)$$

For a small, reversible change in the surface phase close to equilibrium at constant volume:

$$dE^S = TdS^S + \gamma dA + \Sigma\mu_i dn_i^S \quad . \qquad (7)$$

Equation (7) may be derived directly from $dE^S = dE^\sigma - dE^\alpha - dE^\beta$. Subtracting equation (7) from equation (6) gives:

$$S^S dT + Ad\gamma + \Sigma n_i^S d\mu_i = 0 \quad . \qquad (8)$$

For a constant temperature, and defining $n_i^S/A = \Gamma_i$ as excess per unit area:

$$d\gamma = - \Sigma\Gamma_i d\mu_i \quad . \qquad (9)$$

This is the Gibbs equation, and it is as correct as the laws of thermodynamics unless there are factors not considered in the derivation. Gibbs' derivation also included terms for the curvature of nonplanar interfaces; their contribution is negligible if the radius of curvature is large compared with the thickness of the interface. The concept of a surface of zero volume is not necessary for the derivation of the Gibbs equation; Guggenheim arrived at the same form for a surface phase with a physical volume (17).

The surface excesses Γ_i of equation (9) are defined relative to an arbitrarily chosen interfacial position. It is usually convenient to choose this position to make the surface excess of solvent zero. Physically, this means that the liquid containing a unit area of surface contains Γ_i more of each species than the volume of bulk liquid

which contains the same amount of solvent. The effects of other conventions for the interface position are discussed in detail by Guggenheim and Adams (18). Bikerman argues that surface excesses should be defined on an alternative basis (6). For dilute solutions, the several conventions all give identical values for the surface excesses of solutes.

For a two-component system (solvent and a single solute) with a zero surface excess of solvent, the interfacial tension is related to the surface excess of solute Γ by:

$$d\gamma = - \Gamma d\mu_i \quad . \tag{10}$$

For dilute solutions, $d\mu_i = RTd \ln x$, where x is the concentration, R is the gas constant, and Equation 10 becomes:

$$\Gamma = - \frac{1}{RT} \frac{d\gamma}{d \ln x} \text{ or } \frac{\Gamma}{x} = - \frac{1}{RT} \frac{d\gamma}{dx} \quad . \tag{11}$$

II-2 Adsorption Isotherms

The behavior of surface-active solutes may be considered adsorption at the surface and is often well represented by the common adsorption isotherms. The principal assumptions for the Langmuir adsorption isotherm (adsorption only as a monomolecular layer on independent, uniform localized sites) are often good approximations at solution-gas interfaces. Surface excess versus equilibrium concentration (Γ versus x) curves for surface-active solutes have the shapes typical of Langmuir isotherms at low concentrations; electrical repulsions may become important for ionized surfactants at higher surface coverages. Adsorption isotherms are discussed in detail in many books on physical chemistry, particularly in those on interfacial or surface chemistry (3,14), and

will therefore not be discussed further here. Some isotherms, particularly the Langmuir isotherm, may be developed from models in which the constants are rate constants for adsorption and desorption.

II-3 Multicomponent Systems

Forms of the Gibbs equation (Equation 9) and the Langmuir equation exist for several competing surfactants. These can be used with some assumptions to obtain the following equation for surface tension with n solutes (34):

$$\gamma_o - \gamma = \Gamma_m' RT \ln \left[1 + \sum_1^n a_i \alpha_i \right] \quad . \tag{12}$$

Here,

γ_o is the surface tension of pure solvent,

γ is the surface tension of a solution,

Γ_m is the surface concentration of a complete monolayer,

a_i is the activity of the ith solute,

θ_i is the fraction of the total surface area covered by the ith component,

α_i is the constant in the Langmuir adsorption equation in the form,

$$\theta_i = \frac{a_i \alpha_i}{1 + \sum_1^n a_i \alpha_i} \quad .$$

Generally these equations for multiple solutes are not convenient to apply to the continuous countercurrent foam-column calculations, but they serve as a guide to the selection of reasonable simplifying assumptions.

II-4 Chemistry of a Surface-Active Complexing Agent and a Metal

Since the surface activities of simple inorganic salts or metal ions is very small, the foam separation of metals requires the formation of surface-active compounds or complexes of the metals. This means multicomponent systems which are described by the more complex equations previously mentioned. Fortunately, the usual situation is to have an excess of either the surfactant or the metal so that, as an approximation, the concentration of the component in excess can be assumed constant.

The system used for the engineering studies contained a strontium concentration small (about 10^{-6} M Sr) compared with the dodecylbenzenesulfonate (DBS) concentration (about 5×10^{-4} M) which in turn was small compared with the sodium concentration of 0.01 to 0.001 M. Reactions that explain the behavior of this system are:

$$Sr(DBS)_2 \rightleftarrows Sr^{2+} + 2DBS^- , \qquad (13)$$

$$NaDBS \rightleftarrows Na^+ + DBS^- , \qquad (14)$$

$$HDBS \rightleftarrows H^+ + DBS^- . \qquad (15)$$

The DBS was chosen because the strontium salt is poorly ionized and hence more surface-active compared to the sodium salt. This means that the equilibrium constant for equation (13) is very small and almost all the strontium is present as $Sr(DBS)_2$ when an excess of DBS^- is present. The NaDBS is highly ionized, so its concentration is small compared with that of the DBS^-. The acid form, HDBS is less highly ionized so that the DBS^- concentration is greatly reduced at low pH's. The NaDBS and

$Sr(DBS)_2$ have approximately equal surface activity; the lower surface activity of sodium is due to the ionization of the NaDBS to give Na^+ and DBS^- of low surface activity.

Generalizations may be made for this system when there is a large excess of DBS as DBS^- in the solution (28). For example, the strontium distribution factor, $(\Gamma/x)_{Sr}$, is independent of the strontium concentration. This is shown by the Gibbs equation and $d\mu = RTd \ln x$ for dilute solutions. The chemistry of the solution is controlled by the Na and DBS concentrations, and $(\partial\gamma/\partial x_{Sr})$ is a constant for the whole strontium concentration range considered. However, $(\Gamma/x)_{Sr}$ will decrease as either the sodium or DBS concentrations are increased.

II-5 Rates of Adsorption

The rate of adsorption at a surface involves the rate of transfer of material to the surface by diffusion and convection and perhaps the rate of penetration of an oriented surface layer with an energy barrier. Foam separation does not involve transfer of the surface-active solute to the gas phase, and newly formed surface is assumed to have zero surface excess of solutes. Rates of adsorption have been experimentally studied by a number of methods (14). The results have been correlated and compared by using diffusion coefficients or by interpreting Langmuir adsorption isotherm constants as rate constants.

While many experimental results agree with diffusion-controlled rates of adsorption, rates much lower than those calculated for diffusion are reported for many systems. The presence of impurities or the

use of inadequate experimental techniques explain many but not all of the low rates of adsorption.

Equations for diffusion starting with a zero surface concentration were derived by Ward and Tordai (33). The rate of diffusion to the surface for no back diffusion or convection is:

$$\frac{dy}{dt} = \sqrt{\frac{D}{\pi}} \frac{x}{\sqrt{t}} , \tag{16}$$

where

y = surface concentration in moles/cm^2,

D = the bulk phase diffusion coefficient,

x = the bulk phase concentration in moles/cm^3,

t = time.

Integration of Equation 16 from zero concentration gives:

$$y = 2 \sqrt{\frac{D}{\pi}} x \sqrt{t} . \tag{17a}$$

A complete equation allowing for back diffusion, that is, for a finite surface concentration, is also given (33). A second term in an integral form is subtracted from the right side of Equation 17 and reduces the value of y at any finite time.

$$y = 2 \sqrt{\frac{D}{\pi}} \left[x \sqrt{t} - \int_0^{\sqrt{t}} \phi(w) \, d(\sqrt{t - w}) \right] , \tag{18}$$

where $\phi(w)$ is the solute concentration in the liquid immediately below the surface.

Typical values of $D = 5 \times 10^{-6}$ cm^2/sec, $y = 3 \times 10^{10}$ mole/cm^2, and $x = 5 \times 10^{-7}$ mole/cm^3 for foam separation surfactants can be substituted in Equation 17b to give t = 0.056 sec:

$$t = \frac{\pi y^2}{4Dx^2} = \left(\frac{\pi}{4D}\right)\left(\frac{y}{x}\right)^2 . \qquad (17b)$$

However, $t \propto x^{-2}$ or $t \propto (y/x)^2$ so that t can become very large for low bulk liquid concentrations or for materials of high surface activity. For strontium dodecylbenzenesulfonate, with $(\Gamma/x) = 5.5 \times 10^{-3}$ cm at equilibrium, the time for $y/x = 3 \times 10^{-3}$ cm from Eq. (17b) is about 1/2 sec. Impurities of high surface activity and very low concentration come to equilibrium very slowly by diffusion, thus the presence of surface-active impurities explains some of the slow adsorption rates observed experimentally.

Two determinations of the rates of adsorption of straight-chain alcohols show that initial rates for heptyl and octyl alcohol agree with their diffusion coefficients while the rates of lower alcohols are much lower than would be calculated from diffusion (27,33). A cationic and an anionic soap both gave initial rates that were about five times as large as would be predicted from diffusion coefficients (27); this could be attributed to increased diffusion due to ionic charge and electrical double layer effects.

Posner and Alexander reported that their experimental data fit the following equation, which can be derived from a Langmuir type of model for adsorption kinetics (27). Experimental values of k_1 and k_2 were determined (Table I).

$$\ln(y^* - y) = -\left(k_1 x + k_2 \frac{y_F}{\sigma}\right)t + \ln y^* , \qquad (19a)$$

where

TABLE I

ADSORPTION AND DESORPTION RATE COEFFICIENTS (27)

Compound	Temperature (°C)	k_1 10^{-7} (cc/molecule/sec)	k_2^a 10^{-21} (cc/molecule/sec)
n-Butyl alcohol	25	0.084	12.4
n-Hexyl alcohol	25	1.9	9.2
n-Heptyl alcohol	25	5.1	5.5
n-Octyl alcohol	25	10.1	2.3
Cetyl trimethyl ammonium bromide	20	~ 10.	- -

[a] Based on σ = 10 Å, $n_F = 5.10^{14}$ molecules/cm^2.

y_F = the surface concentration when the molecules are close packed,

y^* and y = equilibrium and actual surface concentrations,

x = bulk solution concentration,

t = time, sec,

σ = thickness of surface layer, cm

k_1 = adsorption rate coefficient, cm^3/conc. unit-sec,

k_2 = desorption rate coefficient, cm^3/conc. unit - sec.

An important result for either the diffusion-controlled or film-penetration model is that the time required to approach equilibrium increases for solutes of high surface activity or of low solution concentrations compared with the surface concentration. This can be seen from Eqs. (17b) and (19b):

$$t = \left(\frac{\pi}{4D}\right)\left(\frac{y}{x}\right)^2, \tag{17b}$$

$$t = \frac{-\ln(1 - y/y^*)}{\left(k_1 x + k_2 \frac{y_F}{\sigma}\right)}. \tag{19b}$$

For $y = fy^* = f\Gamma$, where f is the fraction of the equilibrium surface concentrations, these equations become:

$$t = \left(\frac{\pi}{4D}\right) f^2 \left(\frac{\Gamma}{x}\right)^2, \tag{20}$$

$$t = -\frac{\ln(1 - f)}{k_1 x + k_2 \frac{y_F}{\sigma}}. \tag{21}$$

Equation (20) indicates that the time required to obtain a given fractional conversion f is proportional to the square of the equilibrium

distribution coefficient (Γ/x) for the diffusion-controlled transfer. Since k_1, k_2, y_F, and σ are positive constants for a given system, Equation 21 indicates that the time required to obtain a given fractional conversion f increases as x decreases.

II-6 Liquid Diffusivities

Diffusion coefficients in liquids are much smaller than in gases, and the theory of diffusion in liquids is not well developed. Representative values reported in the International Critical Tables are (1 to 10) x 10^{-5} ft^2/hr for common solutes in water, methyl or ethyl alcohol, and benzene at room temperature. A method for estimating these coefficients was developed by Wilke (35) and may be represented by the following equation (32):

$$D_L = \frac{4.0 \cdot 10^{-7} T}{\mu (V^{1/3} - K_1)}, \qquad (22)$$

where

D_L = the liquid diffusivity, ft^2/hr,

T = temperature, °R,

μ = viscosity of solution, lb/hr·ft,

K_1 = 2.0, 2.46, and 2.84 for dilute solutions in water, methyl alcohol, and benzene respectively,

V = the molal volume of the solute at the normal boiling point.

This equation applies only to dilute solutions and does not agree well with the data for small molecules and some elemental gases. Also, it does not apply to electrolytes.

For water at 25°C and converting units to D in cm^2/sec, the equation becomes:

$$D = \frac{25.7 \times 10^{-6}}{(V^{1/3} - 2.0)} \quad . \tag{23}$$

For dodecylbenzenesulfonic acid, the values are: V = 414, and D = $4.7 \cdot 10^{-6}$ cm^2/sec. The surfactants of principal interest to foam separation will have values of V between 100 and 1000 and will thus have diffusion coefficients of (3 to 10) x 10^{-6} cm^2/sec.

CHAPTER III

PHYSICAL CHARACTERISTICS OF FOAMS

The physical properties of foams are important to the stability of the foam, to the surface area, and to the practicality of drainage in a foam column. The configurations of the interfaces of foams were first reported and explained by Plateau (26) over a hundred years ago. The concept of bubble sizes being determined by equating the gravitational force to the surface tension force at the perimeter of an orifice or capillary is also old. There do not appear to be any important or generally accepted improvements or additions to these concepts, although there are a large number of experimentally evaluated corrections and refinements. General reviews of the literature are published in books on foams (5) or surface chemistry (2). Therefore this chapter will be confined to the two basic concepts and the experimentally verified variations which appear most useful to this foam separation study.

III-1 Foam Structure

While foams are usually produced by forming gas bubbles in a liquid, the structure of foams is best visualized as comprising films surrounding gas spaces. The surface tension γ of each film is balanced by a pressure difference, $\Delta P = 2\gamma/R$, where R is the radius of curvature, between the interior and exterior of the bubble. When two bubbles have a common boundary surface, the radius of curvature of this septum, R_s,

must result in a force that balances the pressure difference between the two bubbles:

$$R_s = \frac{R_1 R_2}{R_2 - R_1} . \tag{24}$$

If the two bubble radii are equal, $R_s = \infty$, and the septum is a plane. If they are unequal, the large bubble is deformed more than the small bubble; that is to say, the center of the center of curvature is on the small-bubble side of the septum.

The importance of the space enclosed between three bubbles was initially recognized by Plateau (26) and is named Plateau's border. A schematic diagram is shown below:

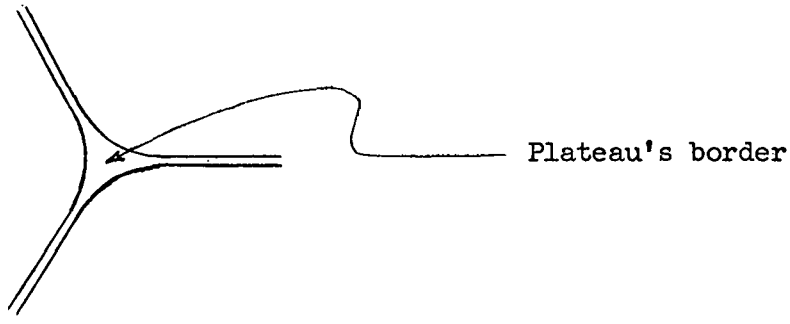

The liquid in the Plateau's border is at a pressure, P_{PB}, lower than that of the liquid in the walls of the bubble, P_s. Since the surface tension γ is the same for all surfaces, this pressure difference is:

$$P_s - P_{PB} = \gamma\left[\frac{1}{R_{PB}} - \frac{1}{R_s}\right] . \tag{25}$$

The three films radiating from a Plateau's border must be at angles of 120° with each other. The forces on the Plateau border from the surface tensions of the films or surfaces must cancel, and this is

possible for three equal forces only if they are at 120° to each other. While four equal forces at 90° could also cancel, such a structure of bubbles would be unstable. Any small pressure difference between two of the bubbles due to a small difference in bubble size or for some other cause would result in a movement of the septum dividing those two bubbles and would thus create two points of three films each. A similar pressure difference does not alter the number of films at a Plateau's border. Since the same Plateau border pressure, P_{PB}, applies to each interface of this border with a bubble, and since $R_{PB} \ll R_s$ for foams, this also shows that the angle between three films is 120°. All three bubbles have equal values of R_{PB}; this is possible only if the angles are equal.

III-2 Bubble Size

A principal method of dispersing a gas into a liquid and the method chosen for foam separation columns is to force gas through small orifices or capillaries below the liquid surface. Studies of the sizes of bubbles produced by a single orifice have been extensively reported. The theoretical model is similar to that for drop weight or other related surface-tension measurements, but the bubble size is the variable of interest, not surface tension.

The idealized assumption is that the bubble leaves the orifice when its buoyancy equals the surface tension times the perimeter of the bubble at the orifice. For a spherical bubble of radius R, and a perimeter of radius r, this equality gives:

$$R^3 = \frac{3r\gamma}{2g\Delta\rho} , \qquad (26)$$

where $\Delta\rho$ is the density difference, γ is the surface tension, and g is the acceleration of gravity. The value of r is the inside radius of an orifice wetted by the liquid or the outside radius of a capillary that is not wetted by the liquid. Since the liquid density is much greater than the gas density for foam bubbles, then $\Delta\rho \simeq \rho$.

The idealized assumption predicts that $2g\rho R^3/3r\gamma$ should be 1; literature values of 0.6 to 1.1 are common, and more extreme values have been reported for the formation of gas bubbles (5). Values for liquid drops falling from a capillary usually vary between 0.52 and 0.65.

Two opposing effects have been reported to give a minimum in the bubble-size-versus-flow-rate curve (23). The bubble size decreases as the bubble rate is increased from a very low rate due to the increasing liquid velocity, which adds to the buoyancy force. The bubbles are torn away from the orifice before the buoyancy force equals the surface-tension force. At very high bubble-formation rates, a second effect becomes more important and causes an increase in the bubble sizes. The bubbles take a definite time to break loose from the orifice. The gas continues to flow into the bubble, and the final bubble size increases as the gas velocity increases. The minimum in the bubble size occurs when these two opposing effects are equal in magnitude.

The correlation of bubble size with bubble rate is even more complex for multiple orifices in a surface such as a porous plate, screen, or perforated plate. For example, for a given gas rate per

orifice, the velocity of the liquid is increased as additional orifices are added. The possibility of coalescence of bubbles from adjacent orifices exists. The wetted perimeter is poorly defined for a flat plate as compared with that for a capillary or with that for a single orifice in a wetted plate. The literature for the release of bubbles by solid surfaces was reviewed by Bikerman (5); it is not adequate for useful quantitative predictions.

III-3 Foam Drainage

Drainage to give a foam of low density or liquid content is desirable to reduce dilution by this liquid when the foam is condensed. Hence, the type of drainage desired is the thinning of films without the rupture of bubbles or loss of surface area. But, the persistence of the foams decreases as the film thickness decreases. Therefore drainage and foam condensation are difficult to separate completely in practice. Drainage rates are commonly measured by forming foam and then measuring the rate of liquid collection under the foam or the foam density versus time.

Drainage of solution from the films between bubbles occurs because of gravitation and because of the lower pressure of the Plateau borders, which thus suck liquid from the films. The lower pressure in the borders, compared with that of the films, is approximately γ/R_{PB}. The radius of the Plateau border, R_{PB}, will be smaller than the bubble radius and will be much smaller than the bubble radius for foams after a small amount of drainage. The gravitational pressure is the liquid head and is thus about 980 dynes/cm^2 per centimeter of

height for aqueous solutions. Also the gravitational pressure has only a vertical component, while the suction of the Plateau borders is effective in all directions. Therefore drainage of the films between bubbles is probably much more due to the Plateau-border effect than to gravitation for the bubble sizes of interest to foam separation (0.01 to 0.2 centimeter in diameter. The vertical Plateau borders will drain due to gravitational pressure drops, and the horizontal borders will drain into the vertical borders because the pressures in the vertical borders decreases as their size decreases.

Equations have been derived from several models for foam drainage with time, and their constants have been evaluated from experimental data. Bikerman (5) reviewed this field up to about 1952. The drainage for very short times and for long times are often anomalous and should probably not be expected to fit any single simple model. For example, the short-time drainage depends on how the foam was formed. Most foams are formed by sparging gas at varying rates into a liquid, but significant amounts of drainage data are for foams made by shaking the liquid in a cylinder or by dripping liquid on top of a porous plate and sucking it through the plate along with gas to form the foam. The long-time drainage would be greatly dependent on the persistence of the foam and any physical bonding of water by the surface layers.

Much of the drainage data is adequately represented by a simple first-order form of equation in which the rate of drainage is proportional to the amount of liquid remaining in the foam, but two other models seem closer to the real situation. Miles, Shedlovsky, and Ross

(24) use a model in which the drainage flow was through a number of vertical capillary tubes of a uniform diameter. Jacobi, Woodcock, and Grove (20) use a model in which the flow channel is a tapered slit, with the width of the taper proportional to the liquid content of the foam. The more correct model would seem to be a combination of these two. Thus, the films between bubbles would drain to the Plateau borders due to their lower pressures. The Plateau borders would be a network of capillaries that would increase in size down a column of foam in which drainage was taking place. This combinational model would have only one stable capillary size for each combination of drainage flow and film dimensions between bubbles. Such a combination model has not been found in the literature and will be developed in the next chapter.

CHAPTER IV

FOAM COLUMN CALCULATIONS: MODELS AND RESULTS

The purpose of this chapter is to present some models and calculations from the models developed for the mass transfer and the foam drainage in foam columns. The continuous, countercurrent nature of foam separation suggests the use of the concepts and methods of calculation found useful for other continuous, countercurrent processes such as solvent extraction. These borrowed concepts do give a very useful basis for foam column calculations, but the differences in foam columns suggest or require revised models and methods.

A model for foam drainage is considered first since it indicates dimensions for subsequent mass transfer models. These dimensions for the Plateau borders and the film thicknesses (confirmed experimentally) indicate that the mass transfer is diffusion controlled since turbulent mixing is absent. The equations to be used for calculations of HTU values from experimental data are justified. Finally, a simplified model for the mass transfer is examined for information on the film concentration gradients. A consistent nomenclature (Figure 1, Table II) is used throughout.

IV-1 Development of a Foam Drainage Model

The purpose of the development of a foam drainage model is to determine the form of the relationships between variables and the theoretical values of constants for comparison with experimental data. The model to be considered comprises capillaries representing the

ORNL-DWG 63-4752

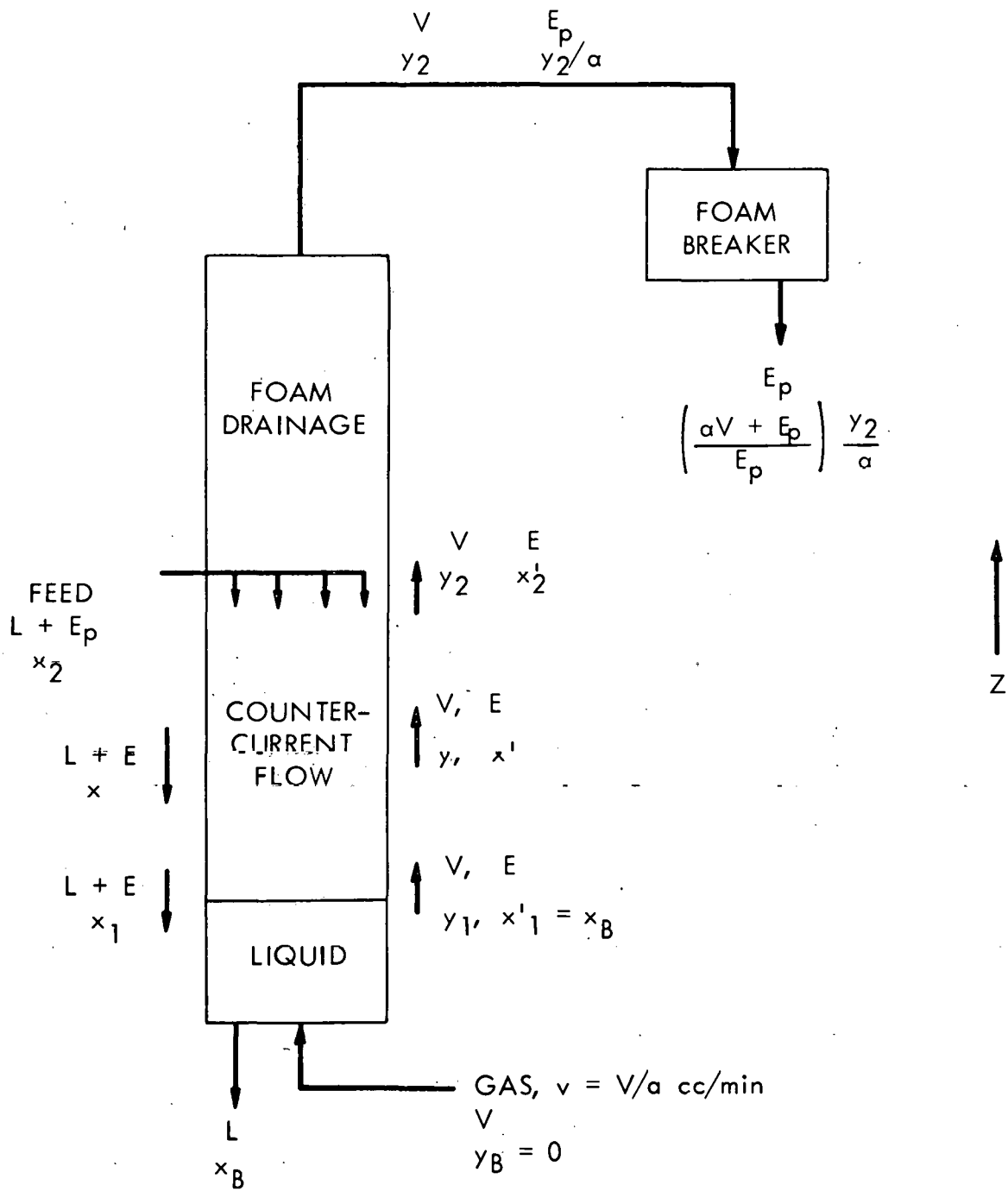

Figure 1. Foam Column Flows and Nomenclature.

TABLE II

FOAM DRAINAGE AND MASS TRANSFER NOMENCLATURE

Symbol	Meaning	Usual Range of Values and Units for this Study	
a	Specific surface area of foams	40-200	cm^2/cc
D	Diffusion coefficient	$(3\text{-}10) \times 10^{-6}$	cm^2/sec
d	Diameter of foam bubbles	0.02-0.2	cm
E	Flow rate of entrained liquid	---	$cc/cm^2 \cdot sec$
h	Fraction of liquid head effective for causing flow	0.6-1.0	cm/cm
L	Superficial net liquid velocity down column	0.02-0.2	cm/sec
ℓ	Vertical length of the foam column section	7-100	cm
N_x	Number of transfer units based on the liquid phase	1-50	
n	Number of Plateau-border capillaries per unit cross section in dry foam	100-200	cm^{-2}
P, ΔP	Pressure, pressure drop	---	
t	Time	---	sec
u	Average liquid velocity in Plateau-border capillaries	---	cm/sec
V	Superficial foam surface flow rate	5-50	sq $cm/cm^2 \cdot sec$

TABLE II

(CONTINUED)

Symbol	Meaning	Usual Range of Values and Units for this Study	
W	Amount of liquid drained from a stationary foam	---	cc/cm^2
v	Superficial foam gas velocity	0.02-1	cm/sec
x	Concentrations in the bulk liquid	---	amount/cc
x′	Average concentration of the entrained liquid	---	amount/cc
y	Surface concentration per unit area; i.e., surface excess	---	$amount/cm^2$
z	Vertical position in the foam column	---	cm
α	Equilibrium constant or (y/x) at equilibrium	---	cm
Γ	Surface excess per unit area (Gibbs model)	---	$amount/cm^2$
δ	Equivalent diameter of Plateau-border capillaries	0.001-0.05	cm
ϵ	Volume fraction of continuous phase or foam density in volume liquid/volume foam	0.001-0.4	cc/cc
μ	Viscosity	---	g/cm·sec
ρ, $\Delta\rho$	Liquid density, density difference	1	g/cc

TABLE II

(CONTINUED)

Symbol	Meaning	Usual Range of Values and Units for this Study	
τ	The film half-thickness	---	cm
τ_{eq}	The equilibrium film thickness for persistent foams	$\sim 10^{-6}$	cm

Plateau borders between foam bubbles. The flows in the capillaries will be due to the gravitational head of the liquid, while the films between bubbles will drain to the capillaries due to the reduced pressures in the Plateau borders. The walls of the capillaries are elastic so that the internal pressure equals the external pressure minus the capillary pressure difference at that point. The external frictional pressure drop for flow of foam through the column is negligible.

This foam-drainage model appears more applicable to foam columns in two respects than any of the models found in the literature. First, the literature models deal with drainage with time as a variable for a fixed volume of stationary foam, while the drainage in a foam involves time steady-state operation with the foam moving through the column. Secondly, the literature models have assumed drainage through capillaries of a constant diameter (24) or between plates separated by a constant or variable distance (20). A tapered capillary of constant pressure drop per unit length appears much closer to the true physical drainage channel in foam than do the other literature models of the process. Also, the effects of the reduced pressures in the Plateau borders on the drainage of the films between bubbles should be considered. The relative importance of gravitation and of the suction of the Plateau borders to film drainage can be shown in terms of the bubble diameter, d. The maximum distance across films will be about d/2, and the gravitational pressure difference for a vertical film will be $gpd/2$ or $490\ d$ dynes/cm^2. The radius of curvature of the Plateau borders will be much less than the radius of curvature of the

film between bubbles. Thus it will be less than d/2, and the pressure drop from the film to the Plateau border required to balance the interfacial tension will be more than $2\gamma/d$ or 600 dynes/cm^2 for γ = 30 dynes/cm and d = 0.1 cm. Thus it can be seen that the films will drain to the Plateau borders due to this "suction" and that gravitation will cause very little of the flow in the films between bubbles.

The starting point for the foam drainage model is to represent the liquid flow in the foam by flow in capillaries of diameter δ. The average liquid velocity in such a capillary which represents a vertical Plateau border is:

$$u = \frac{\rho h g}{32\mu} \delta^2 \ . \tag{27}$$

For a foam of fractional liquid volume, ϵ, and fractional gas volume of $1 - \epsilon$ moving upward due to a superficial gas velocity v, the bubble velocity upward will be $v/(1 - \epsilon)$. The number of Plateau borders per unit of cross section area is defined as n for a dry foam, and thus $n(1 - \epsilon)$ for a wet foam. A fractional cross section for liquid flow for $n(1 - \epsilon)$ capillaries of diameter δ is:

$$\epsilon_{PB} = n(1 - \epsilon)\frac{\pi\delta^2}{4} \ . \tag{28}$$

The use of the same equivalent diameter, δ, in Equations 27 and 28 is an approximation since the Plateau borders are not circular. The net liquid flow per unit cross section is the difference between the down flow in the Plateau borders and the up flow due to the upward foam velocity.

$$L = u\epsilon_{PB} - \frac{v}{1 - \epsilon}\,\epsilon \quad . \tag{29}$$

Since ϵ and ϵ_{PB} are both fractions of liquid volume per unit volume of foam, they were assumed to be related to each other by a proportionality constant k which is independent of d, v, L, or other variables:

$$\epsilon = k\epsilon_{PB} = nk(1 - \epsilon)\frac{\pi\delta^2}{4} \quad . \tag{30}$$

These four equations can be combined to eliminate u, δ, and ϵ_{PB} to give:

$$L + \frac{v}{1 - \epsilon}\,\epsilon = \frac{\rho g}{32\mu}\,\frac{4}{\pi nk^2}\,\epsilon^2 \quad . \tag{31}$$

For the common case of no upward flow of foam or v = 0, Equation 31 reduces to:

$$\frac{\epsilon^2}{L_o n} = \frac{32\mu}{\rho g}\,\frac{\pi k^2}{4} \quad . \tag{32}$$

Equations 31 and 32 are point equations with which experimental results will be compared.

In order to use these equations, values of k and n are needed in addition to the properties of the solution and measured values of the variables, ϵ, L, v, and d. The number of Plateau borders per unit cross section area was estimated from the representation of the foam cross section by close packed circles of diameter, d, in a plane. Each circle (that is, bubble) shares six Plateau borders. Each border is shared by three circles. Then n is given by:

$$n = \frac{1}{3}(6)\,\frac{4}{\pi d^2} = \frac{2.5}{d^2} \quad . \tag{33}$$

The value of k should be greater than 1, but it is difficult to justify

a particular specific value. From consideration of the foam structure, a value of k = 1.5 was selected for use with the reservation that other values between 1.1 and 2. were not improbable. Some such considerations are discussed in Appendix A.

The above equations are based on a number of approximations. Since the Plateau border is not a cylinder, the diameter for the capillary flow equation and for the cross section area are probably not identical. This effect can be considered to be lumped into n; that is, δ is the value which gives the correct value of u using Equation 27 and n is the value which gives the correct value of L from Equations 28 and 29. The effect of flow in Plateau borders at an angle between vertical and horizontal is not mentioned. Since n is defined to give the correct value of L, and k is defined to give the correct value of ϵ, the contributions of all the Plateau borders is included. The constant pressure drop, per unit length, $h\rho g$, in the capillary flow equation results because the capillary cross section adjusts in size so that the frictional head loss per unit length equals the liquid head causing flow; h is capillary length per unit column length. A differential pressure balance would give the following pressure drop:

$$-\frac{dP}{dz} = h\rho g = \rho(1 - \epsilon)g + \frac{2\gamma}{\delta^2}\frac{d\delta}{dz} . \qquad (34)$$

The values of $(2\gamma/\delta^2)\, d\delta/dz$ are small for the foams of interest and were neglected so that h was given by:

$$h = 1 - \epsilon . \qquad (35)$$

The times required for the films between bubbles to drain to the

Plateau borders and for the horizontal Plateau borders to drain into vertical Plateau borders will be considered only for deriving equations for drainage during vertical foam flow. Time is not a variable for steady-state countercurrent foam-liquid flow. The exit foam densities for vertical drainage are calculated on the assumption that equilibrium is approached, so the drainage times do not affect these exit foam densities. For the drainage of stationary foam or with horizontal flow of foam, the times for drainage from the films or the horizontal Plateau borders would impose small time lags on the results obtained without considering these effects. However, the results are expressed in terms of time differences and are not applicable to very short times because the boundary conditions are probably not satisfied at zero time. Therefore the time lags can be neglected for these results. For drainage during vertical flow of foam, the equilibrium Plateau border size and thus the exit foam density would be reached instantaneously or in zero length if the drainage times from the films and the horizontal Plateau borders is neglected. Since the drainage from the films appears to be slower and thus controlling, only this time is actually considered.

The drainage of the films between bubbles may be represented by the viscous flow between parallel plates due to the suction of the Plateau borders if the void volume of ϵ_{PB} are not large (perhaps when ϵ_{PB} is less than 0.1 for foams of d less than 0.1 cm). The reduced pressure effect decreases as the Plateau border diameter increases and is no longer controlling for high foam densities as exist for counter-

current foam-liquid flow in the foam column. The films of persistent foams approach a zero drainage rate at a finite film thickness which will be designated 2 τ_{eq}. The film-to-Plateau-border pressure drop will be γ/R_{PB} and will thus be proportional to γ/δ. The equation for drainage between parallel plates may be written by use of the capillary flow equation:

$$\text{average velocity} = - \frac{k_1 \gamma (\tau - \tau_{eq})^2}{\mu \delta} , \tag{36}$$

$$\text{average flow} = k_2 \gamma \frac{(\tau - \tau_{eq})^3}{\mu \varepsilon} . \tag{37}$$

The constant k_1 would be $g\delta/3R_{PB}$, and k_2 would include the effects of the foam configuration. For three tangent circles, their radius over the hydraulic radius of the Plateau border between them would be 1.6. Therefore a value of $R_{PB} = 2\delta$ appears appropriate. Bikerman (5) reports an equation for the drainage of a circular liquid plate of radius a'. Substituting the notation of this report and the Plateau border pressure of $\gamma/R_{PB} = \gamma/2\delta$, this equation becomes:

$$\frac{1}{(\tau_2 - \tau_{eq})^2} - \frac{1}{(\tau_1 - \tau_{eq})^2} = \frac{8\gamma(t_2 - t_1)}{3 \mu a'^2} . \tag{38}$$

The value of a' will be proportional to d; a value of d/4 may be used:

$$\frac{1}{(\tau_2 - \tau_{eq})^2} - \frac{1}{(\tau_1 - \tau_{eq})^2} = \frac{128\mu}{3\mu d^2 \delta} (t_2 - t_1) . \tag{39}$$

Differentiating to obtain $d\tau/dt$:

$$- \frac{d\tau}{dt} = \frac{256\gamma}{3\mu d^2 \delta} (\tau - \tau_{eq})^3 . \tag{40}$$

Stationary Foam Drainage

While drainage of a stationary foam does not occur in a continuous foam column, the application of the proposed drainage model to this situation is of interest for several reasons. Experimental data for stationary drainage may be used as another verification of the drainage model. The models in the literature are developed for stationary drainage, and a comparison with these literature results is important. By use of a moving origin, the results for stationary foam may be applied to a horizontal drainage section for a foam column.

Simple analytical solutions cannot be expected to apply to all the drainage data for very short times and for very long times. Long-time drainage is controlled by the persistence of the films and surface viscosity effects instead of the hydraulic effects. Short-time drainage depends on the initial conditions as boundary conditions. For example, the effects of boundary conditions are illustrated by drainage when steady-state countercurrent flow is stopped at zero time. The foam density would start decreasing immediately at the top of the countercurrent region when the flows were stopped. The foam density and thus the drainage rate would be constant at the bottom until this decrease had traveled down the column. As the countercurrent length (before zero time) increases, the length of the constant drainage rate time period increases. For an infinite length, the rate would be constant for an infinite time. Formation of foam by sparging gas into a liquid at the bottom of the chamber gives an initial distribution, with the foam density decreasing up the bed. Suction of liquid and gas

through a porous plate at the top of the chamber would probably give a foam density increasing up the bed. Thus widely varying short-time drainage rates would be expected.

For a stationary bed of foam where Equation 32 applies, a material balance with time may also be written:

$$\frac{\partial \epsilon}{\partial t}\, dz = - \frac{\partial L_o}{\partial z}\, dz \ . \tag{41}$$

Combining Equations 32 and 41 to eliminate $\partial L_o/\partial z$:

$$\frac{\partial L_o}{\partial z} = - \frac{\partial \epsilon}{\partial t} = \frac{\rho g}{32\mu} \frac{8\epsilon}{\pi n k^2} \frac{\partial \epsilon}{\partial z} \ . \tag{42}$$

A solution may be obtained by the method of separation of variables (see Appendix B) using:

$$\epsilon(t,z) = T(t)Z(z) \ . \tag{43}$$

$$- \frac{1}{T^2(t)} \frac{dT}{dt} = \frac{\rho g}{32\mu} \frac{4}{\pi n k^2} 2 \frac{dZ}{dz} = c \tag{44}$$

$$T(t) = \left[c(t - t_o) + \frac{1}{T(0)} \right]^{-1} , \tag{45}$$

$$Z(z) = c \left[2 \frac{\rho g}{32\mu} \frac{4}{\pi n k^2} \right]^{-1} (z - z_o) + Z(0) \ , \tag{46}$$

$$\epsilon(t,z) = \frac{\frac{1}{2}\left|\frac{32\mu}{\rho g}\right|\left|\frac{\pi n k^2}{4}\right|(z - z_o) + \frac{Z(0)}{c}}{(t - t_o) + \frac{1}{cT(0)}} \ . \tag{47}$$

Substituting in Equation 32:

$$L_o(t,z) = \frac{\rho g}{32\mu} \frac{4}{\pi n k^2} \left[\frac{\frac{1}{2} \frac{32\mu}{\rho g} \frac{\pi n k^2}{4} (z - z_o) + \frac{Z(0)}{c}}{(t - t_o) + \frac{1}{cT(0)}} \right]^2 \ . \tag{48}$$

Integration with respect to t from t_o to t gives the volume W drained from the foam at position z with $W(t = t_o) = 0$.

$$W = \int_{t_o}^{t} L_o dt \ , \tag{49}$$

$$W(t,z) = \frac{\rho g}{32\mu} \frac{4}{\pi n k^2} \left[\frac{1}{2} \frac{32\mu}{\rho g} \frac{\pi n k^2}{4} (z - z_o) + \frac{Z(0)}{c} \right]^2 \left[cT(0) - \frac{1}{(t - t_o) + \frac{1}{cT(0)}} \right] \tag{50}$$

For the $z = z_o$ position, these equations for ϵ, L_o and W may be simplified to:

$$\epsilon(t,z_o) = \frac{\epsilon(t_o,z_o)}{cT(0)(t - t_o) + 1} \ , \tag{51}$$

$$L_o(t,z_o) = \frac{L_o(t_o,z_o)}{[cT(0)(t - t_o) + 1]^2} \ , \tag{52}$$

$$W(t,z_o) = \frac{\rho g}{32\mu} \frac{4}{\pi n k^2} \epsilon^2(t_o,z_o) \left[\frac{t - t_o}{cT(0)(t - t_o) + 1} \right] \ , \tag{53}$$

$$W(t,z_o) = L_o(t_o,z_o) \left[\frac{t - t_o}{cT(0)(t - t_o) + 1} \right] \ : \tag{54}$$

These results are what would be obtained for a second-order reaction; that is to say, the rate of drainage is proportional to the square of the amount of undrained liquid. The constant $L(t_o,z_o)$ is the initial drainage rate, and $cT(0)$ gives the time dependence of the rate. Equation 47 indicates that $\epsilon(t,z)$ is linear with respect to z. Thus any boundary conditions which require a nonlinear variation of ϵ with z cannot be satisfied by these solutions.

Several other relationships of importance are easily derived.

At the top of column of foam where $z = \ell$ and $L_o = 0$, ϵ must also be zero. From Equation 47, ϵ at any specified time should be a linear function of z. Then an average foam density would be:

$$\bar{\epsilon} = \frac{\int_{z_o}^{\ell} \epsilon dz}{\int_{z_o}^{\ell} dz} = \frac{1}{2} \epsilon(t,z_o) \quad . \tag{55}$$

As the time becomes infinite, drainage is complete, and

$$W_\infty = \frac{L(t_o,z_o)}{cT(0)} = \ell\bar{\epsilon}_o = \frac{\ell}{2} \epsilon(t_o,z_o) \quad . \tag{56}$$

The constant $cT(0)$ may be calculated from experimental data by:

$$cT(0) = \frac{L(t_o,z_o)}{W(t,z_o)} - \frac{1}{t - t_o} \quad . \tag{54a}$$

This constant may be calculated from the observed foam properties as follows:

$$L(t_o,z_o) = \frac{\rho g}{32\mu} \frac{4}{\pi n k^2} \epsilon^2(t_o,z_o) \quad . \tag{57}$$

Substituting for $\epsilon(t_o,z_o)$ from Equation 56 and rearranging:

$$cT(0) = \left[\frac{\rho g}{32\mu} \frac{4}{\pi n k^2} \frac{4}{\ell^2} L(t_o,z_o)\right]^{\frac{1}{2}} \quad . \tag{58}$$

Countercurrent Liquid-Foam Flow. For the region of countercurrent liquid-foam flow in a foam separation column, all properties are constant independent of both time and position. Thus Equations 41 and 44 are satisfied by $c = 0$ and $\partial\epsilon/\partial t = \partial L/\partial z = 0$, and the values of L, v, ϵ, and d should be correlated by Equation 31a:

$$\frac{\epsilon^2}{n} \left[L + \frac{v}{1 - \epsilon}\right]^{-1} = \frac{32\mu}{\rho g} \frac{\pi k^2}{4} \quad . \tag{31a}$$

Substituting for n from Equation 33:

$$\epsilon^2 d^2 \left[L + \frac{v}{1 - \epsilon} \epsilon \right]^{-1} = \frac{32\mu}{\rho g} \frac{\pi k^2}{1.6} \quad . \tag{59}$$

For v = 0, Equations 32 and 33 may be combined to give:

$$\frac{\epsilon^2 d^2}{L_o} = \frac{32\mu}{\rho g} \frac{\pi k^2}{1.6} \quad . \tag{60}$$

This indicated that $\epsilon^2 d^2 / L_o$ should be a constant for a given foam for all values of ϵ, d, and L_o.

Horizontal Foam Flow Drainage

The density of the exit foam for a horizontal drainage section is most conveniently correlated by an adaptation of the stationary drainage equations. A complete description of the foam throughout the drainage section would be complex since both the vertical and horizontal dimensions would be variables. If we consider an origin moving with the foam at the foam velocity, then the drainage occurs in a "stationary" foam with respect to this origin. Using the average density, $\bar{\epsilon}$, Equations 32, 51, 55, and 56 may be combined to give:

$$\frac{1}{\bar{\epsilon}} - \frac{1}{\bar{\epsilon}_o} = \frac{4}{\ell} \frac{\rho g}{32\mu} \frac{4}{\pi k^2} (t - t_o). \tag{61}$$

If $\bar{\epsilon}_o \gg \bar{\epsilon}$, then the second term on the left may be neglected.

Drainage for Vertical Foam Flow

The density of the exit foam for a vertical drainage section

decreases as the height of section increases to approach asymptotically a limit determined by the foam velocity. This limit is the density where the films reach a constant thickness and the average liquid velocity in the Plateau borders equals the foam velocity upward. The manner in which this density is approached, that is, the foam density throughout a vertical drainage section with the initial density at the bottom as one boundary condition, is more complex, and a simple analytical solution was not derived.

The superficial net liquid velocity at the exit will be given (where ϵ_p is for the exit foam) by:

$$L = \frac{- v}{1 - \epsilon} \epsilon_p \quad . \tag{62}$$

The equality of the foam velocity and the Plateau border liquid velocity is expressed as:

$$u = \frac{v}{1 - \epsilon} \quad , \tag{63}$$

Combining Equations 62, 29, and 63:

$$\epsilon_p = (k - 1) \epsilon_{PB} \quad . \tag{64}$$

Combining Equations 27, 28, and 30 and substituting in Equation 64:

$$\epsilon_p = (k - 1) \frac{32\mu}{\rho g} \frac{n\pi}{4} \frac{v}{1 - \epsilon} \quad . \tag{65}$$

Noting that ϵ will be very small and substituting for n from Equation 33

$$\epsilon_p = (k - 1) \frac{32\mu}{\rho g} \frac{\pi}{1.6} \frac{v}{d^2} \quad . \tag{66}$$

From the structure of foams, Equation 66 should contain a

constant term representing the equilibrium film thicknesses, and this constant term should be controlling as v becomes very small. Actually, the foam becomes unstable, and the rupture of foam bubbles becomes controlling before the effects of such a constant term is detectable.

The differential equations for a vertical drainage section can be obtained from a material balance from z to the exit position, $z = \ell$. The volume fraction of liquid in the foam will be given by the following equation, which defines k_3:

$$\epsilon = a(1 - \epsilon)\tau + k_3 n(1 - \epsilon)\frac{\pi\delta^2}{4} . \tag{67}$$

The flows due to the foam velocities are:

$$\text{flow out at } z = \ell \text{ is } \frac{v}{1 - \epsilon}\epsilon = va\tau\,(\ell) + vk_3 n\pi\,\frac{\delta^2(\ell)}{4} ,$$

$$\text{flow in at } z \text{ is } \frac{v}{1 - \epsilon}\epsilon = va\tau + k_3\, nv\,\frac{\pi\delta^2}{4} .$$

The flows of liquid in the vertical Plateau borders are:

$$\text{flow in at } z = \ell \text{ is } u\epsilon_{PB} = \frac{\rho g}{32\mu}\,\delta^2(\ell)\; n[1 - \epsilon(\ell)]\,\frac{\pi\delta^2(\ell)}{4} ,$$

$$\text{flow out at } z \text{ is } u\,\epsilon_{PB} = \left|\frac{\rho g}{32\mu}\right|\delta^2\; n(1 - \epsilon)\frac{\pi\delta^2}{4} .$$

For time steady state, the total net flow is zero or

$$\tau = \tau(\ell) - k_3\,\frac{n\pi}{4a}[\delta^2 - \delta^2(\ell)] - \frac{1}{v}\,\frac{n\pi}{4a}\,\frac{\rho g}{32\mu}\left\{[1 - \epsilon(\ell)]\delta^4(\ell) - (1 - \epsilon)\delta^4\right\} . \tag{68}$$

Substituting $v = v(\ell) = \frac{\rho g}{32\mu}\,\delta^2(\ell)$ and $[1 - \epsilon(\ell)] \simeq 1$,

$$\tau = \tau(\ell) - k_3\,\frac{n\pi}{4a}\,\delta^2 + (k_3 - 1)\,\frac{n\pi}{4a}\,\delta^2(\ell) + \frac{1}{v}\,\frac{n\pi}{4a}\,\frac{\rho g}{32\mu}\,(1 - \epsilon)\delta^4 . \tag{69}$$

Differentiating,

$$\frac{d\tau}{dz} = \frac{n\pi}{4a}\left[\frac{\rho g}{32\mu}\,\frac{1-\epsilon}{v}\,4\delta^3 - 2k_3\delta\right]\frac{d\delta}{dz} \quad . \tag{70}$$

This equation may also be obtained from a liquid material balance for a differential length of the drainage section. Substituting τ from Equation 69 in Equation 67:

$$\epsilon = a(1-\epsilon)\tau(\ell) + \frac{n\pi}{4}(1-\epsilon)(k_3-1)\delta^2(\ell) + \frac{n\pi}{4}\,\frac{\rho g}{32\mu}\,\frac{(1-\epsilon)}{v}\,\delta^4 \quad . \tag{71}$$

From Equation 40,

$$-\frac{d\tau}{dz} = -\frac{(1-\epsilon)}{v}\,\frac{d\tau}{dt} = \frac{256\gamma(1-\epsilon)}{3\mu d^2 v}\,\frac{(\tau-\tau_{eq})^3}{\delta} \quad . \tag{72}$$

Eliminating τ and $\frac{d\tau}{dz}$ from Equations 69, 70, and 72 ,

$$dz = \frac{-\left(\frac{4a}{n\pi}\right)^2 \frac{3\mu d^2 v}{256\gamma(1-\epsilon)}\left[\frac{\rho g}{32\mu}\,\frac{(1-\epsilon)}{v}\,4\delta^3 - 2k_3\delta\right]\delta d\delta}{\left\{\frac{\rho g}{32\mu}\,\frac{1-\epsilon}{v}\,\delta^4 - k_3\delta^2 + (k_3-1)\delta^2(\ell) + \frac{4a}{n\pi}[\tau(\ell) - \tau_{eq}]\right\}^3} \quad . \tag{73}$$

If $(1-\epsilon)$ is assumed constant, this is in the form:

$$dz = k_4\,\frac{d[f(\delta)]}{f^3(\delta)} \quad . \tag{74}$$

An analytical solution for this equation has not been found. Numerical calculations are possible by using the properties of the liquid solution and the average bubble diameter.

VI-2 Estimated Foam Densities

The tests of the foam drainage equations developed will be comparisons with experimental results in Chapter V. At this point, values for the properties of the dodecylbenzenesulfonate solution used experimentally will be substituted. The simplified equations will be used to

estimate the probable values predicted by the drainage model.

For the dilute aqueous solutions of DBS, $\rho = 1.0$ g/cc and $\mu = 1$ centipoise. Values of $n = 2.5/d^2$ and $k = 1.5$ will be used. From these values:

$$\frac{32\mu}{\rho g}\frac{\pi n k^2}{4} = \frac{14.10^{-4}}{d^2} \quad . \tag{75}$$

From Equations 31 and 32:

$$\epsilon^2 d^2 \left[L + \frac{v}{1-\epsilon}\epsilon\right]^{-1} = 14 \times 10^{-4} \quad , \tag{76}$$

$$\epsilon^2 d^2 / L_o = 14 \cdot 10^{-4} \quad . \tag{77}$$

From Equation 58:

$$cT(0) = 53 \frac{d}{\ell} L_o^{1/2} \quad . \tag{78}$$

From Equation 61 where $\bar{\epsilon}$ is small compared to $\bar{\epsilon}_o$:

$$\frac{\ell}{\bar{\epsilon} d^2 (t - t_o)} \simeq 2800 \quad . \tag{79}$$

From Equation 66:

$$\epsilon_p = 3.2 \cdot 10^{-4} \frac{v}{d^2} \quad . \tag{80}$$

The maximum and minimum values of the foam densities were estimated from Equations 76 through 80 for average bubble diameters of 0.06 cm and the experimentally used values of v and L. In the region of countercurrent foam and liquid flow, the minimum densities would be about 0.13 cc/cc and the maximum, 0.48 cc/cc from Equation 76. From Equation 79 for a horizontal drainage section, the average exit

densities would be below 0.01 cc/cc for several minutes of holdup, but would require 10 to 100 minutes to give densities below 0.001 cc/cc. From Equation 80, the exit densities from vertical drainage sections would be 0.01 to 0.001 cc/cc. Since the values of $a\tau_{eq}$ are about 10^{-4}-cc liquid/cc foam, these calculated results indicate that the foam densities for vertical foam flow rates above 0.01 cm/sec are controlled more by the equilibrium Plateau border sizes than by the liquid remaining in the films between bubbles.

IV-3 Justification of Diffusion-Controlled Mass Transfer

The dimensions indicated by the foam drainage model and confirmed experimentally can be used to justify assumption of diffusion controlled mass transfer. The Reynolds number, Re, for flow through packed beds based on the superficial fluid velocity is:

$$Re = \frac{dL\Delta\rho}{\mu} . \tag{81}$$

For the countercurrent flow of foam and liquid, this Reynolds number is 1 to 5, which is well below the 10-to-100 range over which the streamlined-to-turbulent-flow transition occurs in packed beds. The more common form of Reynolds number can be calculated as follows for flow in the Plateau borders as capillaries:

$$Re = \frac{\delta u\rho}{\mu} , \tag{82}$$

$$u = \frac{\rho hg}{32\mu}\delta^2 = 3060\,\delta^2 , \tag{27a}$$

$$Re = \frac{\delta(3060\delta^2)(1)}{0.01} = 0.306\cdot 10^6\delta^3 . \tag{82a}$$

The largest values of δ are about 0.04 cm, which give Re = 20; this is well below the transition zone, which starts at 2000. The flow of liquid through the foam would probably become turbulent at flow rates intermediate between those at which turbulence appears in a packed bed of solids and in a simple capillary tube. From either criteria, streamlined flow and diffusion-controlled mass transfer appear to be well justified assumptions.

IV-4 Calculation of Heights of Transfer Units

The equations commonly applied to countercurrent mass transfer between phases in columns (15,25) were adapted for experimental determinations of the number of transfer units in foam columns. The flow rates, L and V, are constant throughout the column. The equilibrium relationship is given by $(y/x)_{equilibrium} = \alpha$ or $y^* = \alpha x$, $x^* = y/\alpha$, where α is a constant independent of concentration differences in the column. The liquid pot is assumed to be one theoretical stage; that is to say, all streams leaving the liquid pot are in equilibrium with each other. The surface "entering" (i.e., generated in) the liquid pot has a zero concentration. All the above conditions are assured by the proper selection of operating conditions.

The conditions selected to define E and x' determine the simplification possible in the differential expressions for the number of transfer units. If E = 0 or $x' = x$ are selected, the equations reduce to those for linear operating and equilibrium lines as given in the references (15,25). The values for the exit foam are E_p and y_p/α, and

it is logical that the values of E and x' should be defined to be continuous to these values. A constant value of E_p throughout the column would simplify the calculations, while a varying value has no apparent additional utility unless it could be shown to simplify the correlation of HTU results. No such simplification is obvious. Therefore E is defined as $E = E_p$ = constant. We also define $x' = y/\alpha$; this definition greatly simplifies the calculations and will be justified in section IV-5 from consideration of diffusion rates and the film dimensions.

A differential material balance may be written for a point in the column:

$$d[(L + E)\ x\ ] = d(Vy) + d(x'E) \quad . \tag{83}$$

But L, E, and V are constant, and $x' = y/\alpha$

$$(L + E)dx = (V + \frac{E}{\alpha})dy = \frac{\alpha V + E}{\alpha}\, dy \quad . \tag{84}$$

This may be integrated from x_1, y_1 to x, y or x_2, y_2:

$$(L + E)(x - x_1) = \frac{\alpha V + E}{\alpha}(y - y_1) \quad , \tag{85a}$$

$$(L + E)(x_2 - x_1) = \frac{\alpha V + E}{\alpha}(y_2 - y_1) \quad . \tag{85b}$$

Since $x^* = \frac{1}{\alpha} y = \frac{1}{\alpha}\left[y_1 + \frac{(L + E)\alpha}{(\alpha V + E)}(x - x_1)\right]$,

$$x_2^* = \frac{1}{\alpha}\left[y_1 + \frac{(L + E)\alpha}{(\alpha V + E)}(x_2 - x_1)\right] , \tag{86}$$

$$\frac{(L + E)}{(\alpha V + E)} = \frac{(y_2 - y_1)}{\alpha(x_2 - x_1)} = \frac{x_2^* - x_1^*}{x_2 - x_1} \quad . \tag{87}$$

The conventional equations for mass transfer in terms of the liquid phase driving force may be written:

$$d[(L + E)x]=(L + E)dx = k_x a(x - x^*)dz \ , \tag{88}$$

$$N_x = \frac{\text{length}}{HTU_x} = \frac{(z_2 - z_1)k_x a}{(L + E)} \int_{x_1}^{x_2} \frac{dx}{x - x^*} \ : \tag{89}$$

Substituting for x^* and letting $k = \frac{(L + E)}{(\alpha V + E)}$,

$$N_x = \int_{x_1}^{x_2} \frac{dx}{x - \frac{1}{\alpha}[y_1 + \frac{(L + E)\alpha}{(\alpha V + E)}(x - x_1)]} = \int_{x_1}^{x_2} \frac{dx}{(kx_1 - \frac{y_1}{\alpha}) + (1 - k)x} \ . \tag{90a}$$

$$N_x = \frac{1}{1 - k} \ln (kx_1 - \frac{y_1}{\alpha}) + (1 - 1)x \Big]_{x_1}^{x_2} \ , \tag{90b}$$

$$N_x = \frac{1}{1 - k} \ln \frac{x_2 + k(x_1 - x_2) - y_1/\alpha}{x_1 - y_1/\alpha} \ , \tag{90c}$$

$$N_x = \frac{1}{1 - \frac{x_2 - x_1}{x_2 - x_1^*}} \ln \frac{x_2 - x_2^*}{x_1 - x_1^*} \ , \tag{90d}$$

$$N_x = (x_2 - x_1) \left[\frac{\ln \frac{x_2 - x_2^*}{x_1 - x_1^*}}{(x_2 - x_2^*) - (x_1 - x_1^*)} \right] \ , \tag{90e}$$

$$N_x = \frac{x_2 - x_1}{(x - x^*)_{\ln \text{ mean}}} \ . \tag{90f}$$

This result is identical with that for linear operating and equilibrium lines where there is no term for E or x'. If $L/\alpha V$ is 1, $(L + E)/\alpha V + E)$ is also 1, and the slope of the operating line is not changed.

While the assumptions made to define E and x' do not change the form of the equation for N_x from that for E = 0, the assumptions do change the calculation of x_1 and x_2^* from the experimental data. The value of x_2 is known from feed samples. The value of x_1^* is the concentration of the exit liquid stream, x_B, since the liquid pot is assumed to be one theoretical stage. From a material balance for this theoretical stage:

$$x_1 = x_B + \frac{\alpha V}{L + E} x_B = \left(1 + \frac{\alpha V}{L + E}\right) x_B , \tag{91}$$

$$x_1 - x_1^* = x_1 - x_B = \frac{\alpha V}{L + E} x_B . \tag{92}$$

From the condensed foam analyses:

$$x_2^* = \frac{y_2 V + x_2' E_p}{\alpha V + E_p} = \frac{\left(V + \frac{E_p}{\alpha}\right) y_2}{(\alpha V + E_p)} = \frac{y_2}{\alpha} . \tag{93}$$

The values of x_B and of $y_2 V + x_2' E$ are measured experimentally. It is physically obvious that E_p must be used in the calculation of x_2^*, or a fictitiously high value will be obtained. The expression derived for $x_1 - x_1^*$ appears more valid than the expression which results if E = 0. This can be seen by considering columns operated at different conditions all chosen so that $L = \alpha V$. Then $(L + E)/\alpha V + E)$ and $L/\alpha V$ are both one, but $\alpha V/(L + E) = 1 - E/(L + E)$. As $L \to 0$, $V \to 0$, $x_2^* \to x_2$, and $x_1 - x_B \to 0$. This is true if $x_1 - x_B = \left(\frac{\alpha V}{L + E}\right) x_B = \left(1 - \frac{E}{L + E}\right) x_B$ but is not true for $x_1 - x_B = x_B$.

IV-5. Film Concentration Gradients

The concentration gradients that exist in the liquid may be

estimated from calculations for simple configurations. The actual configuration of the foams appeared too complex to permit exact practical solutions. The low Reynolds numbers for the whole range of foam conditions (see Section IV-2) indicate that all liquid flows would be streamlined with respect to the foam bubbles, with no turbulent mixing in the Plateau borders or bubble walls.

A mass-balance equation and the conventional rate equations using x_i and x_j as interface concentrations between the (L + E) and E, and E and V streams may be written for a differential length of the countercurrent flow section.

$$(L + E)dx = Vdy + E\,dx' , \tag{94}$$

$$(L + E)dx/dz = k_x a(x - x_i) , \tag{95}$$

$$V\,dy/dz = k_y a(\alpha x_j - y) , \tag{96}$$

$$Edx'/dz = k_x a(x - x_i) - k_y a(\alpha x_j - y) = k_e a(x_i - x_j) . \tag{97}$$

The values of L, E, and V are assumed constant for the reasons discussed in Section IV-3.

The only systems of interest are for $L \gg E$ and $L/\alpha V$ = about 1. (Certainly, $L/\alpha V$ less than 2 is necessary for transfer of any major fraction of the solute from the liquid to the surface.) The physical meaning of this is that accumulation in the "entrained" liquid phase is not significant throughout the columns; however, transients at the liquid pot surface and in the drainage section must be considered when boundary conditions are selected. Therefore the net amounts transferred to the "entrained" liquid are small compared to the net transfer from the liquid to the surface. For the diffusion-controlled mass

transfer in the liquid, the mass transfer coefficients, k_x or k_e, are equal to D/ℓ, where ℓ is an averaged diffusion length. Therefore the mass transfer coefficients and thus the HTU_x values may be calculated if appropriate values of the average diffusion distance can be estimated.

The model used for foam drainage can be extended to give a model for the mass transfer. A capillary with streamlined flow of liquid represents the Plateau borders. The films between bubbles can be represented by three axial fins, with diffusion to the film surfaces from the capillary. The configuration is very similar to heat transfer for a finned tube, but the boundary conditions at the surface of the fins are not the usual ones for heat transfer.

Since the surface has a capacity proportional to the liquid concentration ($y^* = \alpha x$, or $dy/dz \simeq \alpha\, dx/dz$), the amount transferred to each unit area of surface at a given position of z is a constant. For a thin fin of rectangular cross section and height h (Figure 2), the mass balance differential equation and its solution are:

$$2D\tau \frac{d^2x}{dw^2} - k = 0 , \tag{98}$$

$$x - x_o = \frac{k}{2D\tau} (w^2 - 2hw) . \tag{99}$$

$$\text{Since } \frac{dy}{dw} = \alpha \frac{dx}{dw} , \frac{d^2y}{dw^2} = \alpha \frac{dx^2}{dw^2} \quad \text{then}$$

$$(y - y_o) = \frac{k\alpha}{2D\tau} (w^2 - 2wh) . \tag{100}$$

The mass transfer at w = 0 per unit axial length is 2kh since the film

ORNL-DWG 63-4754

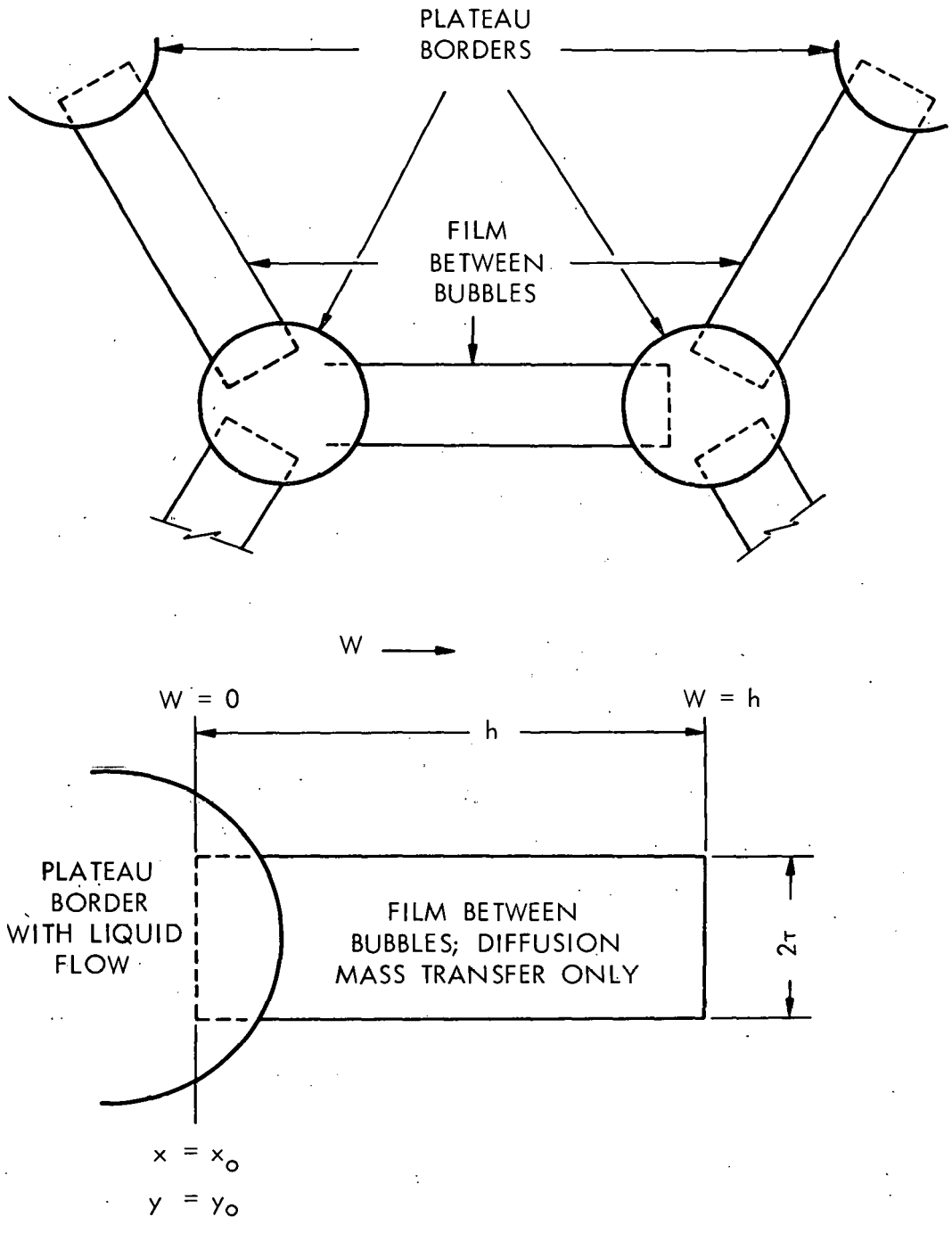

Figure 2. Simplified Mass Transfer Configuration in a Foam.

surface area is 2h cm^2/cm.

The average concentrations as used for HTU_x calculations can be logically assumed to be:

$$x_{ave} = x_o \ , \tag{101}$$

$$y_{ave} = \int_o^h y \, dw = y_o - \frac{kh\alpha^2}{3D\tau} \ . \tag{102}$$

Since the amount transferred per unit area is constant, the average distance is h/2. Then the HTU_x values may be calculated if h is known in terms of d. A value of h = 0.2d appears logical for this model since the edge of a dodecahedron is about 0.45d. The height of a transfer unit for diffusion controlled mass transfer is (15):

$$HTU_x = \frac{L'}{k_x a S} = \left(\frac{L'}{S}\right)\left(\frac{\ell}{D}\right)\left(\frac{1}{a}\right) \ , \tag{103}$$

$L'/S = L$, the superficial liquid velocity

$\ell = h/2 = 0.1d$

$D = 4.7 \cdot 10^{-6}$ cm^2/sec

$1/a = d/6$

$$HTU_x = (L)\left(\frac{0.1d}{4.7 \cdot 10^{-6}}\right)\left(\frac{d}{6}\right) = 3500Ld^2 \tag{104}$$

Mass transfer inside the Plateau border is due both to diffusion and to the flow with a parabolic velocity distribution. The resulting second-order equation with variable coefficients does not appear to have any useful analytical solutions. Numerical solutions with a computer would be possible, but did not appear to be worthwhile. If the distribution of concentrations inside the Plateau border were

known, the volume average concentration could be compared with the average with respect to diffusion. Considering the uncertainty in the average diffusion distance, the comparison of concentration averages is not very important.

CHAPTER V

CORRELATION OF MEASURED FOAM PROPERTIES AND FOAM DRAINAGE

A low density is desirable for the foam discharged from a foam separation column in order to obtain a high volume reduction, that is, in order to obtain the separated surface-active materials in a minimum volume of condensed foam. The usual procedure for increasing the volume reduction is to reduce the vertical foam velocity. Since high foam velocities tend to reduce channeling and reduce the column size, a countercurrent column is usually topped by a "drainage section." Drainage appears to approach equilibrium after several feet of vertical drainage section, and additional drainage at the same foam velocity occurs only because of the loss of surface due to foam condensation. An equilibrium foam density would be expected from foam drainage models at the density where the downward liquid velocity with respect to the foam equals the upward velocity of the bulk foam.

Experimental data were obtained for four foam drainage situations. One was the type most commonly reported in the literature where the collection of liquid below a stationary column of foam was observed as a function of time. The other three were from time-steady-state operation of foam columns. These time-steady-state situations were for the region of the column with countercurrent flow of the foam and liquid, for drainage of liquid from the foam as it flowed upward through a drainage section, and for drainage of liquid from foam flowing horizontally. The data were not adequate to determine the rates at

which the films between bubbles drain to the Plateau borders. The numbers of greatest practical interest were the densities of the relatively dry foams leaving drainage sections and successful correlations of these results with measured foam properties were possible.

V-1 Drainage in Stationary Foam

The drainage of solution from a stationary column of foam (the type of data most frequently reported in the literature) should be represented by Equations 47, 48, and 50 if they satisfy the boundary conditions on the foam. The accumulation of liquid at the bottom of such a column as a function of time, $W(t,z_o)$, should be represented by Equation 54. These equations are in the form of those for a second order reaction with the rate of drainage proportional to the square of the amount of undrained liquid.

Experimental measurements were made for a 6-in.-ID foam column in which uniform, countercurrent, steady state flow of liquid had been established. The gas and liquid flows were shut off simultaneously and the liquid-foam interface position, which is equivalent to $W(t,z_o)$ was recorded periodically. For the region of countercurrent liquid-foam flow, all properties would be constant, independent of both time and position. When the flows were shut off, the foam would drain as a stationary column; the zero time conditions would be the same values of ϵ and L_o as for the steady state countercurrent flow.

Typical experimental data for $W(t,z_o)$ (Figures 3 and 4, also Table XXXIV in the Appendix) show a constant rate period until the

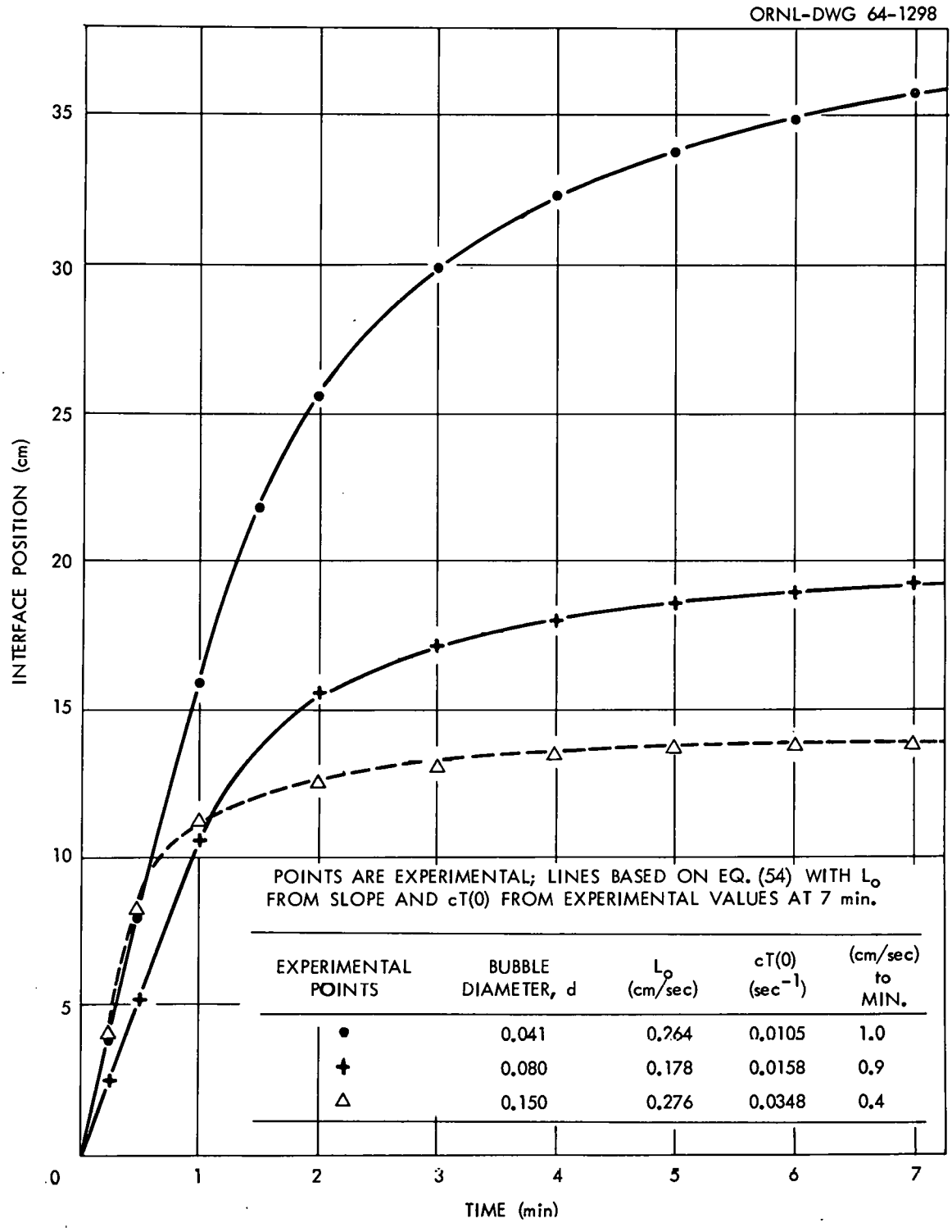

Figure 3. Drainage of a Bed of Foam after Counter-Current Flow.

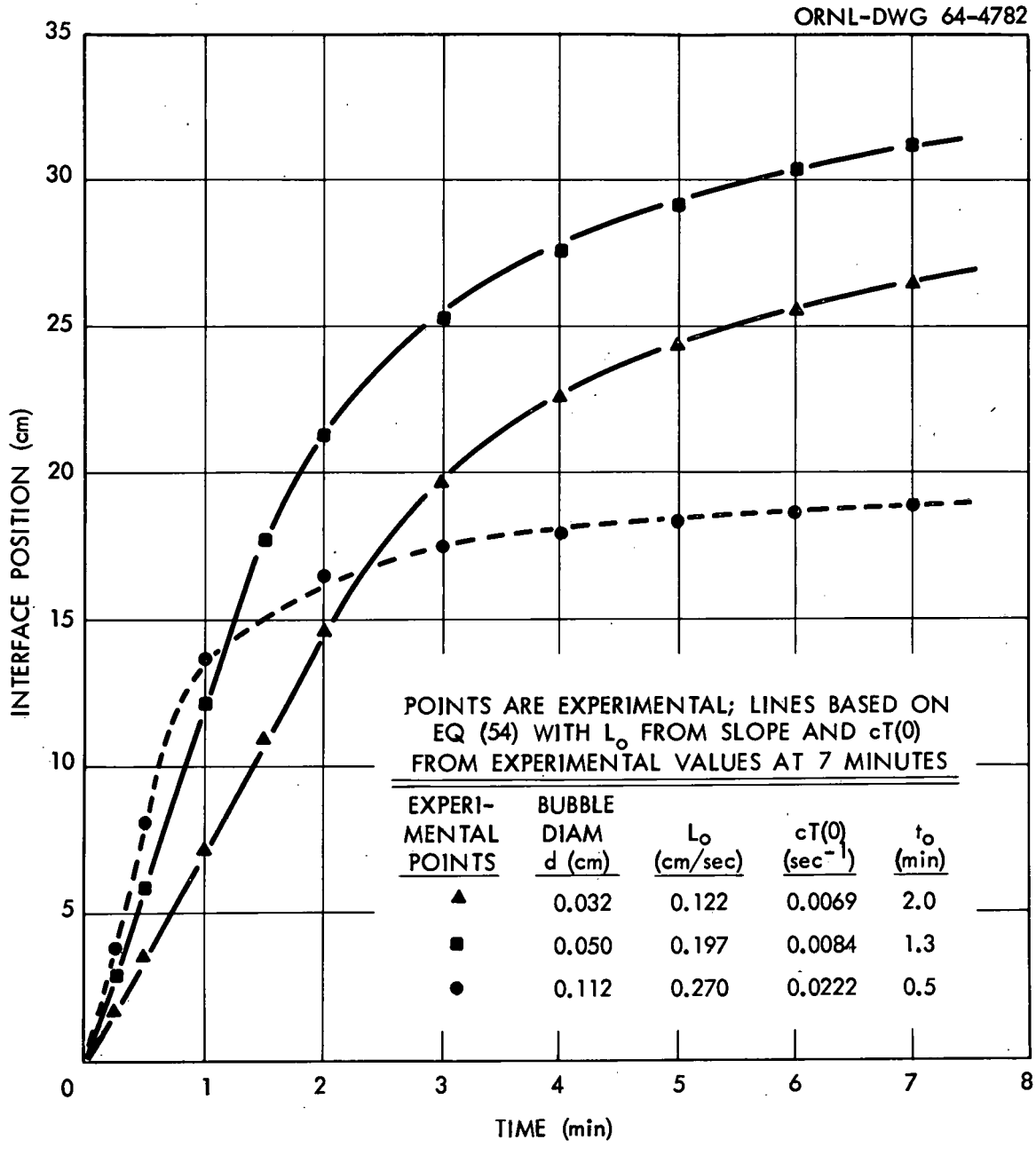

Figure 4. Typical Drainage of Beds of Foam after Countercurrent Flow.

first liquid from the top of the countercurrent region reaches the bottom. The foam density starts decreasing immediately at the top, but the foam density is constant at the bottom until this decreasing density has traveled down the column. During the periods when ϵ or L are constant, equations 51, 52, and 54 are satisfied by $\partial\epsilon/\partial t = -\partial L_o/dz = 0$ and $c = 0$.

Equation 54 gives an excellent fit of the experimental data as shown by typical curves (Figures 3 and 4). The slope of the constant rate period where $c = 0$ is used as the value of $L(t_o,z_o)$. By using the end of the constant rate period as time t_o with the value of $L(t_o,z_o)$ from the slope, $cT(0)$ is evaluated using the value of $W(t = 7 \text{ min}, z_o)$. The experimental data of other authors such as Jacobi et al. (20) also show good agreement with the form of Equation 54 by evaluating $L(t_o,z_o)$ and $cT(0)$ as empirical constants.

A much more severe test of drainage models would be to relate the constants to the foam properties. Equation 58 or 78 provides such a test:

$$cT(0) = \left[\frac{\rho g}{32\mu} \frac{4}{\pi n k^2} \frac{4}{\ell^2} L(t_o,z_o)\right]^{\frac{1}{2}} , \tag{58}$$

$$cT(0) = 53 \frac{d}{\ell} L_o^{\frac{1}{2}} . \tag{78}$$

Values of $cT(0)$ calculated from Equation 78 show very good agreement with the empirical values obtained by curve fitting (Table III). This result indicates that ϵ, L, and W throughout a stationary column of foam as a function of time could be predicted from the values of ρ, μ,

TABLE III. A TEST OF A DRAINAGE MODEL FOR A STATIONARY BED OF FOAM

Bubble Diameter d, cm	Column Height ℓ, cm	Superficial Liquid Velocity L_o, cm/sec	Empirical $cT(0)$, sec^{-1}	Theoretical $cT(0)$, sec^{-1}
0.032	112	0.063	0.0047	0.0038
	112	0.122	0.0069	0.0053
0.033	109	0.137	0.0075	0.0060
0.041	110	0.181	0.0075	0.0084
		0.220	0.0087	0.0092
		0.264	0.0105	0.0104
0.050	112	0.197	0.0095	0.0105
0.055	111	0.053	0.0061	0.0061
0.059	107	0.060	0.0071	0.0072
	111	0.118	0.0096	0.0097
		0.264	0.0103	0.0145
		0.335	0.0130	0.0163
0.080	110	0.068	0.0102	0.0100
		0.130	0.0126	0.0139
	109	0.178	0.0158	0.0165
	103	0.230	0.0200	0.0198
0.112	110	0.158	0.0173	0.0214
	108	0.270	0.0222	0.0284
0.150	109	0.185	0.0254	0.0314
	110	0.276	0.0348	0.0380

ℓ, d, and a single measurement of ϵ, L, or W at one point. This conclusion is only valid, of course, if the boundary conditions can be satisfied by the equations which were derived. The methods used to form the foam may give initial boundary conditions which the simple equations cannot fit. However, the effects of boundary conditions which only apply at zero time will damp out and the simple solutions may be adequate after a short time.

The most realistic model found in the literature is that of Jacobi et al. (20) who represented the foam drainage by the capillary flow of liquid between plates whose separation varied with height and time. Equations similar to Equations 32, 52, and 54 were obtained except that the rate of drainage was proportional to the third power of the amount of undrained liquid. Also both constants were evaluated empirically without consideration of their theoretical relationship. If both constants are evaluated empirically, the equations of this report or of Jacobi will fit the experimental data of this report or of Jacobi about equally well.

The best comparison of the two models would be to compare experimental values of $\epsilon^2 d^2/L_o$ and $\epsilon^3 d^2/L_o$ with the constant theoretical values since the equivalent of Equation 60 for Jacobi's model is (see Appendix B):

$$\frac{\epsilon^3 d^2}{L_o} = \frac{12\mu}{\rho g} \frac{d^2}{k_4{}^3 S'} \quad . \tag{105}$$

When the equation is arranged in this form, $d^2/k_4{}^3 S'$ is dimensionless

and would have a value of 13.5 for $k_4 = d/3$ and $S' = 2/d$ consistent with previous calculations. Such a comparison for the data for this report (Table IVa) show that $\epsilon^2 d^2/L_o$ is more constant than $\epsilon^3 d^2/L_o$. In Table IVa the theoretical value is closer to the experimental value for $\epsilon^2 d^2/L_o$ ($14 \cdot 10^{-4}$ as compared to $9 \cdot 10^{-4}$ - $24 \cdot 10^{-4}$) than for $\epsilon^3 d^2/L_o$ ($17 \cdot 10^{-4}$ as compared to $0.7 \cdot 10^{-4}$ - $6 \cdot 10^{-4}$). The theoretical value of $\epsilon^3 d^2/L_o$ is based on the value of 13.5 for d^2/k_1^3 since Jacobi did not suggest values for k_4 and S. Jacobi generated all the foams for which data is reported by using a constant gas rate of 90 cc/min through a 20-mm-diam sintered glass disk of 40-60μ porosity. For DBS solutions, this would give foams of 0.02 - 0.04 cm average bubble diameter. For the data of Jacobi (Table IVb), $\epsilon^2 d^2/L_o$ is more constant and closer to the theoretical value than $\epsilon^3 d^2/L_o$.

V-2 Countercurrent Flow of Foam and Liquid

The hydraulic behavior of foam and liquid flowing countercurrently was observed in order to estimate the capacities of foam separation columns and to determine the validities of the drainage models previously developed (Chapter IV). The appearance was observed visually through the column walls, and the foam densities and drainage rates were measured. For the region of countercurrent liquid-foam flow, all properties are constant independent of both time and position. Thus Equations 41 and 44 are satisfied by $\partial\epsilon/\partial t = -\partial L/\partial z = 0$ and $c = 0$.

The values of L, v, ϵ, and d should be correlated by Equation 76 for the DBS solution.

TABLE IV

A COMPARISON OF TWO DRAINAGE MODELS FOR A STATIONARY BED OF FOAM

Source of Data: For DBS solutions, procedure of this report as described, illustrated by Figure 3, and tabulated in Table III. For other surfactants, data of Jacobi et al., Table I (20).

	Surfactant	Bubble Diameter d, cm	Superficial Liquid Velocity L_o, cm/sec	$\bar{\epsilon}_o = \frac{W_\infty}{\ell}$	$\frac{\epsilon^2 d^2}{L_o}$ 10^{-4} cm·sec	$\frac{\epsilon^3 d^2}{L_o}$ 10^{-4} cm·sec
a.	Data of the author DBS	0.032	0.063	0.119	9.3	0.90
			0.122	0.158	8.4	1.1
		0.033	0.137	0.168	8.5	1.3
		0.041	0.181	0.220	17.9	3.4
			0.220	0.230	16.3	3.2
			0.264	0.235	14.2	2.8
		0.050	0.197	0.210	22.2	4.0
		0.055	0.053	0.078	13.9	0.92
		0.059	0.060	0.079	14.5	0.98
			0.118	0.110	14.5	1.3
			0.264	0.231	28.3	5.5
			0.335	0.232	22.6	4.4
		0.080	0.068	0.060	13.8	0.68
			0.130	0.085	14.1	0.99
			0.178	0.104	15.4	1.4
			0.230	0.112	13.8	1.3
		0.112	0.158	0.083	22.0	1.5
			0.270	0.113	23.7	2.3
		0.150	0.185	0.067	21.9	1.2
			0.276	0.074	17.9	1.1
b.	Data of Jacobi					
	Sodium dodecyl-sulfate	0.03[a]	0.167	0.200[b]	8.6	1.5
	Sodium tetra-decylsulfate		0.159	0.200[b]	9.1	1.5
	Sodium hexa-decylsulfate		0.122	0.110[b]	3.6	0.33
	Miranol SM (C_{10})		0.143	0.189[b]	7.5	1.5
	Miranol HM (C_{12})		0.127	0.164[b]	7.7	1.1
	Miranol MM (C_{14})		0.085	0.119[b]	6.0	0.60
	Triton X-100		0.066	0.095[b]	4.9	0.39
	Merlfoam		0.035	0.104[b]	11.1	0.98

[a] As Jacobi did not report values of d, this value of 0.03 was assumed since a 40-60 μ porosity sintered glass disk was used.

[b] From the foam expansions reported by Jacobi.

$$\epsilon^2 d^2 \left[L + \frac{v}{1 - \epsilon} \epsilon \right]^{-1} = 14 \cdot 10^{-4} \quad . \tag{76}$$

The values of $\epsilon(t_o, z_o)$ were calculated from $L(t_o, z_o)$ and $cT(0)$ using Equation 56:

$$\epsilon(t_o, z_o) = 2\bar{\epsilon}_o = \frac{2L(t_o, z_o)}{\ell cT(0)} \quad . \tag{56a}$$

Substitution gives $8 \cdot 10^{-14}$ to $19 \cdot 10^{-4}$ (Table V) for $\epsilon^2 d^2/[L + v\epsilon/(1 - \epsilon)]$ in good agreement with the theoretical value of $14 \cdot 10^{-4}$ from Equation 76. By noting that $u\epsilon_{PB}$ in Equation 29 is the same for L and v during countercurrent flow and for L_o and $v = 0$ after the flows are stopped, an independent expression for ϵ is obtained:

$$\epsilon = \frac{L_o - L}{v + L_o - L} \quad . \tag{106}$$

The values of ϵ from Equation 76 are probably the best. The liquid drained in 7 min divided by the foam volume (Table V) gives a low estimate of the foam density because of the liquid which remains in the foam. This difference should be most significant for small values of d or L. The values of ϵ from Equation 106 are low due to channeling of liquid through the foam during countercurrent flow. This effect is most important for high liquid flow rates.

Equation 31 may be used to estimate the limiting flow rates for countercurrent foam columns:

$$L + \frac{v}{1 - \epsilon} \epsilon = \frac{\rho g}{32\mu} \frac{4}{\pi n k^2} \epsilon^2 \quad . \tag{31}$$

For the DBS solution, this reduces to Equation 76.

TABLE V

A TEST OF A DRAINAGE MODEL FOR COUNTERCURRENT FLOW OF LIQUID AND FOAM

Bubble Diameter d (cm)	Superficial Gas Velocity v (cm/sec)	Superficial Liquid Velocity L (cm/sec)	Superficial Liquid Velocity for v = 0 L_o (cm/sec)	$\epsilon(t_o, z_o)$ from Eq. 56 (cc/cc)	$\frac{\epsilon^2 d^2}{L + \frac{v\epsilon}{1-\epsilon}}$ 10^{-4} (cm·sec)	$\frac{L_o - L}{v + L_o - L}$ (cc/cc)	$\frac{W(t=7)}{\ell}$ (cc/cc)
0.032	0.067	0.046	0.063	0.239	8.7	0.202	0.165
		0.101	0.122	0.316	7.6	0.239	0.238
0.033	0.125	0.101	0.137	0.335	7.5	0.224	0.253
0.041	0.254	0.101	0.181	0.439	10.9	0.240	0.286
		0.134	0.220	0.460	10.2	0.253	0.294
		0.188	0.264	0.470	9.0	0.230	0.334
0.050	0.364	0.101	0.197	0.419	12.1	0.274	0.280
0.055	0.067	0.046	0.053	0.156	10.5	0.095	0.081
0.059	0.129	0.046	0.060	0.158	12.5	0.098	0.115
		0.101	0.118	0.221	14.4	0.117	0.149
	0.507	0.101	0.264	0.462	14.0	0.244	0.314
		0.172	0.335	0.465	12.3	0.244	0.323
0.080	0.267	0.046	0.068	0.121	11.3	0.079	0.112
		0.101	0.130	0.169	11.7	0.098	0.151
		0.134	0.178	0.207	13.4	0.142	0.177
		0.190	0.230	0.223	12.0	0.130	0.208
0.112	0.525	0.101	0.158	0.166	16.8	0.084	0.142
		0.182	0.270	0.225	19.1	0.111	0.176
0.150	0.930	0.101	0.185	0.134	16.5	0.075	0.112
		0.163	0.276	0.148	15.2	0.094	0.126

$$\epsilon^2 d^2 \left[L + v\epsilon/(1 - \epsilon) \right]^{-1} = 14 \times 10^{-4} \quad . \qquad (76)$$

Channeling becomes excessive for conditions which give $\epsilon > 0.30$ in these equations while channeling can be avoided for $\epsilon < 0.26$ if the liquid is uniformly distributed and the foam bubbles are uniform in diameter. Fluidization of the foam bubbles would be expected at about $\epsilon = 0.26$ since this is the void volume of close packed spheres. These observations on channeling are based on visual appearance, on heights of transfer units for countercurrent mass transfer (Chapter VII) and on the comparison of densities calculated from Equations 56 and 106.

This limiting flow rate or "flooding rate" increases as the bubble diameter increases even when V/L or v/dL are held constant to give an operating line of constant slope (Figure 5). Values from these curves in units commonly used for solvent extraction are:

ϵ	V/L (sq cm/cc)	L for d = 0.06 cm (cm/sec)	L for d = 0.06 cm ($gal \cdot ft^{-2} \cdot hr^{-1}$)	L for d = 0.10 cm (cm/sec)	L for d = 0.10 cm ($gal \cdot ft^{-2} \cdot hr^{-1}$)
0.26[a]	900[b]	0.04	37.	0.08	70.
0.26[a]	180[c]	0.11	95.	0.24	210.

[a] "Flooding" value.

[b] Ratio required for LLW decontamination.

[c] Ratio required for stripping of strontium from demineralized water.

V-3 Drainage with Horizontal Foam Flow

Drainage in a channel with horizontal flow of foam would not be limited by the velocity equilibrium between the liquid and the foam

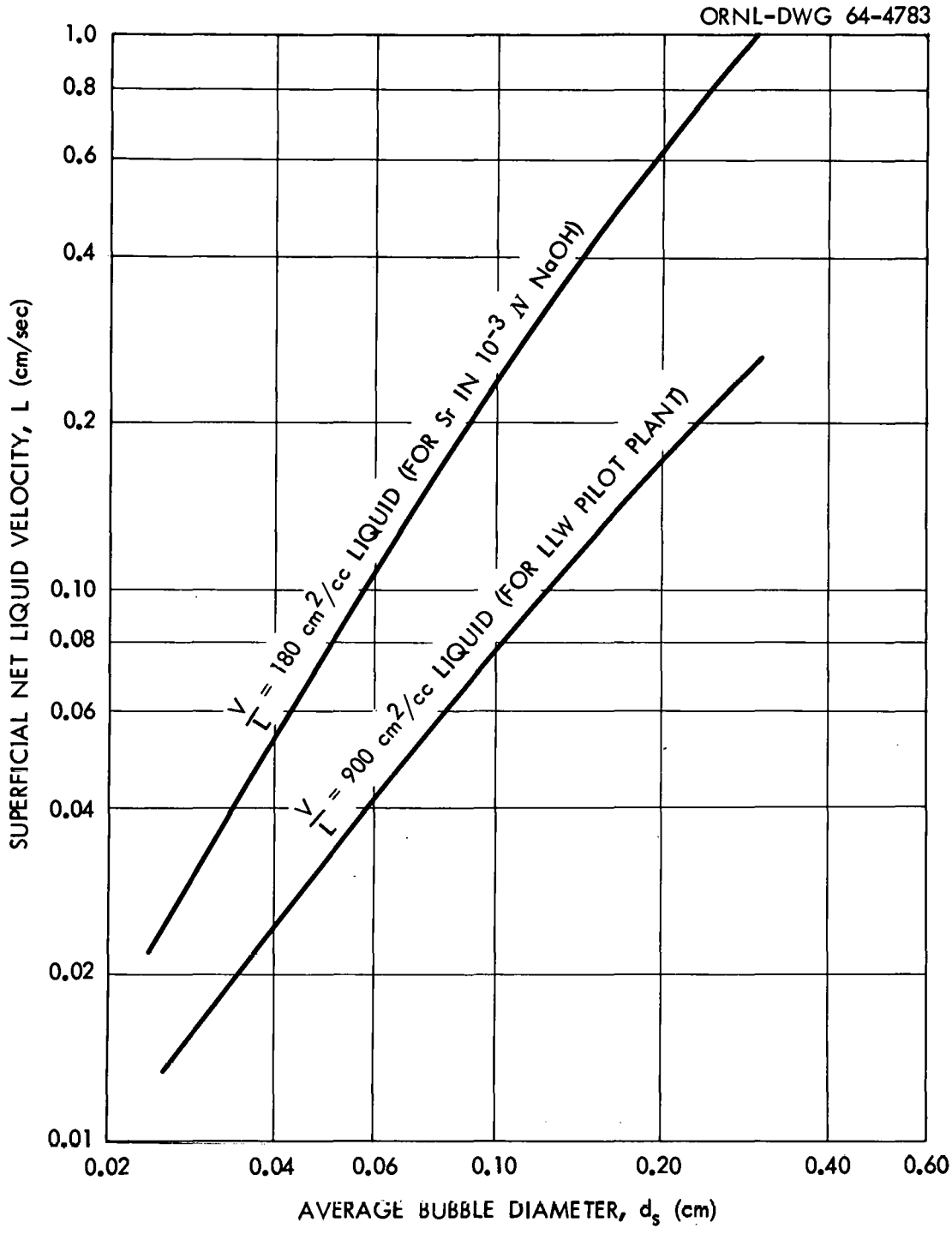

Figure 5. Limiting Flow Rates (ϵ = 0.26) for Foam Columns.

since the two flows would be at right angles to each other. Liquid would collect at the bottom of the horizontal channel, where it could be drained off and returned to the column. The use of a larger diameter would not be necessary for such a horizontal drainage section. Since the maximum liquid drainage distance would be the diameter of the channel, a larger diameter might actually be less effective than the same volume of a smaller diameter.

Drainage with horizontal flow of foam was measured experimentally in a 48-in. length of 6-in.-diam horizontal glass pipe as the drainage section for a short 6-in.-diam foam column (Figure 6). The pipe was at about a 2° angle to the horizontal (with the foam exit at the low end) to ensure collection of the drained liquid by a cross in the middle. The gas rate was set at a selected value, and the pump was set to recycle all the condensed foam and drained liquid. When the system appeared to be at equilibrium, the drained liquid and condensed foam rates were measured. Measurements were made for gas rates of 1100 to 18,400 cc/min and for two surfactant concentrations.

Good drainage was obtained, and foam densities were below 6 mg/ml even at very high foam flow rates (Figure 7). The lower curve shows the densities of the exit foam as determined by the condensed foam rate. The upper curve shows the foam densities into the horizontal section, as indicated by the sum of the condensed foam and drained liquid rates. For comparison, the exit foam densities for about the same volumes of vertical drainage were 5 to 8 mg/ml for about 7 cm/min velocities in either a 6-in.-diam or 10.5-in.-diam

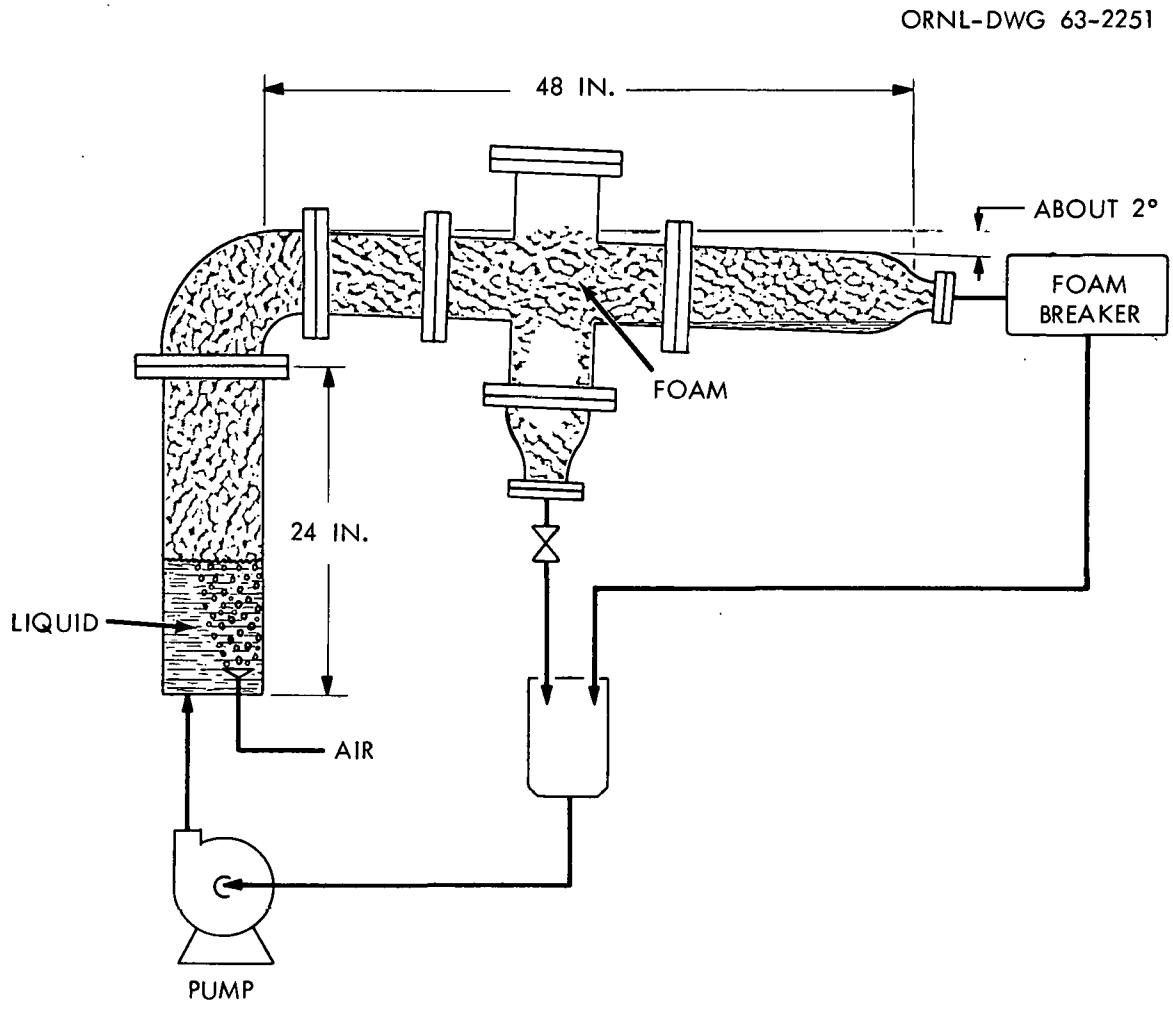

Figure 6. Drainage Test Apparatus with Horizontal Foam Flow.

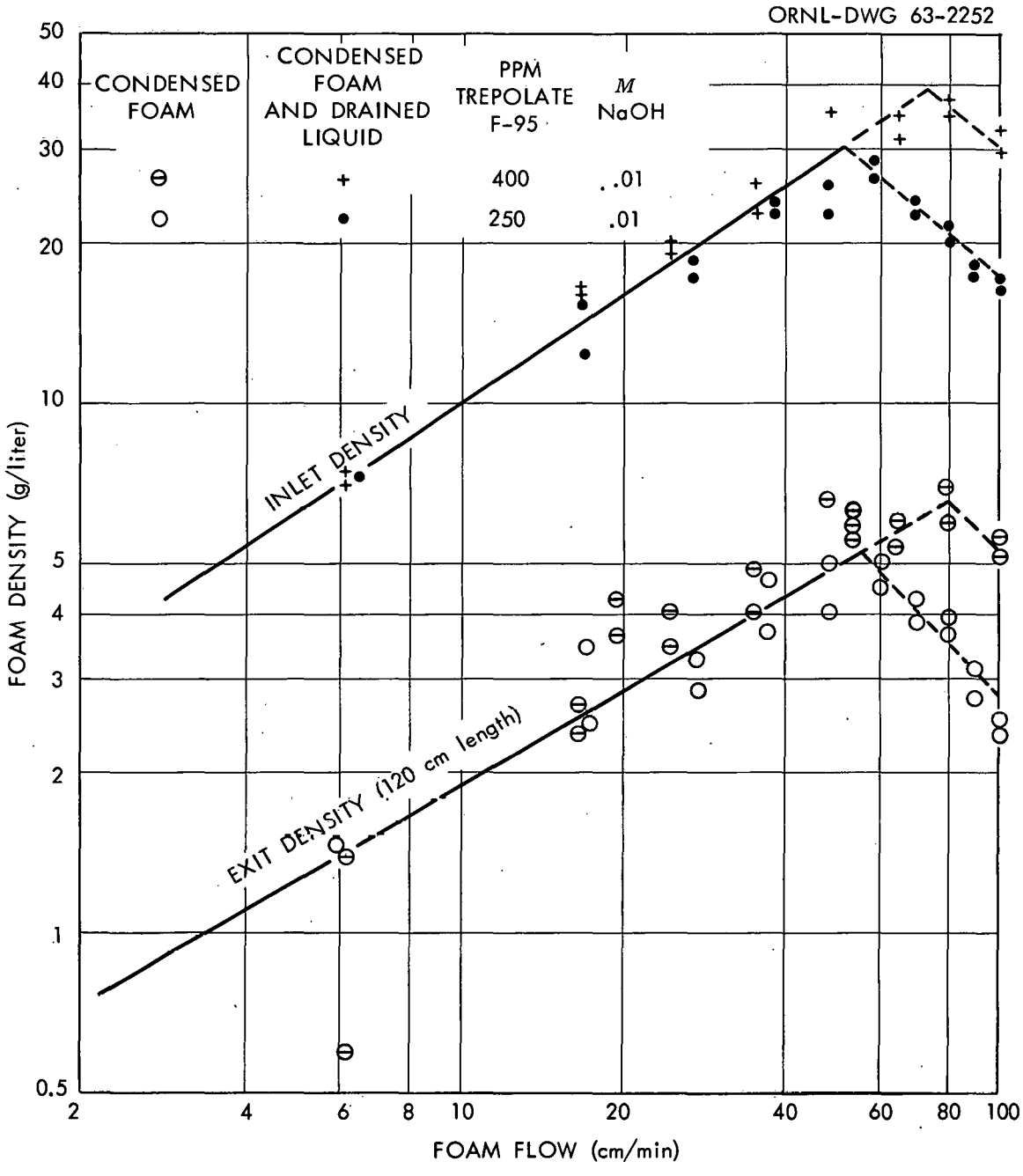

Figure 7. Foam Densities in a Horizontal Drainage Section for an Extra-Coarse Fritted Glass Gas Sparger.

drainage section.

The foam densities entering and leaving the horizontal drainage section may be used to check foam drainage models using Equation 61:

$$\frac{1}{\bar{\epsilon}} - \frac{1}{\bar{\epsilon}_o} = \frac{4}{\ell}\left(\frac{\rho g}{32\mu}\right)\frac{4}{\pi n k^2}(t - t_o) \quad . \tag{61}$$

For the previously used values of n, k, ρ, and μ, this becomes:

$$\left(\frac{1}{\bar{\epsilon}} - \frac{1}{\bar{\epsilon}_o}\right)\frac{\ell}{d^2(t - t_o)} = 2800 \quad . \tag{107}$$

The experimental results show good agreement in that the values of $(\ell/td^2)(1/\bar{\epsilon} - 1/\bar{\epsilon}_o)$ were mostly 1900 to 3500 as compared to about 2800 predicted from Equation 107 (Table VI).

This model indicates several results of importance to applications of horizontal foam drainage. The wetness of the foam entering such a drainage section is of small importance for good drainage since $1/\epsilon_o$ becomes of little significance when $\epsilon_o \gg \epsilon$. The total time in the horizontal drainage section is controlling, while the foam velocity, which is the controlling variable in a vertical drainage section, does not appear directly. Since the surface area per cubic centimeter of foam is proportional to $1/d$, the amount of liquid per square centimeter of area is given by:

$$\frac{\epsilon}{a} \propto \frac{d}{d^2 t} = \frac{1}{dt} \quad . \tag{108}$$

For a specified constant area rate, the volume rate is proportional to d, or the time in the drainage section is proportional to $1/d$. Thus the grams of liquid per square centimeter of surface is a constant

TABLE VI

A TEST OF A DRAINAGE MODEL FOR HORIZONTALLY FLOWING FOAM

Solution: DBS as 250- to 400-ppm Trepolate F-95, 0.002 or 0.01 N NaOH in demineralized water.

Drainage section: 120- or 140-cm length of 6-in.-ID glass, ℓ = 12 cm assumed, pipe at 1° slope to liquid removal port.

Bubble Diameter d (cm)	Time $t - t_o$ (sec)	$\bar{\epsilon}_o$ (cc/cc)	$\bar{\epsilon}$ (cc/cc)	$\frac{\ell}{td^2}\left[\frac{1}{\bar{\epsilon}_o} - \frac{1}{\bar{\epsilon}_o}\right]$ (cm·sec)
0.054	1200	0.007	0.0014	1920.
0.056	720	0.010	0.0019	2260.
0.063	360	0.016	0.0029	2340.
0.076	180	0.026	0.0043	2240.
0.086	131	0.032	0.0052	2000.
0.117	72	0.018	0.0029	3500.
0.095	370	0.007[a]	0.0012	2500.
0.150	150	0.009[a]	0.0006[b]	5500.
0.150	150	0.009[a]	0.0011[c]	2000.[c]
0.050	380	0.03[a]	0.0044	2450.
0.077	170	0.03[a]	0.0045	2250.
0.077	170	0.03[a]	0.0053[c]	1850.[c]

[a] Estimated values.

[b] Accuracy of measurement poor for this very dry foam.

[c] These results for a slope of about 4° toward exit; i.e., 3-in. rise in 48 in.

independent of bubble diameter for a given horizontal drainage section volume and given surface area flow rate.

V-4 Drainage with Vertical Foam Flow

The experimental data collected for the vertical flow of foam in the drainage section are in the form of exit densities, with the foam velocity as the principal independent variable. The drainage times, bubble sizes, and solution concentrations were also varied over limited ranges. These data are compared with the drainage model result, assuming that the Plateau borders approach the equilibrium size given by:

$$v = \frac{\rho g}{32\mu} \delta^2(\ell) \quad . \tag{109}$$

The equation for the exit foam density from this model is:

$$\epsilon_p = 3.2 \times 10^{-4} \frac{v}{d^2} \quad . \tag{80}$$

A more accurate approximation for very low foam velocities would be a simplification of Equation 67 to give:

$$\epsilon_p = a\tau_{eq} + 3.2 \times 10^{-4} \frac{v}{d^2} \quad . \tag{110}$$

The foam densities measured during HTU_x determinations or during foam breaker tests are plotted, along with curves from the above equation (Figures 8, 9, 10, 11). Since the bubble sizes for all the spargers become proportional to the square root of the gas flow rate at high gas flow rates, all the curves calculated from the equation level off to constant foam densities. The trends of the experimental points appear to agree reasonably well with the calculated curves.

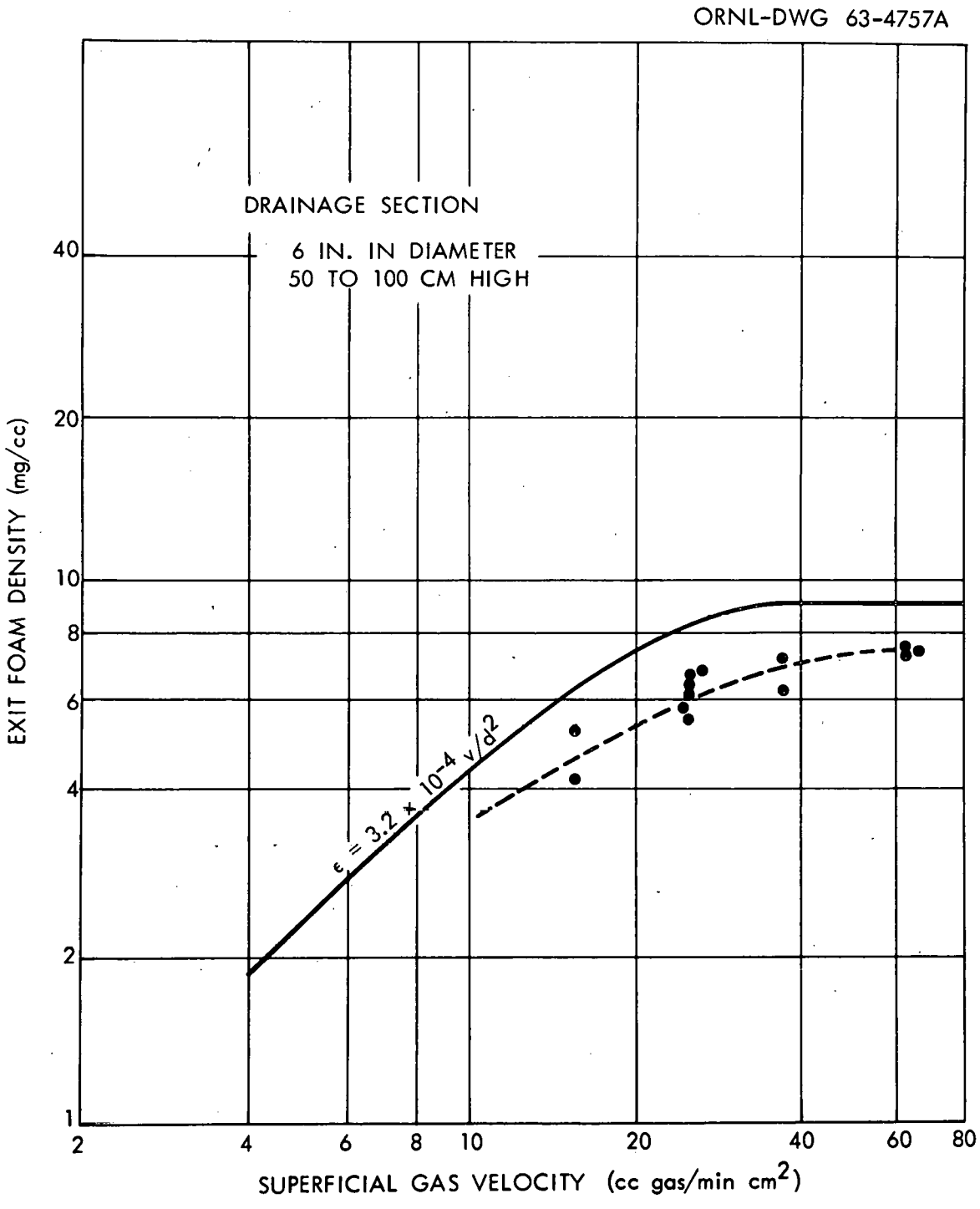

Figure 8. Foam Densities for 275-ppm Concentration of Trepolate F-95 and Spinneret Gas Sparger with 80-μ-diam Holes.

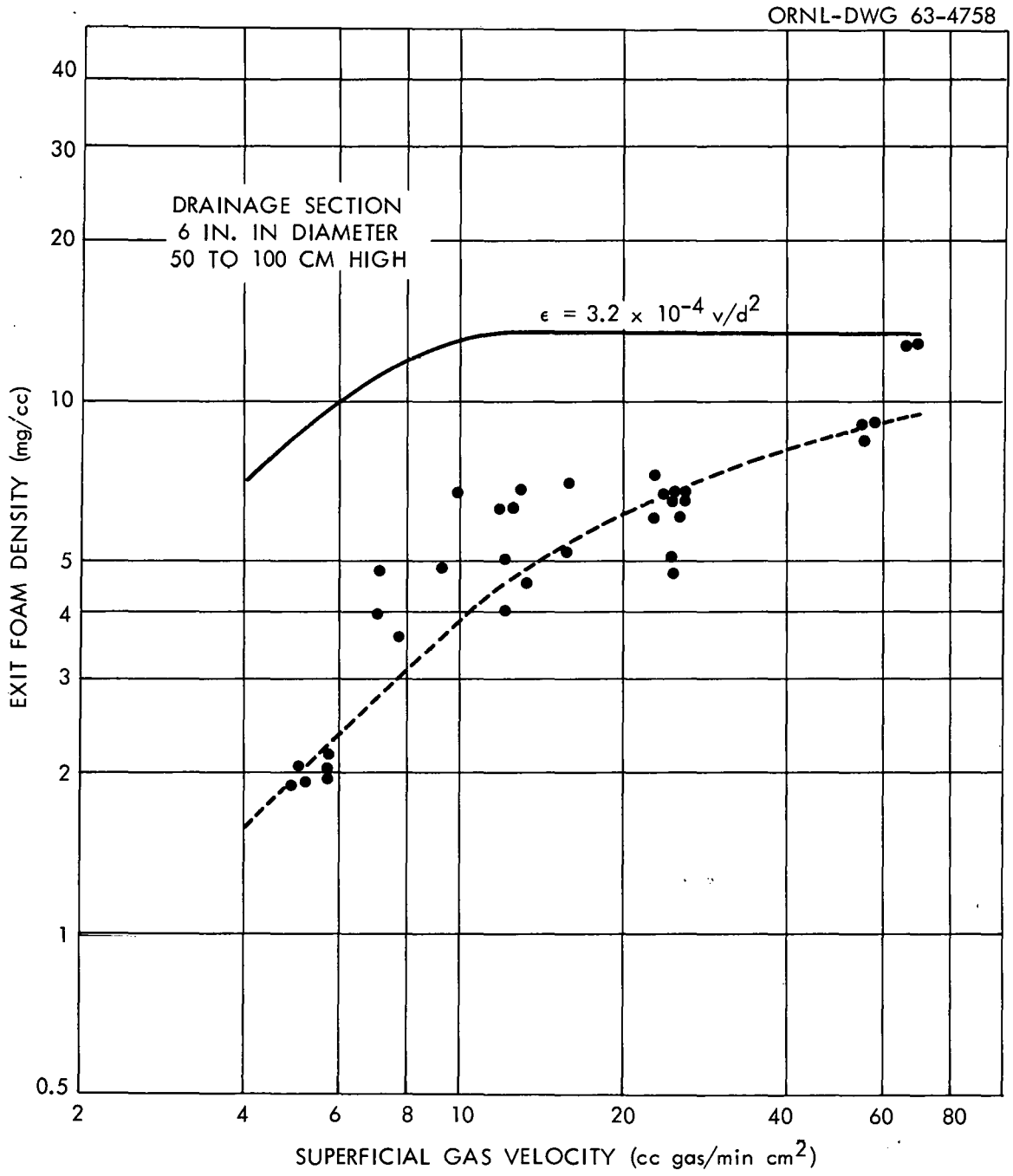

Figure 9. Foam Densities for 275-ppm Concentration of Trepolate F-95 and Spinneret Gas Sparger with 50-μ-diam Holes.

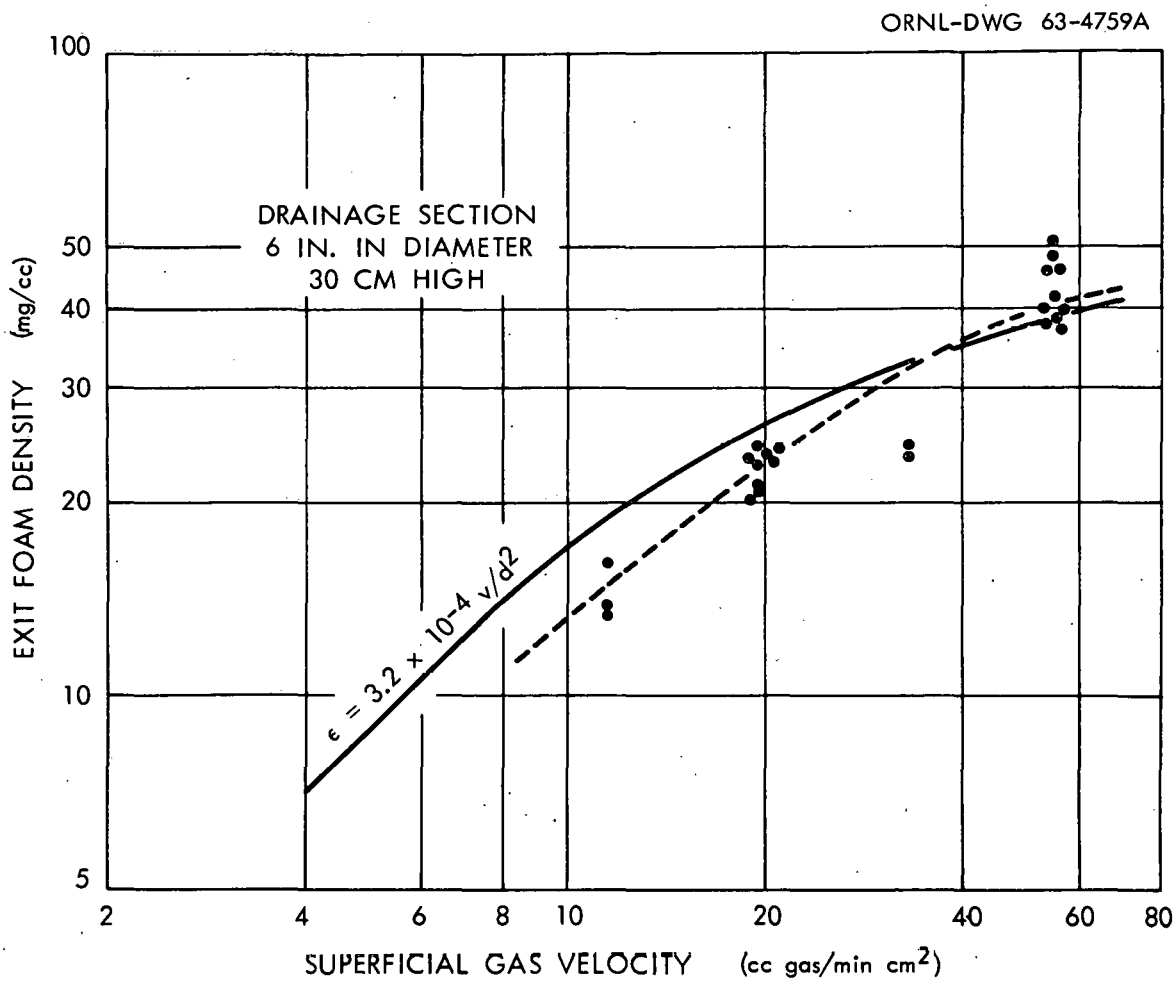

Figure 10. Foam Densities for 250-ppm Concentration of Trepolate F-95 and Extra-Coarse Porosity Fritted Glass Disk Gas Sparger.

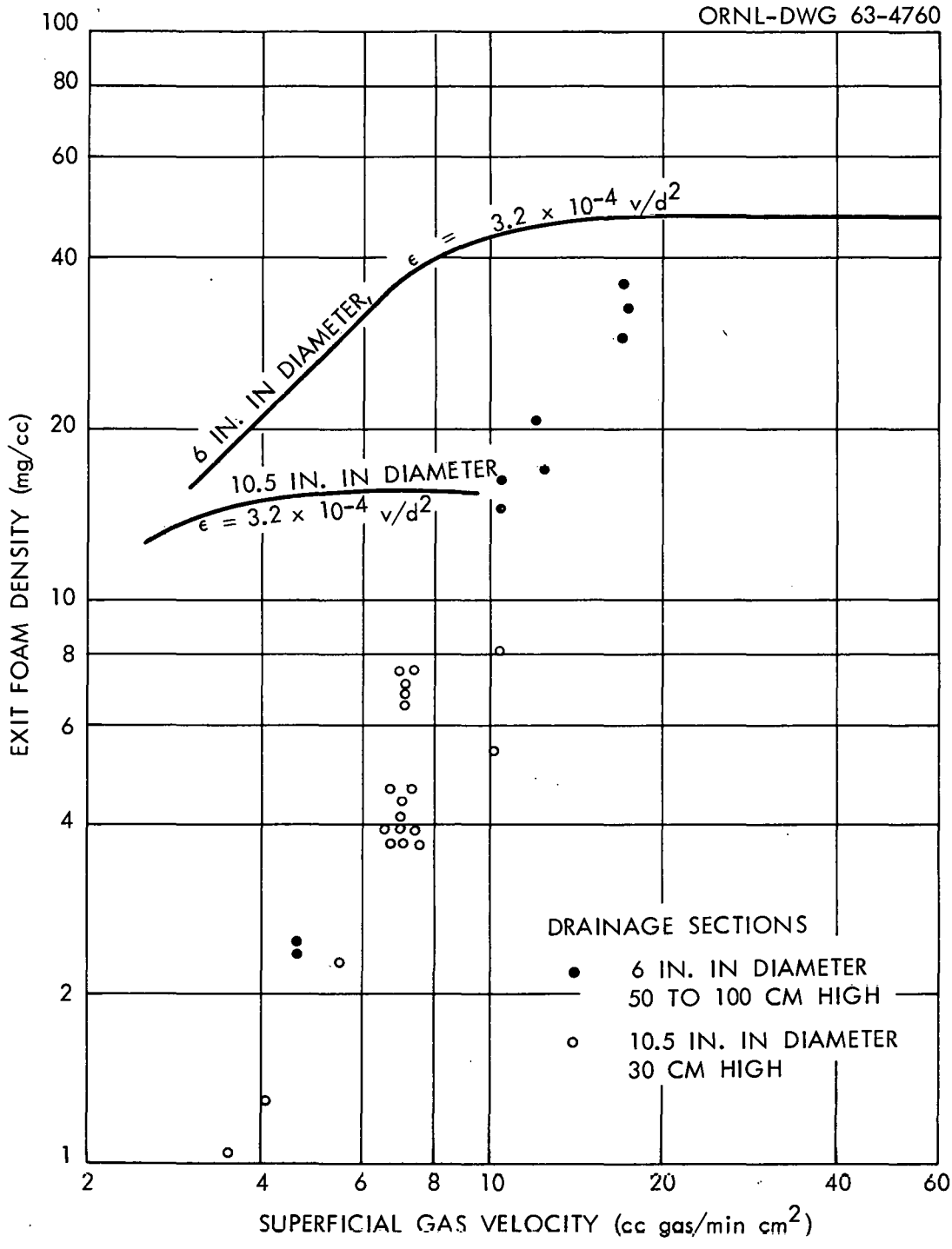

Figure 11. Foam Densities for 275-ppm Concentration of Trepolate F-95 and Extra-Coarse Porosity Fritted Glass Cylinder Gas Spargers.

The experimental values are as low as one-tenth of the calculated values; the differences show a consistent pattern. As the foams drain, collapse of individual bubbles and loss of Plateau borders occurs. The spinneret sparger with 80-μ-diam holes gave the most uniform and stable bubbles, and the experimental values for this sparger are about eight-tenths the calculated values (Figure 8). The spinneret with 50-μ-diam holes gave less uniform bubbles. The experimental points were about half the calculated values at high gas flow rates, but decreased to about two-tenths the calculated values at low gas flow rates (Figure 9). Data were obtained for a wider range of flow rates (5 to 67 cm/min) for this spinneret than for the spinneret with 80-μ-diam holes (15 to 65 cm/min). Foam densities for the extra-coarse-porosity fritted glass disk used for centrifugal foam breaker tests were about two-thirds the calculated values (Figure 10). Because of the relatively short residue times in this short drainage section (1/2 to 3 min compared with 1 to 10 min for the previous two spargers), drainage was less complete. The assumption of a capillary liquid velocity equal to the foam velocity at the exit may have been a poor approximation, particularly at the highest flow rate. The results for the extra coarse porosity fritted glass cylinders (Figure 11) show the effects of extensive bubble collapse. The experimental foam densities were two-thirds the calculated densities at the highest flow rate, which represented about 4 min in the drainage section. At the lower flow rates, which resulted in 6 to 15 min in the drainage section, extensive bubble collapse was observed visually and resulted in experimental foam

densities of a fifth to a tenth of the calculated values. This decreased bubble stability, compared with stability of bubbles produced by the spinnerets, appears to be due to the less uniform foam bubble size. Since greatly simplified concepts were used to estimate $n = 2.5/d^2$ and $k_2 = 1.5$, the experimental agreement appears acceptable. Because of the foam collapse which occurs at very low foam flow rates and the difficulties for measuring condensed foam rates below 1 cc/min, it was not practical to obtain data for which the $a\tau_{eq}$ term of Equation 10 would be controlling.

Foam condensation during drainage is shown by a plot of the surfactant rate in the foam surface versus the surface area generated (Figure 12). The surfactant rate is the concentration times the weight of the condensed foam and the surface area rate was that entering the drainage section. If there were no condensation, the points would give a single straight line whose slope would be the surface concentration, Γ, in equilibrium with the 275 ppm liquid concentration. Actually spinneret B gives the highest values, spinneret A somewhat lower values, and the extra-coarse-porosity glass gives much lower values in agreement with the foam stability effects previously described. The correct value of Γ/c for the surfactant would probably be given by a line through the higher points. A value of $\Gamma = 2.3 \cdot 10^{-10}$ mole/cm or $\Gamma/c = 3.3 \cdot 10^{-4}$ cm was reported from laboratory measurements (29).

Some of the initial foam density data collected during tests of a cyclone foam breaker illustrate the difficulty of obtaining reproducible data. Variations in the foam densities with the linear foam

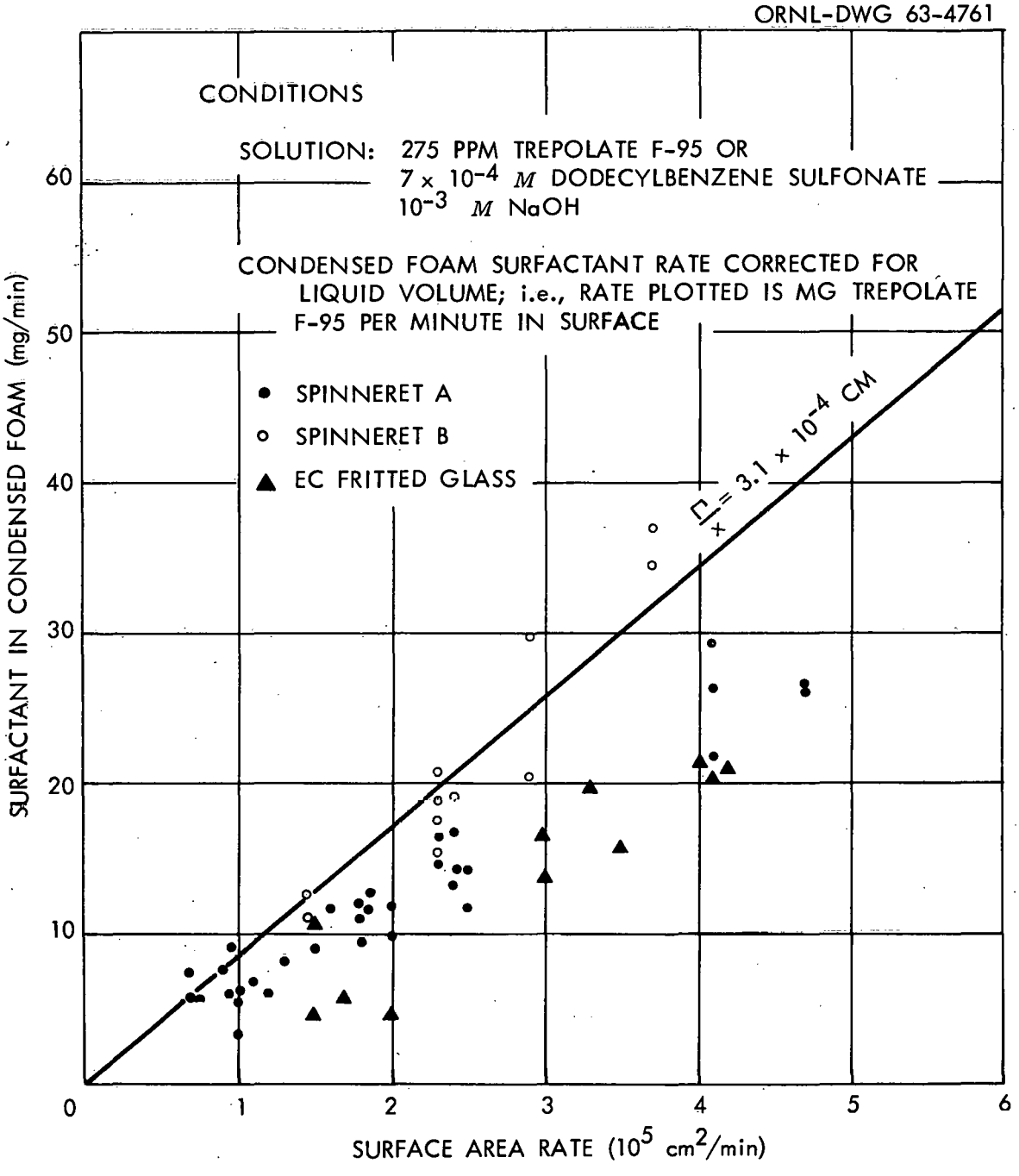

Figure 12. Surfactant in Surface vs Surface Area Rates for Continuous Runs.

rate during drainage, the pH, and the surfactant concentrations were expected, but the immediate previous history of the solution was an unexpectedly important variable. While reproducible foam densities were obtained after foaming and return of the condensed foam had continued for long periods, the initial foam densities with new solution or for solution that had stood overnight were as much as six times greater than the reproducible steady-state values (Figure 13). The results in Table VII and the points for less than 0.4 hr in Figure 13 illustrate the type of behavior observed. The porous metal spargers gave the least uniform foam bubble sizes of any of the spargers tested, and all the data shown (Figure 13) are probably affected by foam collapse. The bubble-size-versus-gas-flow curve was not determined for the porous metal spargers. The bubble size at low gas flow and the drainage conditions were almost identical to those for the extra coarse fritted glass disk (Figure 11), but the steady-state experimental foam densities were a half to a quarter of those for the fritted glass.

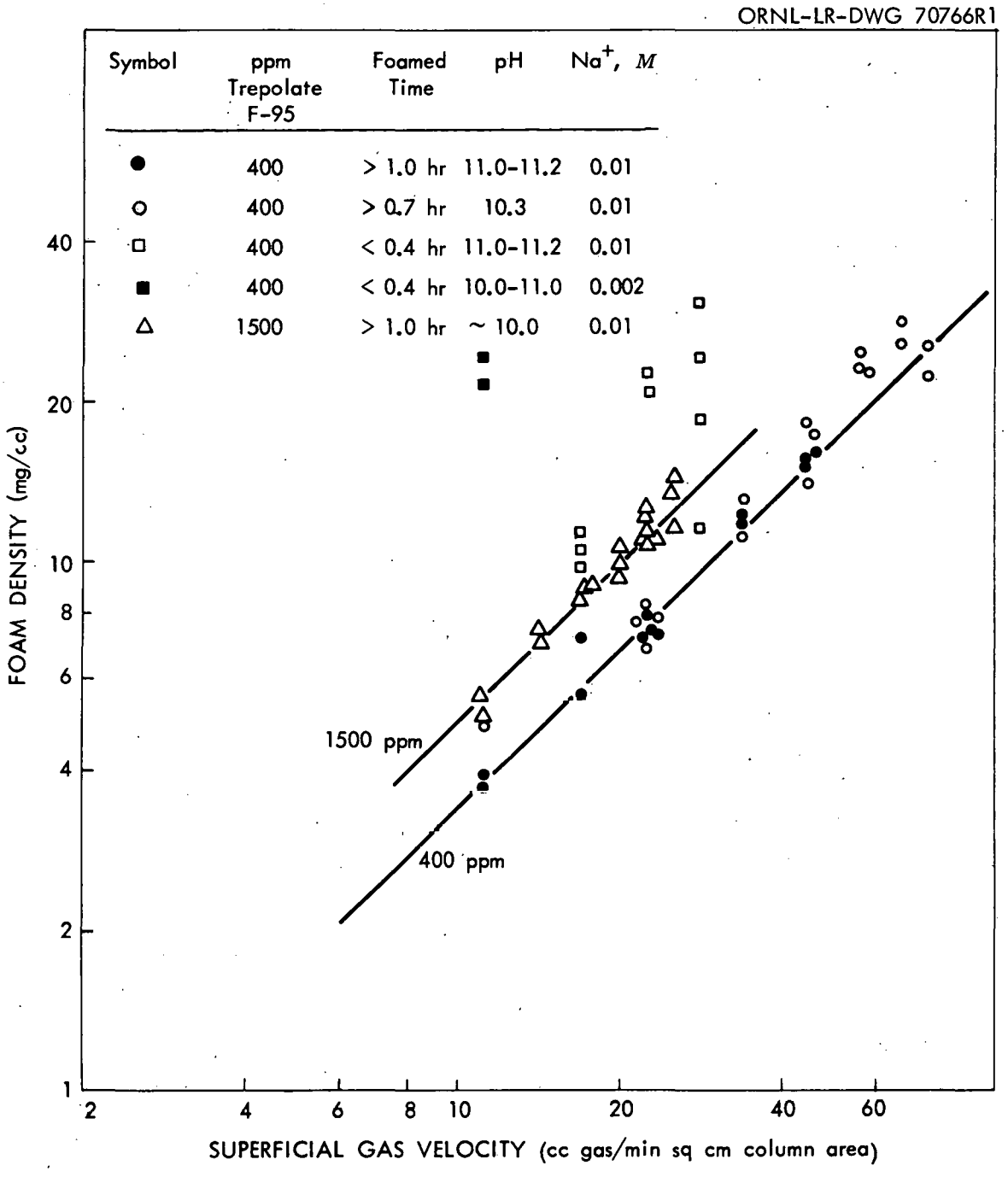

Figure 13. Foam Densities for a Dodecylbenzenesulfonate Surfactant, Bubbles of about 0.6 mm in Diameter.

TABLE VII

FOAM DENSITIES FOR A DODECYLBENZENESULFONATE SURFACTANT

Conditions: Trepolate F-95 surfactant, about 0.01 N Na^+ and pH of 10-11; gas rate of 4000 cc/min, or 221 cm/sec superficial velocity, porous stainless steel spargers.

Accumulated Time (min)	Foam Density (mg/cc) or Remarks for 400 ppm Trepolate F-95 Solution[a]	Foam Density (mg/cc) or Remarks for 1500 ppm Trepolate F-95 Solution[b]
0	Foam gas started	Foam gas started
6-15	23	22,21
65	8.6	--
165-180	--	10.9, 10.9, 12.1
190-200	7.7	11.4, 10.6, 12.4
205	--	Foam gas shut off
245	--	Foam gas started
249-254	--	21.2, 19.8, 23.0
267-270	--	19.8, 16.8, 15.3
290-305	7.3	12.5, 12.5, 12.0
400	7.3	
410	Foam gas shut off	--
1515	Foam gas started	--
1523	21.7	--
1580	8.2	--
1665	6.8	--
1685	Foam gas shut off	--
1700	Foam gas started	--
1708	9.3	--

[a]The 400-ppm solution was not foamed previously.

[b]The 1500-ppm solution was used the previous day and stood overnight.

CHAPTER VI

EXPERIMENTAL DEVELOPMENT OF FOAM SEPARATION EQUIPMENT

The foam separation columns required operations not common to chemical engineering equipment. The requirements included the generation of a uniform and stable foam, the continuous, countercurrent contacting of foam with a liquid, and foam drainage and condensation. The experimental measurements and the development of equipment for these operations are described in this section. The performance of gas spargers, liquid feed distributors, and foam breakers were measured. Measurements of countercurrent foam-liquid flow and foam drainage were compared with proposed models in Chapter V.

VI-1 Gas Spargers and Surface Area Measurements

The ability of gas spargers to give controlled distributions of foam bubble sizes was important to two distinct problems for this study. One problem was to obtain a stable and uniform foam in order to avoid channeling in the countercurrent region and to avoid excessive condensation in the drainage section. The other problem was to convert gas rate measurements into foam surface rate measurements. Foams from three types of spargers (Figures 14, 15, 16) and from two or three hole sizes or porosities for each type were first observed visually and then considered for foam column use (Table VIII). The two spinnerets and the extra-coarse porosity of fritted glass were the only ones used extensively. Accordingly, procedures for measuring surface area rates were developed and applied to these three spargers.

ORNL-PHOTO 56712

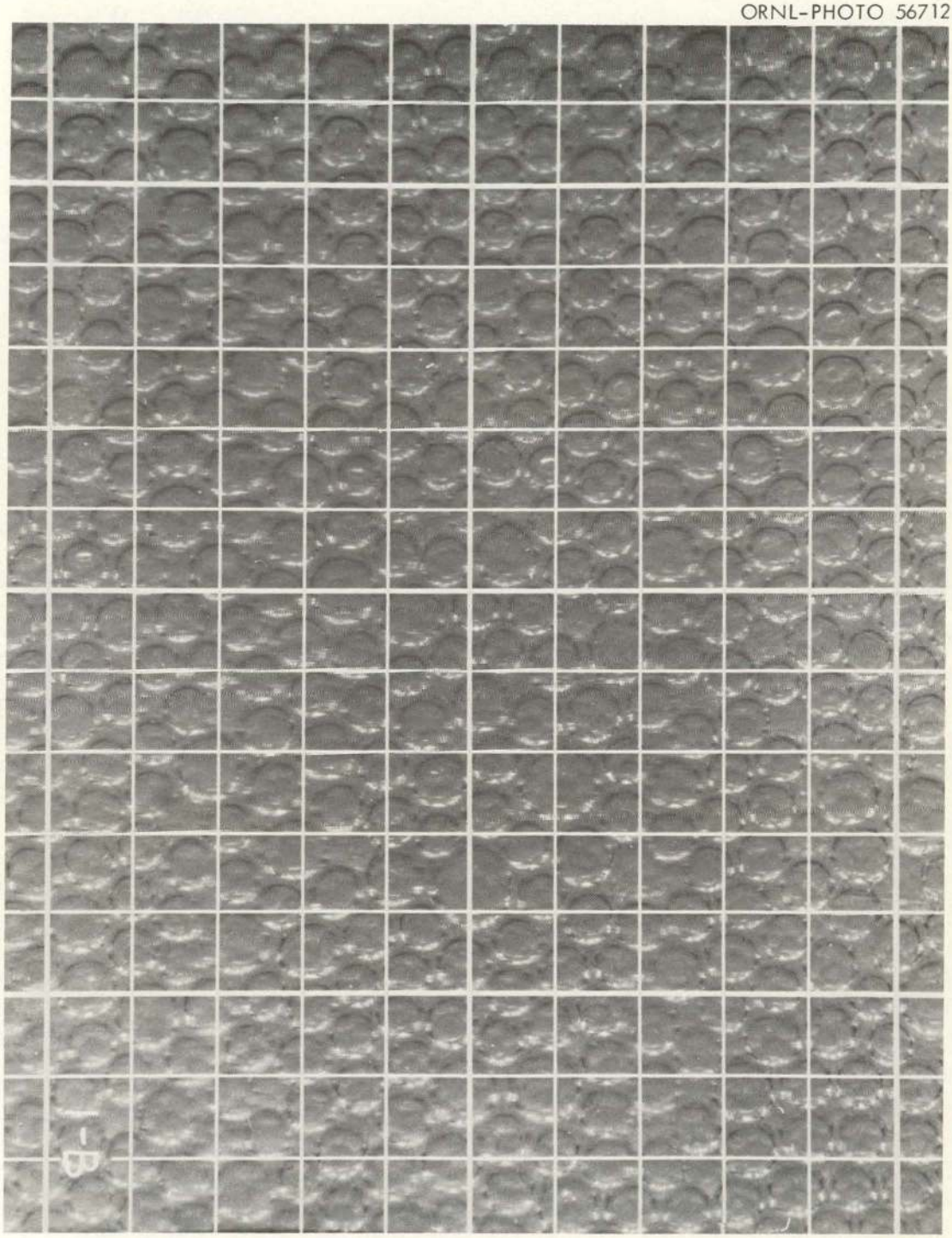

Figure 14. Foam from N_2 through 50-μ-diam Holes of Spinneret into 275-ppm Trepolate F-95 in 10^{-3} M NaOH; 1-mm Grid.

ORNL-PHOTO 58385

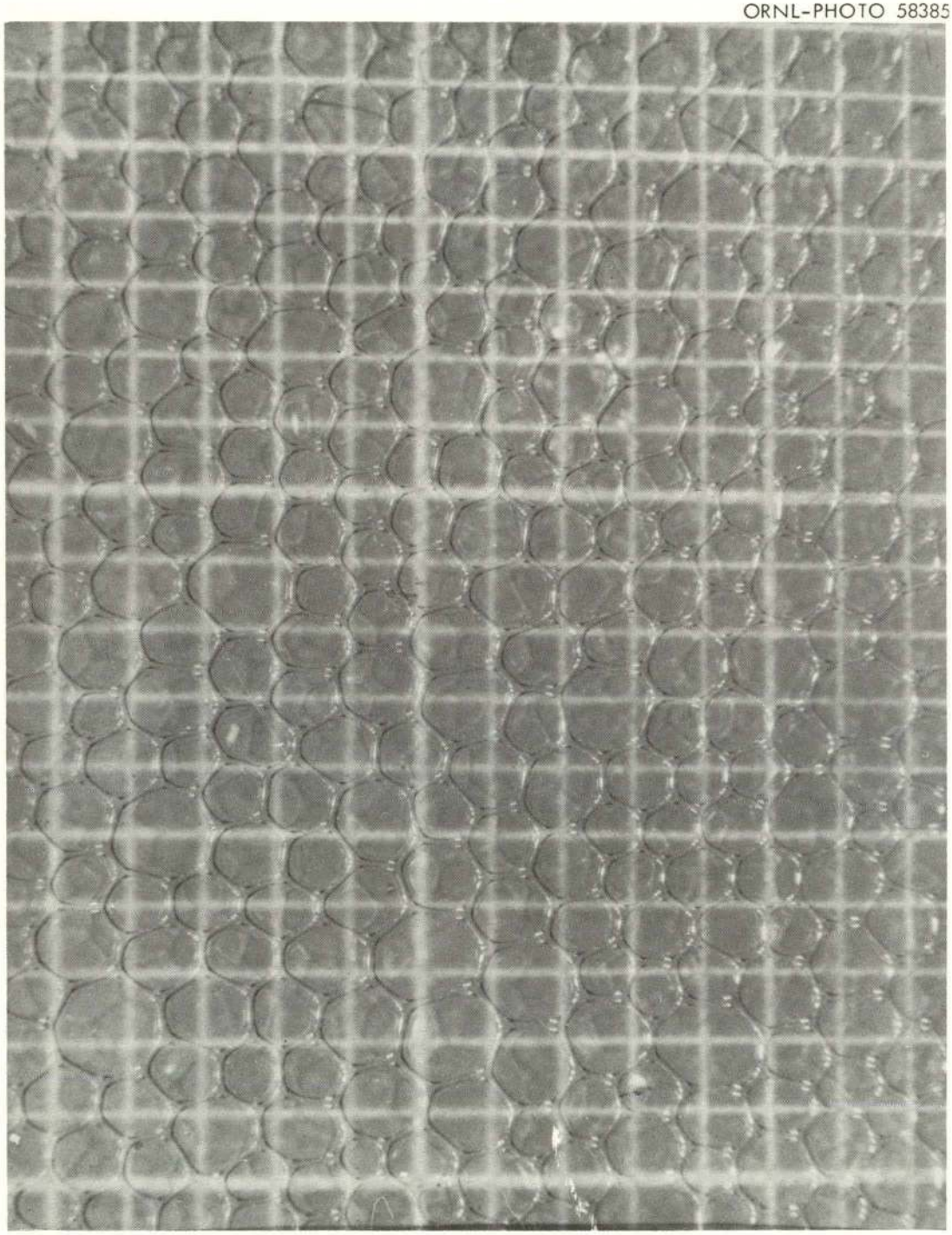

Figure 15. Foam from N_2 through 80-μ-diam Holes of Spinneret into 275-ppm Trepolate F-95 in 10^{-3} M NaOH, 1-mm Grid.

ORNL-PHOTO 56713

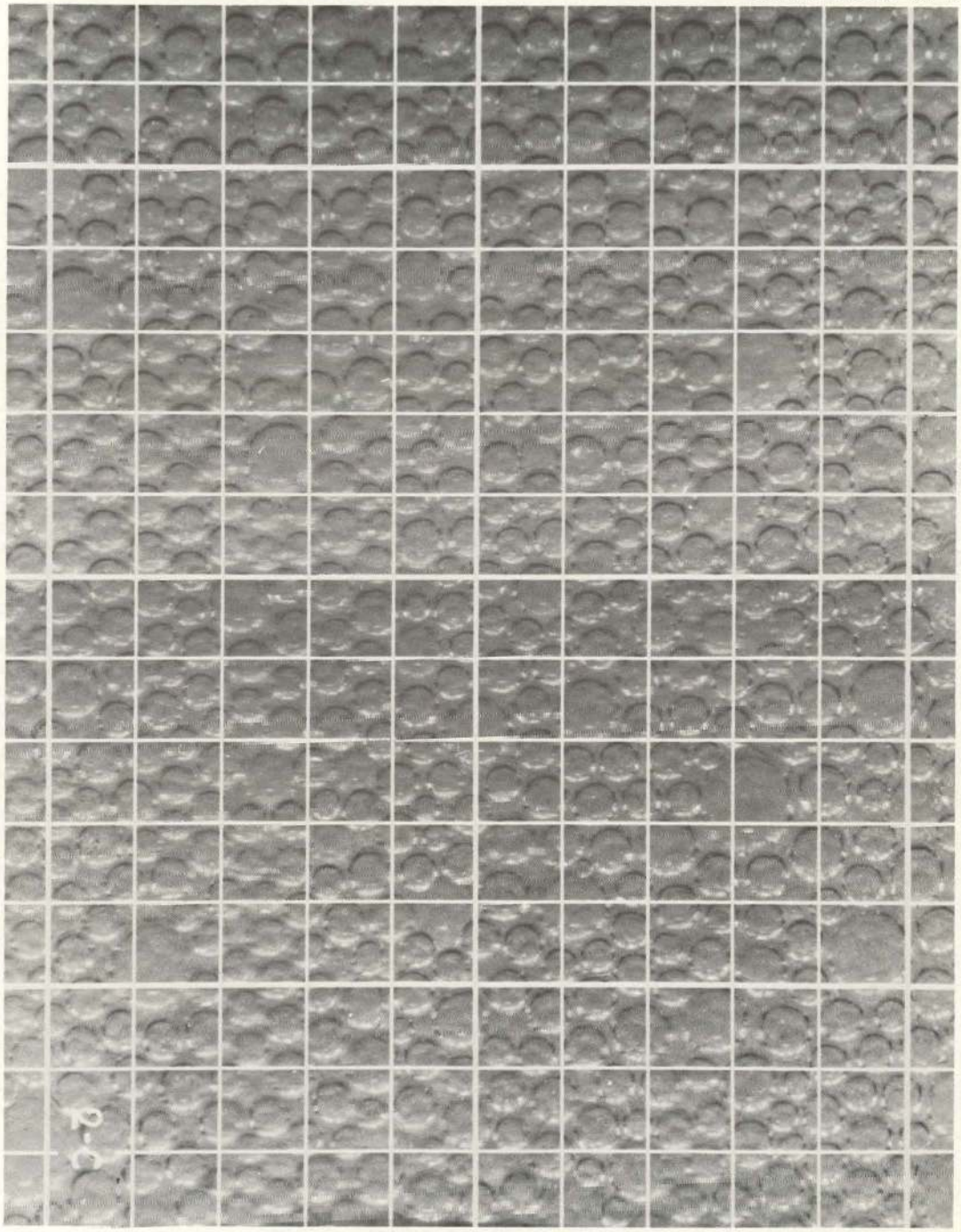

Figure 16. Foam from N_2 through Extra-Coarse Sintered Glass Gas Spargers into 275-ppm Trepolate F-95 in 10^{-3} M NaOH; 1-mm Grid.

TABLE VIII

QUANTITATIVE EXAMINATIONS OF GAS SPARGERS

Type	Hole Size-Manufacturer's Rating (μ)	Manufacturer	Bubble diam (cm)[a]	Remarks
Spinneret[b]	50	J. Bishop & Co.	0.055	Uniform bubbles; holes of uniform size but not regular in shape
Spinneret[b]	80	J. Bishop & Co.	0.11	Very uniform bubbles; circular holes
Fritted glass[b,c]	EC porosity (200, max)	Corning Glass Works	0.032	Uniformity intermediate to those of spinnerets and porous stainless steel
Fritted glass[c]	C porosity	Corning Glass Works	-	Less uniform than EC porosity Bubbles excessively small
Porous stainless steel	D porosity (65)	Micro Metallic	0.06	Much less uniform than either spinnerets or fritted glass; therefore, poor foam stability
	E porosity (35)	Micro Metallic	-	Least stable foam of any spargers tested: less uniform than D porosity and excessively small bubbles
	F porosity (20)	Micro Metallic		Same as E porosity

[a]Mean diameter at low gas rates.

[b]These three spargers used for nearly all of the experimental studies.

[c]These were standard 12-mm-OD fritted cylinders; plate of the same porosity appeared to give larger bubble diameters.

Quantitative Differences Between Spargers

All the gas spargers used for foam generation were of standard commercial fabrication. The spinnerets were of the construction used by the rayon industry with 50- or 80-μ-diam holes in a cup of gold-platinum alloy (about 70% Au--30% Pt). The holes were spaced with a uniform pitch from row to row and from hole to hole in a row diameter of of 0.039 in. This was an approximation to a triangular spacing with a 1-mm pitch. The spinnerets were about 2 in. in diameter, with 1794 or 1800 holes. The extra-coarse-porosity glass was used as three gas dispersion tubes, Corning No. 39533 in the 6-in.-diam column. Other items with flat disks of extra-coarse porosity were used in a 24-in.-diam column or in other experimental tests. The porous stainless steel spargers were bought as standard 1-in.- or 2-1/8-in.-diam gas spargers from the Micro Metallic Corporation. The E and F grades of porous stainless steel gave the least stable foam of any of the spargers tested, with initial formation of many small bubbles and a few large bubbles. Large voids quickly appeared in the foam from these spargers. The D porosity gave larger and more uniform bubbles than the E and F porosities, and more stable foams. The D porosity was used for some initial experimental runs. The spinnerets gave the most uniform and most stable foams. The 50-μ spinneret hole is about the minimum hole diameter normally available. Since there were no obvious advantages of larger bubble sizes, the holes of 80-μ diameter in a second spinneret were the largest tested. The foam from fritted glass was more uniform than that from porous stainless steel. Only the extra-coarse porosity

was used since the coarse generated a less stable foam of smaller and less uniform bubble size. None of the three spargers is a best first choice for all applications. The uniform and stable foam of easily measured surface area from the spinnerets made them the most suitable type for engineering studies. The glass spargers are convenient and cheap to assemble into laboratory-scale equipment, and they give a large surface area per unit volume if the exact area or maximum foam stability are not of major importance. The spinnerets are expensive (about 5¢ per hole for fabrication and 5¢ per hole material costs, which can be recovered) and are more affected by plugging since the number of holes is much smaller than for the porous glass or metal. The glass is fragile and difficult to seal into metal systems. The porous metal would probably be preferred for large-scale radioactive systems if the uniformity of the pore size can be improved. The pressure drops for the useful ranges of flow rates for the spargers were due more to the capillary pressure of water for the small holes than to the frictional pressure drops. A pressure-drop curve for the spinneret with 50-μ-diam holes is given in Chapter VII (Figure 26).

Bubble Size Distributions. A mathematical model for the distribution of bubble sizes observed in photographs of the column wall would be very convenient for the description and correlation of these distributions. Such a model would also simplify calculations by allowing use of the parameters of the model. The numbers of bubbles within ranges of diameters were counted for areas of photographs showing from

40 to 340 bubbles for each photograph of interest. The mean diameter $\bar{d}$ and the variance s^2 were calculated from these measurements. The histograms from these observations showed bell shapes which indicated that they might be fitted by normal distributions (as well as other, more complicated distributions). The Chi-Square test (19) with a 95% significance level was used as a test of the fit of the normal distribution with mean $\bar{d}$ and variance s^2.

The results from use of the Chi-Square test show adequate representation of the photograph bubble diameter distribution by normal distributions of mean $\bar{d}$ and variance s^2 for the foams from spinneret gas spargers (Table IX). Tests for foams from extra-coarse fritted glass or sintered porous stainless steel spargers usually resulted in rejection of normal distributions for bubble diameters in these foams (Table IX).

A typical calculation is included as an example of the procedure (Table X). The compatibility of the observed frequencies and the normal distributions is measured by the quantity, χ^2, which is defined by:

$$\chi^2 = \sum_{i=1}^{k} \frac{(n_i - E_i)^2}{E_i} , \qquad (111)$$

where n_i is the observed frequency in the ith interval and E_i is the frequency expected for this interval for the distribution to be tested and sample size of $\sum_{i=1}^{k} n_i$. The Chi-Square test is a good approximation only when all $E_i \geq 5$ and $k \geq 5$. The required test criterion is obtained from tables for Chi-Square distributions using k - 2 degrees of freedom

TABLE IX

RESULTS FROM CHI-SQUARE TEST OF $N(d,\bar{d},s^2)$ AS THE SIZE DISTRIBUTIONS OF FOAM BUBBLE DIAMETERS

Gas Sparger		Gas Flow	Sample	$\bar{d}$	s		Test	Normal Distribution
Type	Description	(cc/min)	Size	(mm)	(mm)	χ^2	Criterion	Accepted
Spinneret	80-μ-diam holes	1,000	88	1.019	0.165	3.76	7.82	Yes
		5,000	67	1.229	0.287	8.40	9.49	Yes
		18,000	42	1.940	0.815	2.47	9.49	Yes
Spinneret	50-μ-diam holes	600	188	0.519	0.125	9.26	9.49	Yes
		800	224	0.540	0.074	6.62	9.49	Yes
		800	91	0.578	0.112	8.42	11.1	Yes
Fritted glass	Extra-coarse porosity	800	328	0.434	0.106	55.47	9.49	No
		800	78	0.436	0.135	15.22	7.81	No
Porous stainless steel	Porosity "D"	1,200	210	0.549	0.339	30.45	7.81	No
		3,000	77	0.705	0.309	7.10	7.81	Yes

TABLE X

APPLICATION OF THE CHI-SQUARE TEST TO PHOTOGRAPH BUBBLE DIAMETERS: AN EXAMPLE

Gas Sparger: extra-coarse sintered glass, 800 cc/min or about 30 cc/min·cm^2
Solution: 250 ppm Trepolage F-95, 10^{-3} M NaOH

Interval										
Lower Limit (mm)	Upper Limit (mm)	d_i Midpoint (mm)	Observed Frequency, n_i	$d_i n_i$	$d_i^2 n_i$	$\frac{UL-\bar{d}}{s}$	Area to $\frac{UL-\bar{d}}{s}$	Area in Interval	Expected Frequency E_i	$\frac{(n_i - E_i)^2}{E_i}$
$-\infty$	0.15	-	0	0	0	-2.68	0.004	0.041	13.5	11.58
0.15	0.25	0.20	1	0.20	0.04	-1.736	0.041			
0.25	0.35	0.30	50	15.00	4.50	-0.792	0.214	0.173	56.7	0.79
0.35	0.45	0.40	169	67.60	27.04	0.151	0.560	0.346	113.3	27.40
0.45	0.55	0.50	76	38.00	19.00	1.093	0.863	0.303	99.5	5.55
0.55	0.65	0.60	21	12.60	7.56	2.038	0.979	0.116	38.1	7.69
0.65	0.75	0.70	4	2.80	1.96	2.980	0.999			
0.75	0.85	0.80	4	3.20	2.56	3.93	1.000	0.021	6.89	2.46
0.85	0.95	0.90	1	0.90	0.81	4.87	1.000			
0.95	1.05	1.0	2	2.00	2.00	-				
1.05	∞	-	0	0	0	∞	1.000			
Total of column			328	142.3	65.47				328.0	55.47[a]
				$\bar{d}$ = 0.434						
				s = 0.106						

[a]For four degrees of freedom, 55.47 > 9.49; therefore normal distribution is rejected.

since $\bar{d}$ and s^2 were obtained from the same data. The normal distribution of mean $\bar{d}$ and variance s^2 is accepted with a 95% significance level if χ^2 is less than:

$$\begin{aligned} 7.82 &\text{ for } k = 5, \\ 9.49 &\text{ for } k = 6, \\ 11.07 &\text{ for } k = 7, \\ 12.59 &\text{ for } k = 8. \end{aligned}$$

Surface Area Rate Measurements. The foam surface areas could be accurately calculated for the case of uniform spherical bubbles from the diameters of the bubbles and the gas volume rates in the column. In practice, the gas rates are indicated by rotameters and the bubble diameters by photographs taken at the column wall. The simplest diameter measurement from photographs is the average diameter given by $D/\sqrt{n}$, where n is the number of bubbles visible in a circle of diameter D. The following sources of error were considered or corrected for as described.

1. Part of the foam volume is occupied by liquid.
2. The bubbles are deformed by the glass column wall.
3. The bubbles at the wall are not representative of the true bubble-size distributions.
4. The bubbles do not have a single uniform diameter.
5. The bubbles are polyhedrons instead of spheres.
6. The gas volume rates indicated by the rotameters require correction for the effects of gas density, temperature, pressure, humidity, etc.

The photographs show the cross sections of bubbles in a layer of

foam about one-bubble-diameter thick at the column wall. Even though the the liquid volume is a significant fraction of the foam volume for most countercurrent flow rates, the photographs show a complete layer of bubbles, with very little area not occupied by bubbles. The effect of two volume percent unoccupied area on the value of $D/\sqrt{n}$ is of small significance, compared with other errors. If the foam is photographed in the drainage section above the region of countercurrent flow, the liquid volume would be less than one percent of the column volume for normal column geometries and flow rates.

At high gas rates, the bubbles just above the interface are suspended as spheres in liquid. The most common diameters at these conditions are not distinguishably different from the most common diameters for bubbles of polyhedron shape which are not separated from the wall by liquid. Thus, the wall does not appear to distort the bubble shape enough to change the observed cross section.

While nonrepresentative distributions may be observed visually during operation with channeling or at high flow rates, they are not visible when the column is operating efficiently. Channeling of liquid results in large variations in linear foam velocities and increased foam condensation at particular locations. Areas of abnormal appearance were avoided when photographs for determining surface areas were taken. When the column is operated efficiently, as indicated by no visible channeling, uniform bubble diameters, and low HTU_x values, the visible bubble-size distribution is approximately the same at all parts of the 6-in.-ID column wall. If the bubble-size distributions at the

column wall are not representative of the interior of the column, variations with axial position up and down the column would probably occur. However, an independent verification that the bubbles at the wall are representative of the interior does appear desirable. Studies of the structure of foams using a quick freeze technique have been reported. Bubble sizes and bubble size distribution of the outer surface of a foam mass and those within the foam mass were almost the same; the occasional small differences were not statistically significant (13).

For a single bubble of diameter d, the surface area, volume, and surface area per unit volume are given by:

$$\text{surface area} = \pi d^2 ,$$

$$\text{volume} = \frac{\pi}{6} d^3 ,$$

$$\text{area/volume} = \frac{\pi d^2}{(\pi/6)d^3} = \frac{6}{d} .$$

For a sample of n bubbles of diameters d_i, i=1, 2 ... n, several "average" diameters may be defined by:

$$\text{mean diameter} = \bar{d} = \frac{1}{n} \sum_{i=1}^{n} d_i , \qquad (112)$$

$$\text{total surface area} = n\pi \bar{d}_A^{\,2} = \sum_{i=1}^{n} \pi d_i^{\,2} , \qquad (113)$$

$$\text{total volume} = n\frac{\pi}{6} \bar{d}_V^{\,3} = \sum_{i=1}^{n} \frac{\pi}{6} d_i^{\,3} , \qquad (114)$$

$$\text{area/volume} = \frac{6}{d_s} = \frac{\sum_{i=1}^{n} \pi d_i^2}{\sum_{i=1}^{n} \frac{\pi}{6} d_i^3} = 6 \frac{\sum_{i=1}^{n} d_i^2}{\sum_{i=1}^{n} d_i^3} . \tag{115}$$

The values of $\bar{d}$, d_A, d_V, and d_s will differ from each other and from the $D/\sqrt{n}$ from the photographs with the diffences dependent on the diameter size distribution of the foam. Relationships between these diameters may be obtained if a mathematical expression for the size distribution is available. In the previous section of this report, the distribution of bubble diameters was shown to be adequately represented by normal distributions of mean $\bar{d}$ and variance s^2 for foams generated by use of spinnerets as gas spargers. Expression for d_A, d_V, and d_s in terms of $\bar{d}$ and s^2 are easily derived for normal distributions. The relationship between $\bar{d}$, d_A, or d_s and $D/\sqrt{n}$ will be considered separately.

These average diameters for a normal distribution of mean $\bar{d}$ and variance s^2 are most conveniently obtained by the use of the moment-generating function as follows:

$$M_d(t) = \exp\left[\bar{d}t + \frac{s^2t^2}{2}\right] , \tag{116}$$

$$\bar{d} = M_d'(0) , \tag{117}$$

$$\pi d_A^2 = \pi M_d''(0) = \pi(\bar{d}^2 + s^2) , \tag{118}$$

$$\frac{\pi}{6} d_V^3 = \frac{\pi}{6} M_d'''(0) = \frac{\pi}{6} (\bar{d}^3 + 3\bar{d}s^2) , \tag{119}$$

$$\frac{6}{d_s} = \pi d_A^2 / \frac{\pi}{6} d_V^3 = 6 \left(\frac{\bar{d}^2 + s^2}{\bar{d}^3 + 3\bar{d}s^2} \right) = \frac{6}{\bar{d}\left[1 + \frac{2s^2}{\bar{d}^2 + s^2}\right]} \quad . \qquad (120)$$

These results may be rearranged to give:

$$\frac{d_A}{\bar{d}} = \left[1 + \frac{s^2}{\bar{d}^2}\right]^{1/2}, \qquad (121)$$

$$\frac{d_V}{\bar{d}} = \left[1 + \frac{3s^2}{\bar{d}^2}\right]^{1/3}, \qquad (122)$$

$$\frac{d_s}{\bar{d}} = 1 + \frac{2s^2}{\bar{d}^2 + s^2} \quad . \qquad (123)$$

Use of values of $\bar{d}$ and s^2 for the bubbles shown by photographs (Figures 14, 15, 16) gives values of $d_s/\bar{d}$ from 1.04 to 1.30 for the spinnerets (Table XI). The values using $\bar{d}$ and s^2 for foams from the fritted glass and porous metal are listed although the normal curves with these parameters are not acceptable fits for these foams. The expression for $d_A/\bar{d}$ is exact for any distribution. However, $d_V/\bar{d}$ and $d_s/\bar{d}$ are exact only for normal distributions (for the spinnerets) and should be considered estimates of unproven validity for the other gas spargers.

The average diameter given by $D/\sqrt{n}$ may differ from $\bar{d}$ because $D/\sqrt{n}$ represents a cross section area average, spherical bubbles would leave voids between bubbles, or because the surface layer of bubbles were not representative of the bubble population. Both the surface area and cross section area of a sphere are proportional to d^2; therefore, the values of $d_A/\bar{d}$ in Table XI show the effect of bubble-size

TABLE XI

AVERAGE DIAMETERS OF FOAM BUBBLES

Gas Sparger		Gas Flow	$\bar{d}$	s			
Type	Description	(cc/min)	(mm)	(mm)	$d_A/\bar{d}$	$d_V/\bar{d}$	$d_s/\bar{d}$
Spinneret	80-μ-diam holes	1,000	1.019	0.165	1.013	1.025	1.051
		5,000	1.229	0.287	1.027	1.052	1.10
		18,000	1.940	0.815	1.08	1.15	1.30
Spinneret	50-μ-diam holes	600	0.519	0.125	1.029	1.055	1.11
		800	0.540	0.074	1.009	1.019	1.037
		800	0.578	0.112	1.018	1.036	1.072
Fritted glass	Extra-coarse porosity	800	0.434	0.106	1.030	1.057	1.11
		800	0.436	0.135	1.050	1.09	1.18
Porous stainless steel	Porosity "D"	1,200	0.549	0.339	1.18	1.29	1.55
		3,000	0.705	0.309	1.09	1.16	1.32

distributions on $\bar{d}$ versus $D/\sqrt{n}$. If the photograph showed uniform, close packed circles, the area within the circles would be 0.91 of the total area. For n such circles (or bubbles):

$$n\frac{\pi}{4} d^2 = 0.91 \frac{\pi}{4} D^2 ,$$

$$d = 0.955 \frac{D}{\sqrt{n}} .$$

Actually, the fitting together of large and small bubbles and only a small amount of distortion of bubbles can give the low liquid volumes in the foam reported for normal column operating conditions. As previously discussed, the bubble distribution is believed to be homogeneous throughout the column when the column is operating efficiently without channeling.

The surface-area-to-volume ratio of a sphere, which may be considered a regular polyhedron of infinite faces, is easily shown to be 6/d, where d is the diameter. A similar ratio, 6/e, applied to other regular polyhedrons, where e is the minimum distance through the centroid from surface to surface.

For a cube of edge e,

$$\text{surface area/volume} = \frac{6e^2}{e^3} = \frac{6}{e} .$$

For a right cylinder of diameter and length e,

$$\text{surface area/volume} = \left[2\left(\frac{\pi}{4} e^2\right) + \pi e \cdot e\right] / \frac{\pi}{4} e^3 = \frac{6}{e} .$$

For a dodecahedron of edge ℓ,

$$e = 2.23\, \ell = \text{distance between two parallel faces} ,$$

$$\text{surface area/volume} = \frac{20.65\ \ell^2}{7.66\ \ell^3} = \frac{2.69}{\ell} = \frac{6.00}{e} .$$

The cross section of individual bubbles as shown by the photographs at the column walls are hexagons of unequal sides whose vertices are approximately on circles. The individual faces of such bubbles are predominantly pentagons. For the relatively uniform bubble diameters desired for countercurrent foam column operation, the use of 6/d (where d is the minimum diameter of the bubble cross section) appears to be a good approximation of the surface area/volume ratio of the polyhedron bubbles.

The rotameters used for gas-rate measurements were calibrated by using air at atmospheric pressure and wet test meters. The manufacturers ratings for standard volumes at 70°F were also available. All gases were metered and used at room temperature. Corrections were necessary for the use of nitrogen in place of air, and for the pressures above atmospheric due to the gas sparger pressure drops and the depth of solution above the sparger. These corrections are given in more detail in the appendix.

Experimental Surface Rates and Average Diameters. Gas rates corrected as described, and surface rates from the corrected gas rate times $6/d_s$ were calculated for the spinneret gas spargers (Figures 17, 18). Many of these points represent values determined for countercurrent run calculations. The low-flow-rate straight-line parts of the curves through zero represent flows where the bubble size is a constant, independent of gas flow. The bubble size increases as the gas flow

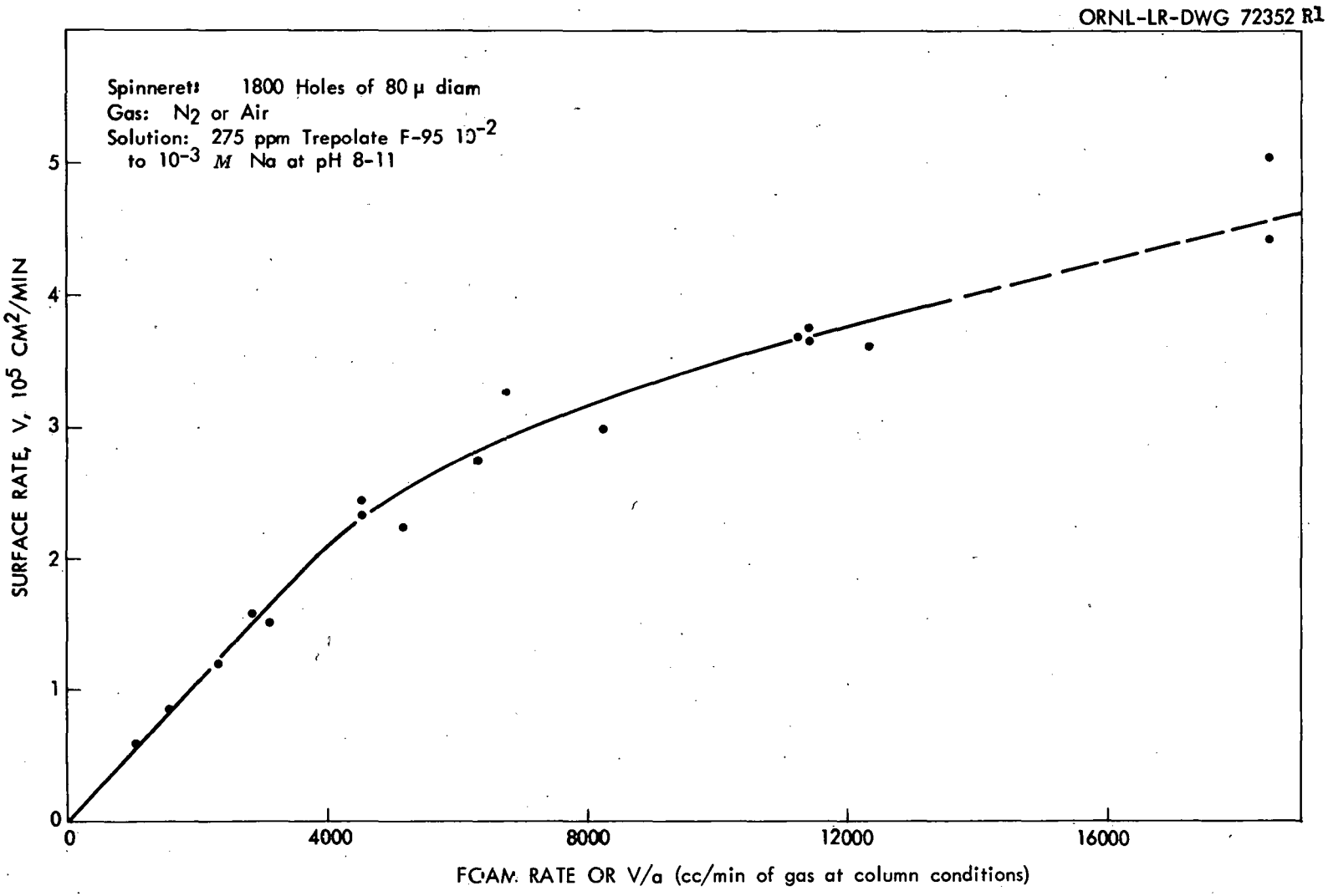

Figure 17. Surface Rates vs Gas Rates for B Spinneret.

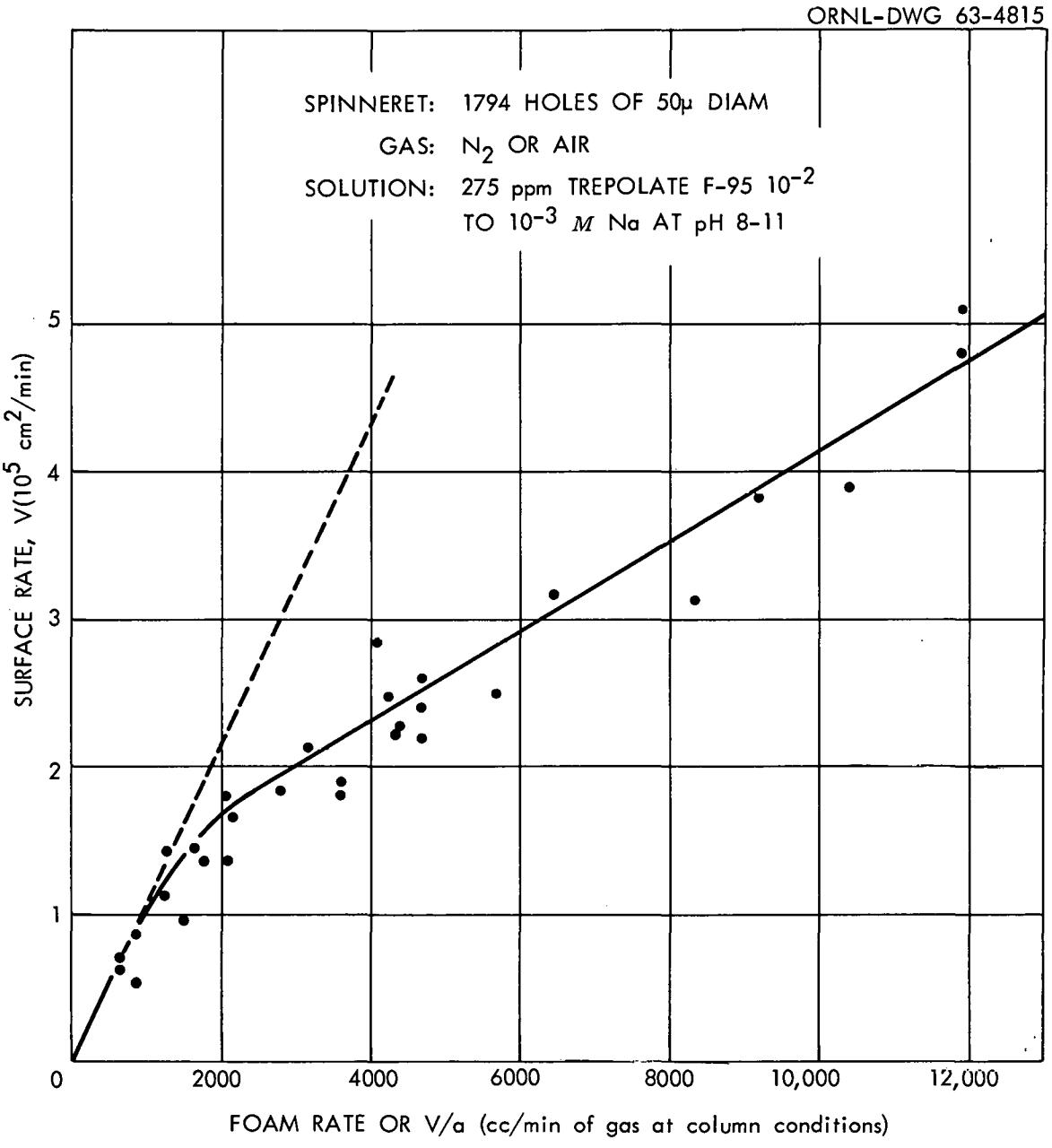

Figure 18. Surface Rates vs Gas Rates for Λ Spinneret.

increases (Figure 19), and a decreasing slope of the foam rate versus the surface rate results. The bubble sizes calculated from the equality of buoyancy and surface tension forces ($R^3 = 3r\alpha/2g\Delta\rho$) would be 0.082 and 0.097 cm for r = 50 μ and 80 μ, respectively.

The individual points for the spinneret were determined in three ways. Where bubble sizes were measured, the total volume and the total area were calculated by summation. Where $\bar{d}$ and s^2 were determined for measured bubble sizes, the value of d_s was calculated assuming normal distributions. Where individual bubble sizes were not measured, normal distributions were assumed, and $\bar{d}$ and s^2 may be estimated from:

$$d_A = \frac{D/\sqrt{n}}{1.03} = \sqrt{\bar{d}^2 + s^2}\ , \tag{124}$$

$$d_{90} = \bar{d} + 1.28\ s\ , \tag{125}$$

where ten percent of the bubbles are larger than d_{90}. Since d_s was the quantity desired, it was calculated by using $D/\sqrt{n}$ and d_{90} directly from the approximation:

$$d_s = \frac{D/\sqrt{n}}{1.03}\left[1 + 1.2\left(\frac{d_{90}}{D\sqrt{n}} - 1\right)^2\right]. \tag{126}$$

Values calculated in this way were within ±3% of the values of d_s obtained by measuring bubble diameters on the same photograph.

Surface rate and bubble-diameter-versus-gas-rate curves were determined similarly for the extra-coarse-porosity fritted glass cylinders (Figures 20, 21), even though the normal distributions of bubble sizes were not accepted for this sparger.

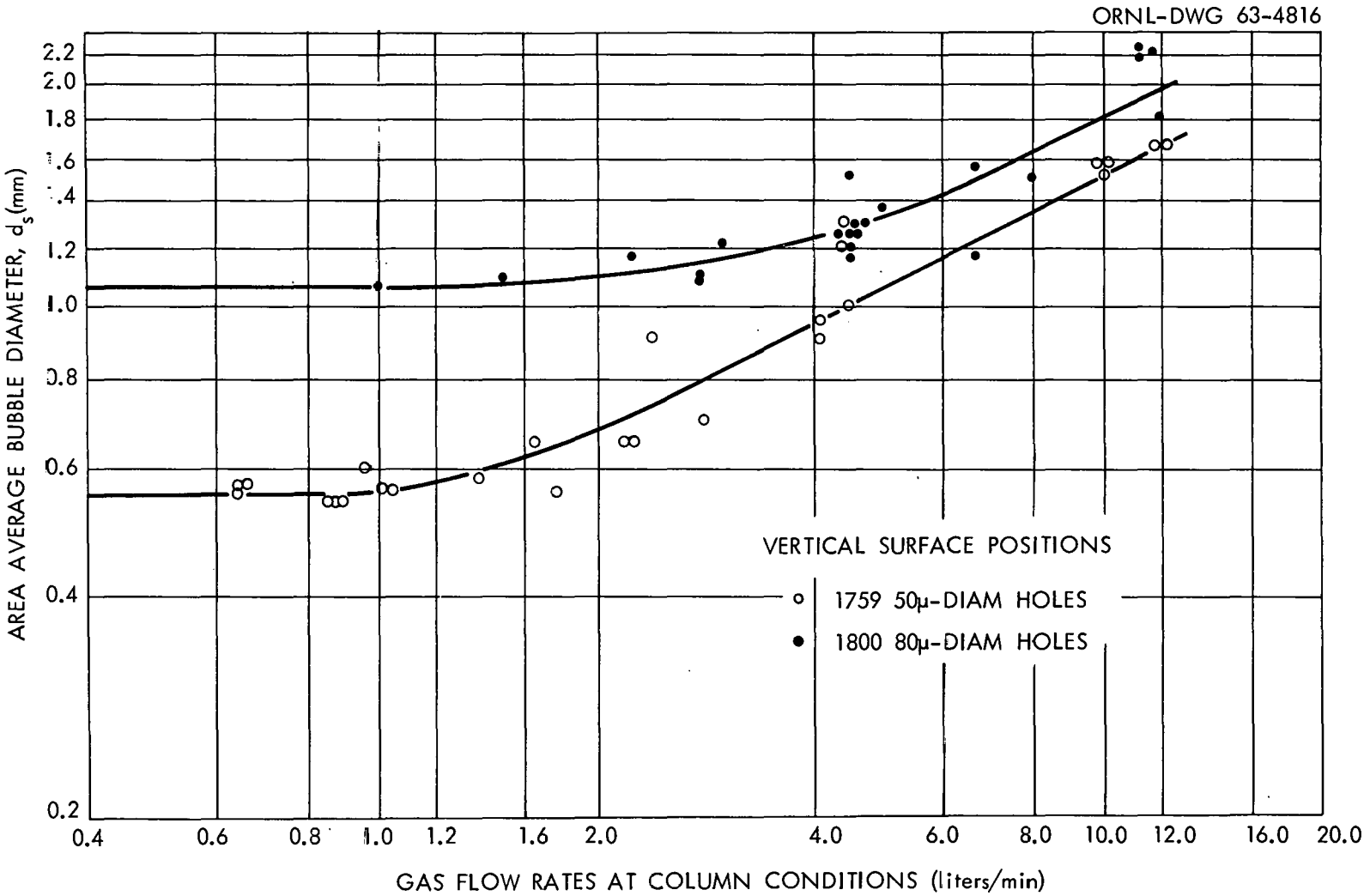

Figure 19. Area Average Foam Bubble Diameters from Spinneret Gas Spargers with 275-ppm Trepolate F-95 Solution.

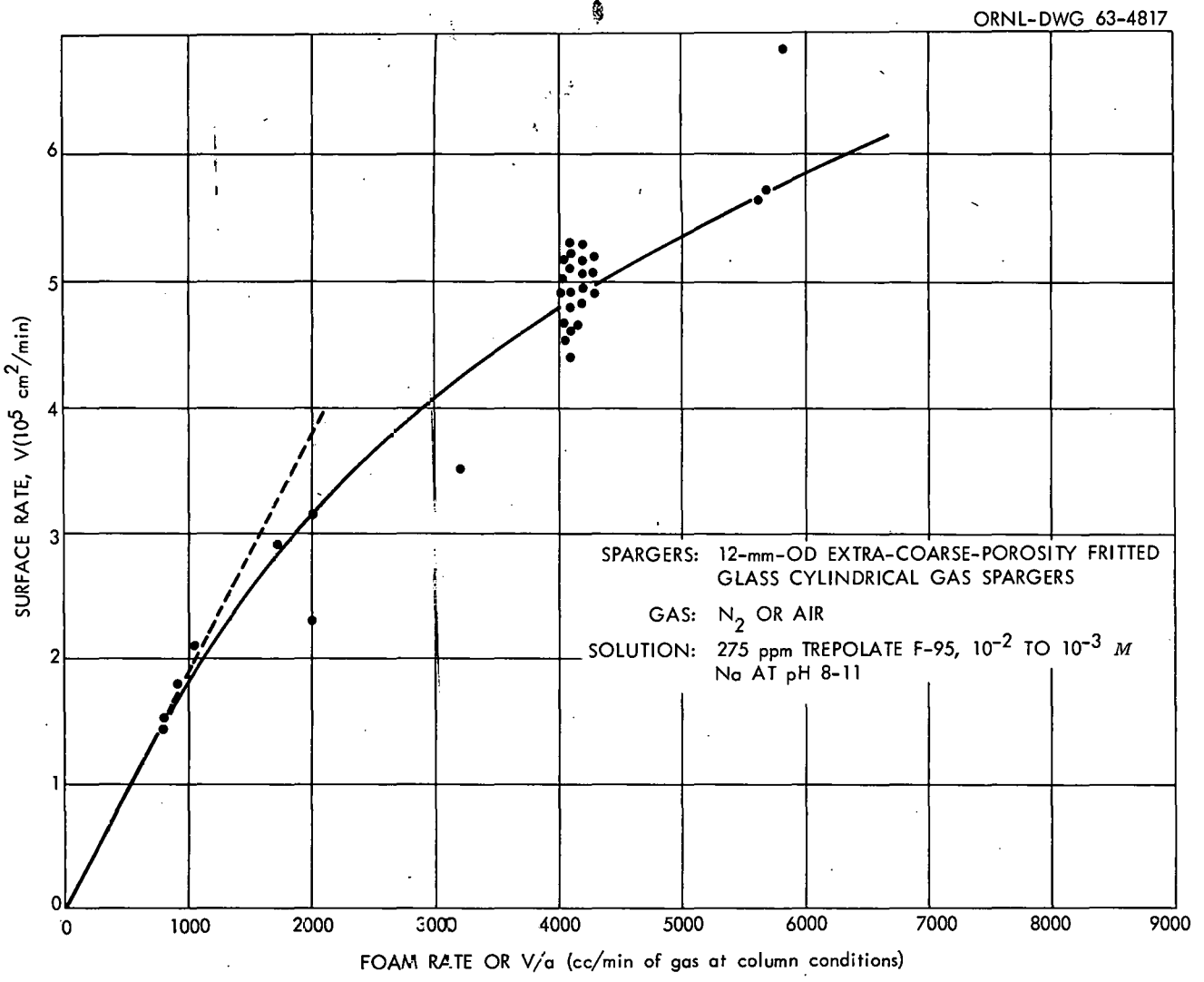

Figure 20. Surface Rates vs Gas Rates for Extra-Coarse Porosity Fritted Glass.

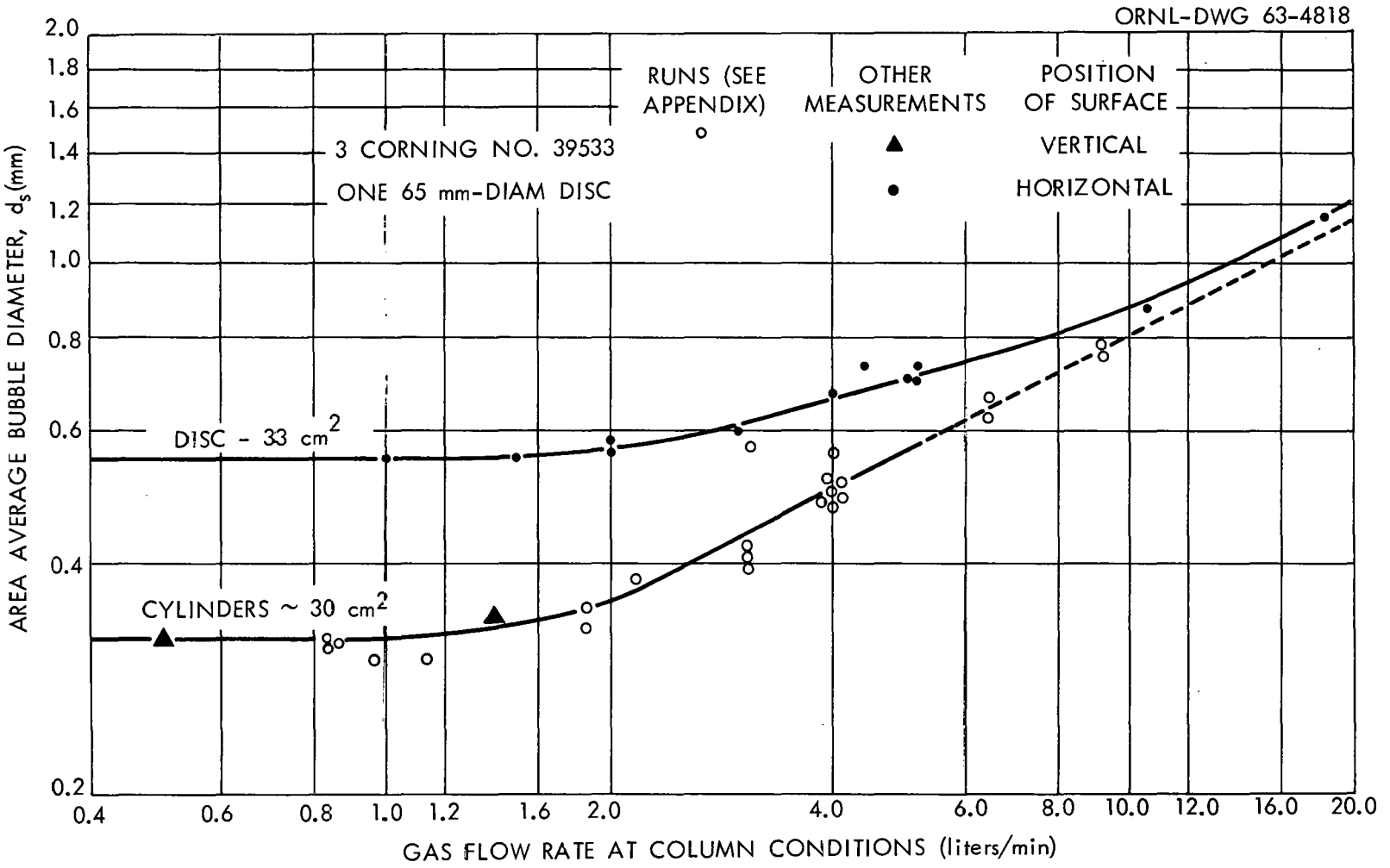

Figure 21. Area Average Foam Bubble Diameters from Extra-Coarse Porosity Fritted Glass Gas Spargers with 275-ppm Trepolate F-95 Solution.

VI-2 Liquid Distributors

Eight liquid feed distributors were fabricated for the 6-in.-ID foam column (Table XII) and their performance observed in and out of the column. Experimental HTU_x results for six of these distributors (reported in section VII-2) confirmed the visual observations. Distributors of two designs for a 24-in.-diam column were also fabricated and then observed visually. Use of a screen across the column cross section below the liquid distributor was tested briefly.

Five of the liquid distributors were of a seven-pronged "spider" design, with six tubes spaced on a 4-in.-diam circle and one at the center with all seven joined to a single feed line (Figure 22a). One distributor had ten 1/8-in.-wide slots as weirs cut into 1/2-in.-OD tubing; eight of the slots were equally spaced around a 4-1/4-in.-diam ring of tubing, and two were on a cross bar (Figure 22b). Drip points of weld beads were attached below the weirs. One was a single tube of 1/2 in. in diameter, with a 5/8-in.-diam splash plate 1/4-in. below the open end of the tube (Figure 22c).

The initially fabricated "0" distributor clearly indicated the two major problems. This 0 distributor was a ring of 1/4-in.-diam tubing with twelve 1/32-in.-diam holes drilled with a uniform spacing around the 4-in.-diam doughnut and the liquid entering the doughnut ring at one point. The flows from the twelve holes were not equal. The individual flows decreased with distance from the liquid entry line and decreased for higher elevations on the doughnut. The streams from the holes broke the foam and created large voids or channeling.

TABLE XII

DIMENSIONS OF THE FEED DISTRIBUTORS

Designation	Type	Number of Exits	Size of Exits (cm)	Area of Exits (cm^2)	Estimated Efficient Capacity[a] (cc/min)
O	Ring with holes	12	0.080 diam	0.060	None
A	Spider	7	0.122 diam	0.082	200 - 500
B	Spider	7	0.155 diam	0.132	500 - 800
C	Spider	7	0.240 diam	0.32	1400 - 1900
D[b]	Spider	7	0.476 diam	1.26	3000[b] - 7500
E	Ring with weirs	10	0.32 slots	~1.0	2000 - 6000
F	Spider	7	0.376 diam	0.78	3500 - 4700
G	Single tube	1		~1.0	- - - -

[a]Capacity range for frictional pressure drop >0.5 cm/cm and average velocity < 6000 cm/min.

[b]An orifice of 0.125 in. in diameter was used at the upper end of each spider D capillary and controlled the frictional pressure drop.

ORNL-PHOTO 58382

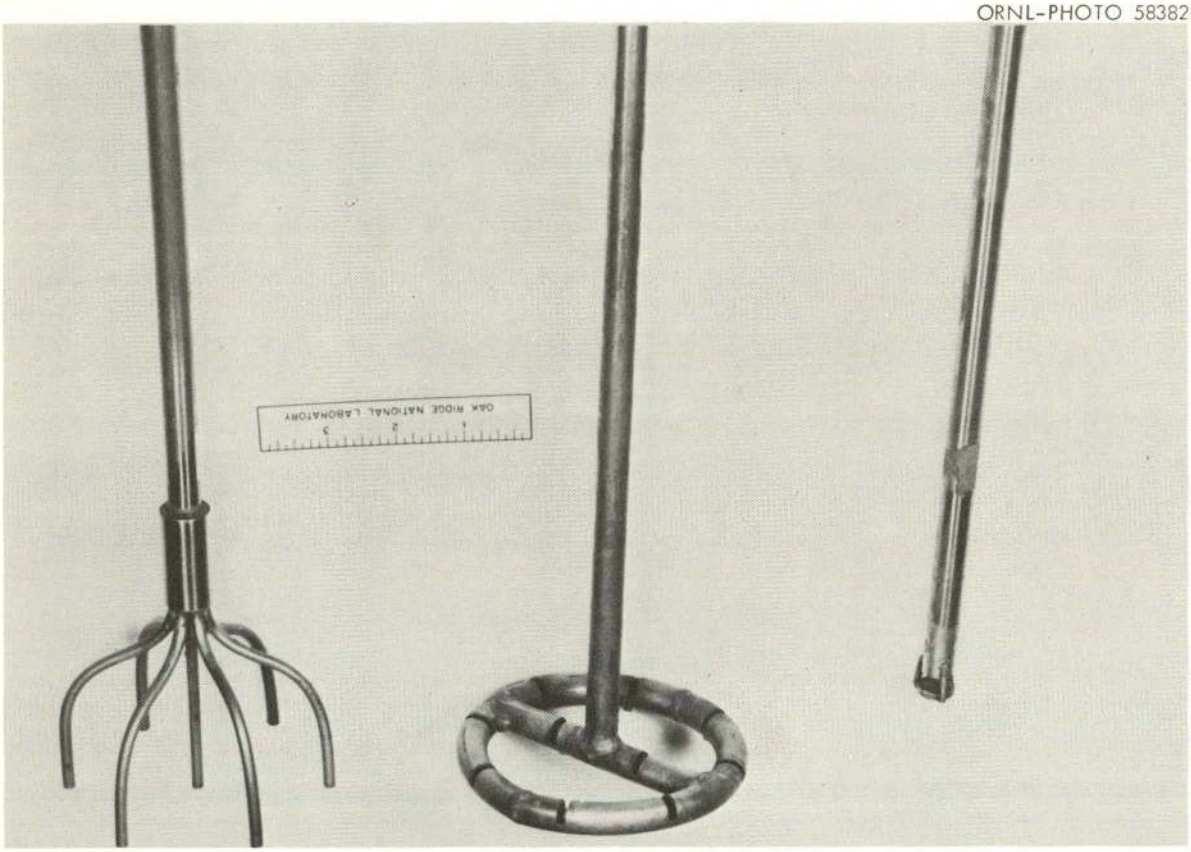

a. "Spider" of seven 0.148-in.-ID tubes; distributor F.

b. Weir with ten 1/8-in.-wide slots; distributor E.

c. Single tube of 1/2-in.-OD, 5/8-in.-diam splash plate about 1/4-in. below open end; distributor G.

Figure 22. Liquid Feed Distributors for the Foam Column.

Each of the spider-type distributors solved these two problems for a limited range of flow rates. As the flow rate is decreased until the pressure drop across the capillaries is less than the gravitational head, unequal flows appear because of siphoning. For capillary frictional pressures drops of 0.5 cm/cm these average minimum velocities would be from 23 cm/sec for distributor B, to 80 cm/sec for distributor F. The frictional pressure drops for D were controlled by a 0.125-in.-diam orifice for each tube. The maximum flows are determined by the occurrence of excessive foam breaking due to the high velocity of the entering liquid. For the B and C spider distributors, inlet velocities of 60 cm/sec showed little effect, while velocities of over 100 cm/sec caused excessive voids.

Estimated capacity ranges from these criteria (Table XII) are somewhat higher than the flow rates that gave uniform flows in air (Table XIII) or higher than the flows that were usable in the foam column for the D, E, and F distributors. The foam breaking probably depends on the total momentum in the entering liquid, and the maximum allowable liquid velocities are probably lower for higher liquid flow rates.

A 24-in.-diam foam column (Figure 23) was operated with feed introduced through 19 tubes in a 5-in. triangular spacing. The about-0.21-in.-ID tubes were fed from a common liquid reservoir through 3-in. lengths of 0.083-in.-ID tubes as flow control orifices. Visible channeling was observed for tubes positioned at varying distances 0 to 2-1/2 in. from the column wall. This channeling persisted for 18 to

TABLE XIII

FLOW CHARACTERISTICS OF THE FEED DISTRIBUTORS

Designation	Flow Velocity Conversion $\left(\frac{cc/min}{cm/sec}\right)$	Continual Drip		Short Solid Stream		Long Solid Stream	
		Total Flow (cc/min)	Variation[a] from Average (%)	Total Flow (cc/min)	Variation[a] from Average (%)	Total Flow (cc/min)	Variation[a] from Average (%)
O	3.6	-	-	-	-	-	-
A	4.9	-	-	-	-	-	-
B	7.9	280	~ ± 5	390	± 4	-	-
C	19.	400	±20	1000	± 7	1400	± 6
D	75.	720	±35	1500	±10	1900	±10
E	~ 60.	900	±50	1900	±35	4000	±20
F	47.	400	±18	600	±10	2000	± 3
G	~ 60.	-	-	-	0	-	0

[a]The maximum variations among the six outer tubes or the eight outer slots. The center tubes of the spiders showed high flow rates which were usually slightly higher than the "plus" variation tabulated, but this location was symmetrical and is not considered a poor distribution of liquid.

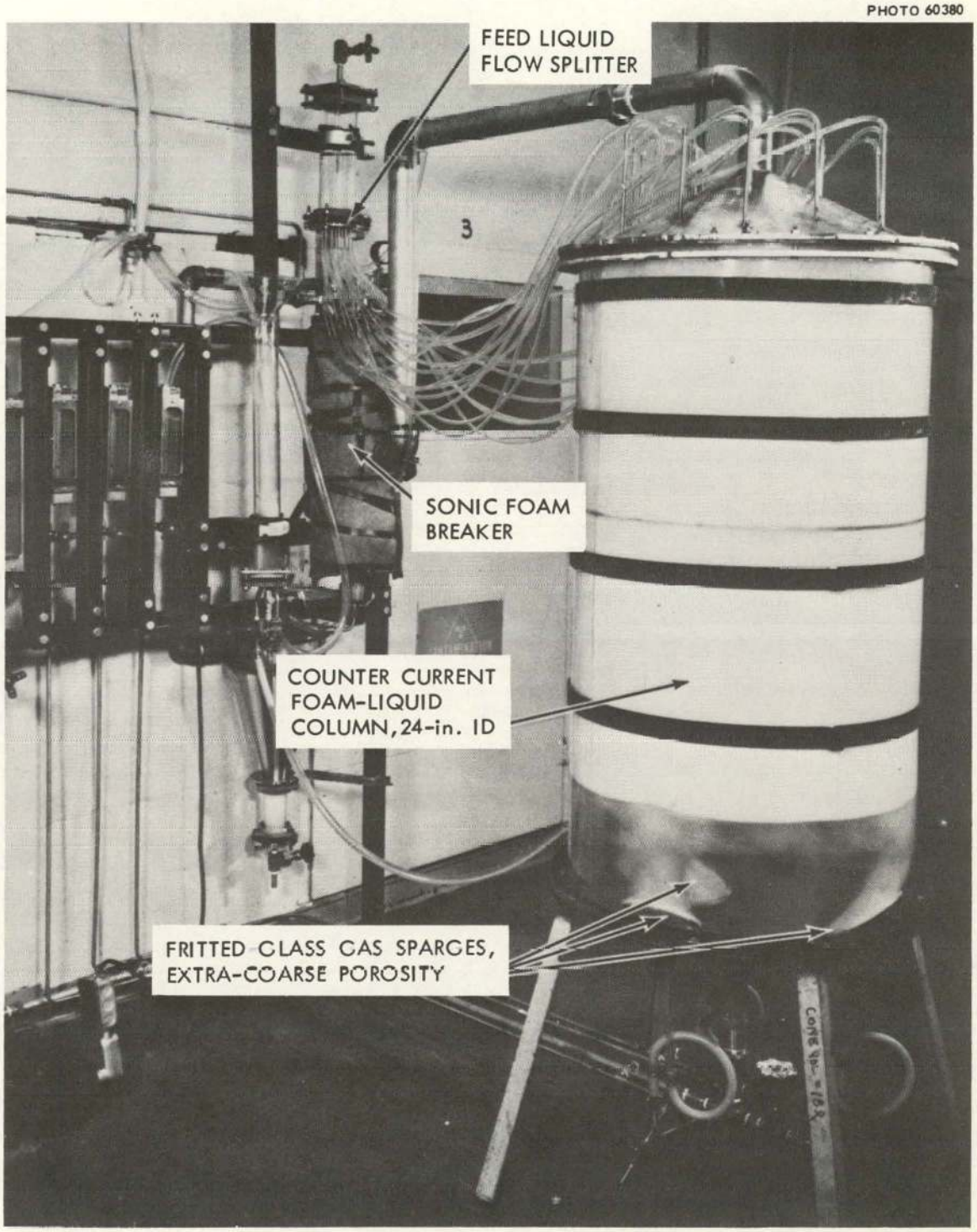

Figure 23. Twenty-four-inch-diameter Column and Associated Apparatus for Foam Separation Studies.

30 in. below the tube ends for 40 gal/hr·ft^2 and 10 to 22 in. for 15 gal/hr·ft^2. The flow appeared to be uniformly divided among the 19 tubes except when siphoning caused a complete loss of liquid and flow from some tubes at low flow rates. Smaller orifices would have prevented this difficulty. A distributor designed to give 37 feed streams on approximately 3-3/4-in. triangular spacing did not cause significant channeling. This design used parallel, horizontal tubes spaced across the column cross section with 0.094-cm-diam metering orifices drilled in the tubes. The orifice streams impinged on baffles and then dripped into the foam with little kinetic energy. This design also eliminated the siphoning at low flow rates which was observed for the 19 tubes or for spiders in the 6-in. columns.

The use of screens across the column below the liquid distributor was considered as a means of obtaining better feed distribution. First, a 40-mesh screen was supported about 8 in. below the liquid feed point in the 24-in.-diam column. Nearly all the liquid flow and much of the foam flow appeared to bypass the screen through the small gap (0 to 1/16 in.) between the screen and the column wall. A 20-mesh screen was then installed, and a rubber ring was used to seal the screen to the wall. No channeling was visible below the screen, while 10 to 30 in. of channeling below the feed point was visible at the flows without the screen. Large bubbles or small voids appeared in the foam during passage through the screen, and some liquid accumulated on the screen. A 20-mesh screen, sealed between two gaskets at a joint, was then used below the single tube (G) liquid distributor

in the 6-in.-diam column. Liquid accumulated on the screen and "dumped" through at irregular intervals (10- to 40-sec intervals were common) to cause very severe channeling. It is probable that the same type of "dumping" occurred in the interior of the 24-in. column where the screen had several slight depressions. The only visual evidence of dumping in the 24-in. column was slight variations in the levels of accumulated liquid on the screen at the column walls.

VI-3 Foam Breakers

Application of foam separation requires the condensation of the foam to a solution or slurry that is either a product stream or a stream part of which may be returned to the column as reflux. Initial tests of possible foam breaker systems showed that their performance varied with the characteristics of the foam fed to them. Foam breaker studies were limited to determining the capacities of an orifice, a cyclone, a centrifugal foam breaker, and sonic foam breakers for typical foams from dodecylbenzenesulfonate solutions. Chemicals and heat may also be used to cause foam condensation, but they seemed less applicable to foam columns than the mechanical breakers tested.

The quantitative reproducibility of foam-condensation test results was poor; this might be expected from the variations observed for foam drainage (see previous section). The relations between variables were consistent, and the relative advantages of the several foam breakers tested are not confused by the poor reproducibility. This fact emerges: The exact performance of any large foam breaker

will be uncertain until it is determined by tests of full-scale units on foam from the system on which it is to be used.

Orifice Foam Breakers. The idea of an orifice as a foam breaker was developed from consideration of the foam breaking mechanism in the sonic, cyclone, and centrifugal foam breakers. The sonic foam breaking mechanism is ascribed to pressure-cycling effects (10). The 2-to-1 inlet-to-outlet pressure ratio found necessary to make an effective foam breaker would produce a very rapid pressure change. Foam flowing through either a stationary fine mesh screen or through a coarse-screen centrifuge bowl is broken very poorly, compared with the effectiveness of a fine-screen centrifuge bowl. This could be attributed to a pressure change as the foam leaves the centrifugal field in the bowl. Since sharp pressure changes and even pressure discontinuities are possible in an orifice, the performance of orifices as foam breakers was tested.

Experimental data were collected for four orifice diameters, using foam from extra-coarse-porosity fritted-glass-disk gas spargers. Foam generated from a 200- to 275-ppm Trepolate F-95 solution was drawn through the orifice by vacuum, with the top of the column vented to the atmosphere (Figure 24). The amount of uncondensed foam was measured by operating the orifice for 2 to 5 min and then venting the vacuum pot and discharging the liquid and foam into a graduate. The orifice diameter, the foam rate, the pressure drop across the orifice, the foam density, the distance from the orifice to the vacuum chamber wall, and the wall material were varied.

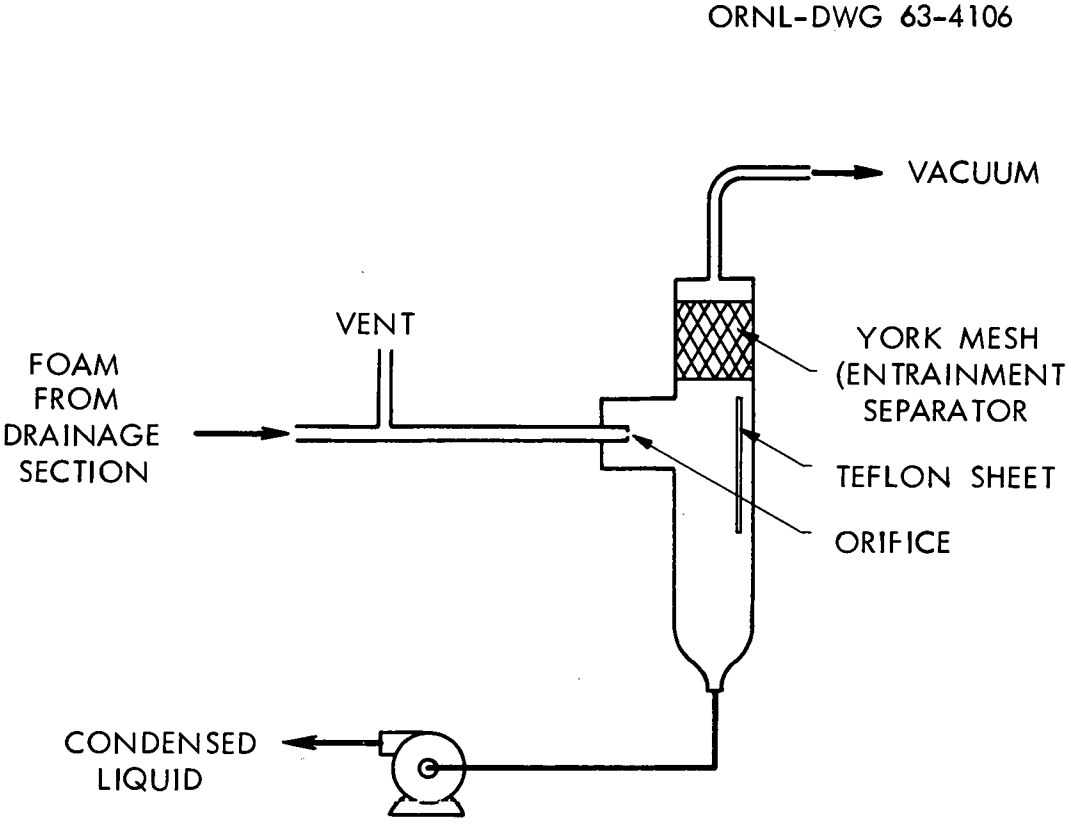

Figure 24. Orifice Foam Breaker Test Apparatus.

The experimental results show that foams are easily condensed by an orifice, with residual foam volumes being about a thousandth of those of the inlet volumes for the well-drained foams (Table XIV). Pressure drops from atmospheric for the inlet foam to one-half atmosphere in the vacuum pot were adequate. The same pressure ratio would probably apply at other pressures; that is to say, an upstream-to-downstream pressure ratio of 2 is probably adequate. With the inlet foam at atmospheric pressure, condensation was less complete for 30 or 25 cm of mercury pressure drop as compared to 50 or 65 cm mercury and became very poor for lower pressure drops.

The results indicate that the condensation occurs as the bubbles pass through the orifice and that orifices smaller than the bubble and impingement of the bubbles on a surface are not necessary. The condensation of foam was about equally efficient for 0.015-, 0.100-, and 0.250-cm-diam orifices. The 0.015-cm-diameter one would be smaller than nearly all the bubbles, while the 0.250-cm-diameter orifice would be larger than nearly all the bubbles (mean bubble diameters of 0.05 to 0.08 cm). For most tests, the stream from the orifices impinged on a Teflon sheet placed 2 to 3 in. from the orifice. The amount of uncondensed foam was slightly decreased by placing the orifice 24 in. from the Teflon sheet. The amount of uncondensed foam was slightly greater for a glass surface in place of the Teflon sheet. It appeared that the foam bubbles broke before they hit the surface and that the liquid striking the surface caused some formation of new foam bubbles, depending on the material and position of the surface.

TABLE XIV

TESTS OF ORIFICE FOAM BREAKERS

Orifice		Opposing Wall		Foam Column		Pressure	Foam	Foam	Average Bubble	Fraction of Uncondensed
No.	Diam (cm)	Material	Distance	Diam (in.)	Foam Drainage Flow	Drop (cm Hg)	Rate (cc/min)	Density (mg/cc)	Diam (cm)	Foam (cc/cc)
12	0.015	Glass	~ 3	6	Horizontal	~ 65	1,000	~ 2	0.05	< 0.001
1	0.100	Glass	~ 2	6	Horizontal	~ 65	5,600	4	0.07	0.0016
							3,700	3	0.06	0.0005
						50	5,600	4	0.07	0.0019
							3,700	3	0.06	0.0011
						30	5,600	4	0.07	0.0012
							3,700	3	0.06	0.0010
						25	3,700	3	0.06	0.0040
		Teflon	~ 2	6	Horizontal	~ 65	5,600	4	0.07	0.0005
							3,700	3	0.06	0.0006
						30	5,600	4	0.07	0.0012
							3,700	3	0.06	0.0014
		Teflon	~ 2	6	Vertical	~ 65	3,700	12	0.07	0.0040
							1,900	9	0.06	0.0016
							700	4	0.05	< 0.0005
						50	3,700	12	0.07	0.0040
						30	3,700	12	0.07	0.0032
							1,900	9	0.06	0.0021
							700	4	0.05	< 0.0005
		Teflon	~ 24	6	Vertical	~ 65	3,700	12	0.07	0.0016
							1,900	9	0.06	0.0013
						30	3,700	12	0.07	0.0027
							1,900	9	0.06	0.0048
						~ 60				
1	0.250	Teflon	~ 3	24	Vertical	~ 60	40,000	4	0.07	0.0010
							32,000	3.5	0.06	0.0011
							16,000	1	0.05	0.0005
							8,000	0.5	0.05	0.0005

The drier foams from lower foam rates or better drainage gave smaller fractions of uncondensed foam. This may have been due to less formation of new foam bubbles on the Teflon surfaces when the inlet foam was drier.

The capacity of the orifices seemed to be inversely proportional to the square root of the foam density as would be expected from orifice equations. Using the form of equation expected for orifices, the observed capacities agree with:

$$q = 6000\ (2r)^2 \sqrt{\frac{\Delta P}{\epsilon}} \quad , \tag{127}$$

where

$2r$ = orifice diameter in cm,

ΔP = pressure drop in cm of Hg,

ϵ = foam density in cc/cc,

q = capacity in cc/min.

This equation indicates slightly higher flows than would be calculated for gases of the same densities as the foams.

Cyclone Foam Breaker. Experimental data were collected for foam breaking by a 0.40-in.-ID cyclone. Foam generated at 500 to 14000 cc/min using "D" porosity sintered stainless steel gas spargers and 300 to 1500 ppm Trepolate F-95 was drawn through the cyclone by vacuum, with the top of the column vented to the atmosphere (Figure 25). The capacity for feed foam at atmospheric pressure and about 22 in. mercury vacuum in the collection pot was 14,000 cc/min foam; the capacity for foam-free air would be about 30 liters/min for these pressures.

ORNL-LR-DWG 70765

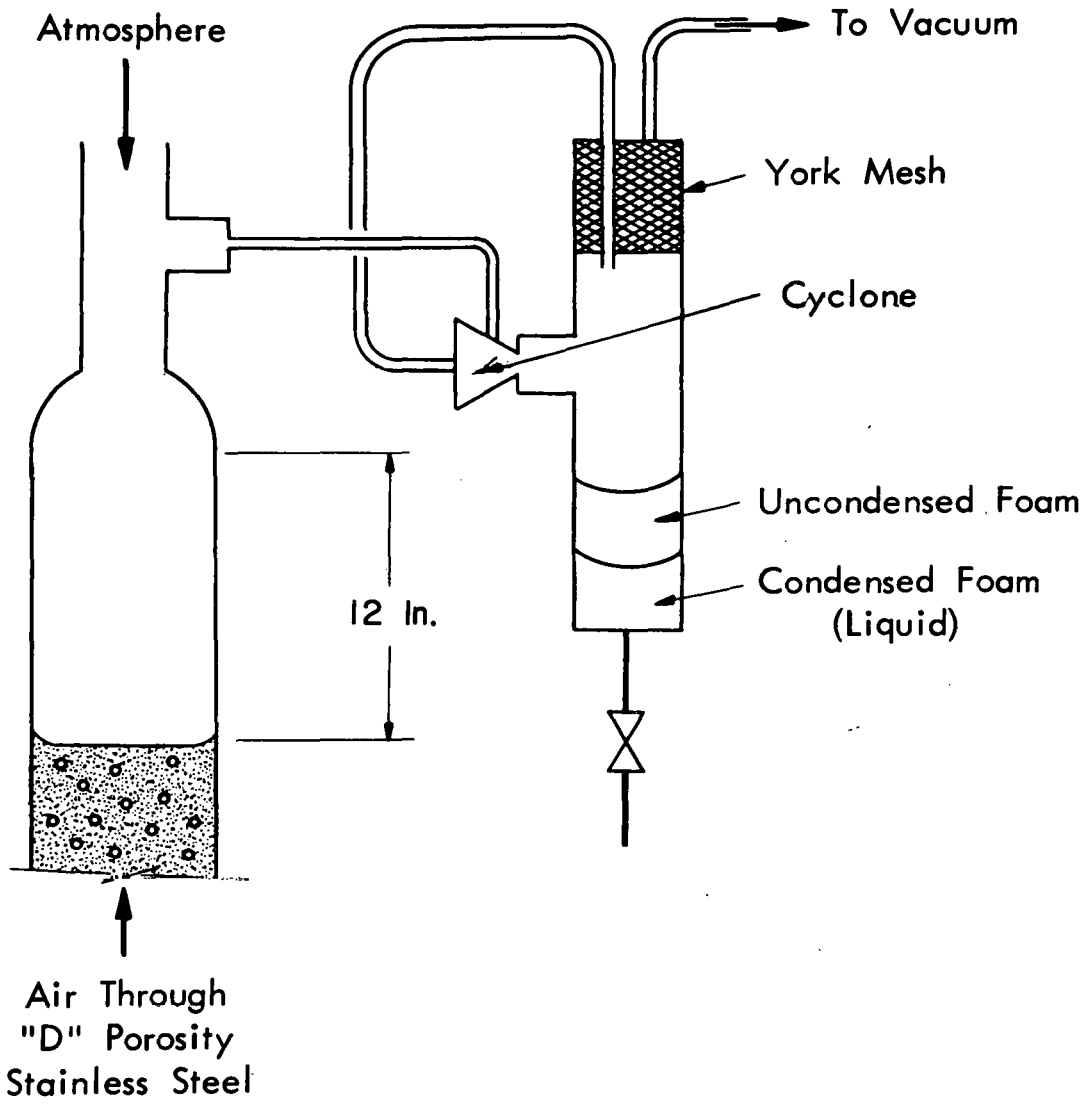

Figure 25. Cyclone Foam Breaker Apparatus.

The effectiveness of foam breaking appeared to decrease as the wetness of the foam increased. The uncondensed foam was a wet, slow-to-break foam of very small bubble diameter. For collection periods of 10 min, the volumes of uncondensed foam (measured at atmospheric pressure), compared with the feed foam volumes, were less than 0.2% for 500 to 800 cc/min foam rates and usually 0.4 to 1.0% for 1200 to 2000 cc/min foam rate, and for 20 liters of feed foam, 1 to 4% for 4000 to 8000 cc/min foam rate. The data did not reproduce well, and variations by factors of two for identical conditions were common. The variations with surfactant concentrations were not significant. The addition of 20 cc/min of water to the cyclone feed line for foam rates of 1000, 2000, and 4000 cc/min resulted in a small increase in the volume of uncondensed foam.

A pump was used to pump the liquid and foam as they collected from the cyclone receiver pot to a settler, with overflow of the foam to the cyclone feed line. The results indicate that such an arrangement would permit the application of cyclone foam breakers without removal of uncondensed foam from the system. The gas to generate the foam and to operate the cyclone could be recycled to contain contamination or to minimize inert-gas requirements if an inert atmosphere were desired.

Centrifugal Foam Breaker. The use of a screen-lined centrifuge bowl as found convenient for laboratory condensation of foam (30) was investigated. Two bowls were made of perforated metal sheet to permit changing the screen liners. Either of these bowls was coupled directly

to a universal-type electric hand-grinder motor. The speed was controlled by a variable-voltage transformer in the motor power supply and was measured by use of a stroboscopic light. Foam from a 6-in.-ID column with about 1 ft of 6-in.-diam drainage section was introduced 1 to 3 in. below the top edge of the bowl. The rate of accumulation of uncondensed foam was measured, with centrifuge speed, foam rate, screen-mesh size, and solution concentrations as the variables (Table XV). If the foam overflowed the centrifuge top, the flow rate was considered to be in excess of the capacity at those conditions.

The most significant conclusions from the test data were:

1. The percentage of uncondensed foam is lower for a low rate of dry foam than for a higher rate of wetter foam.
2. Screen sizes of 100 or 120 mesh per inch give less uncondensed foam than 200 or 40 mesh per inch screens.
3. The capacity increases as the speed is increased.
4. Lower speeds give less uncondensed foam if the capacity is not exceeded.
5. The amount of uncondensed foam at higher speed was greatly decreased by use of a Teflon sheet liner instead of glass as the stationary wall around the centrifuge.

The capacities of the centrifugal foam breakers decreased rapidly as the speed decreased below 2000 rpm. Typical values for the 4-in.-diam, 4-in.-high bowl with 120-mesh screen were 3500 cc/min at 1515 rpm, 4000 cc/min at 1670 rpm, and 10,000 cc/min at 2000 rpm for foam from the 6-in.-diam column (Table XVI). These effects are shown

TABLE XV

TEST OF CENTRIFUGAL FOAM BREAKER

Bowl: 4-in. ID., 4-in. height of perforated sheet; 1/8-in.-diam holes on 3/16-in. triangular spacing
Foam: "EC" fritted glass gas sparger; 6-in.-diam, 12-in.-high drainage section.

Foam Rate	Screen Mesh (per inch)	Stationary Wall	Foam Breaker (rpm)	For 250 ppm Trepolate F-95 and 0.01 N NaOH Uncondensed Foam (cc/min)	(%)	For 500 ppm Trepolate F-95 and 0.01 N NaOH Uncondensed Foam (cc/min)	(%)
2,000	120	Glass	2,000.	4.	0.2		
			2,500	6.	0.3		
			3,000	12.	0.6		
			3,500	12.	0.6		
3,500	120	Glass	2,000	13.	0.4	110.	3.1
			2,500	25.	0.7	160.	4.6
			3,000	19.	0.6	240.	6.9
			3,500	46.	1.3	380.	11.
	200	Glass	2,000	10.	0.3		
			3,500	123.	3.5		
	200	Teflon	2,000	11.	0.3		
			2,500	9.	0.3		
			3,000	21.	0.6		
			3,500	30.	0.9		
6,000	120	Glass	2,000	72.	1.2		
			2,500	100.	1.7		
			3,000	310.	5.2		
			3,500	290.	4.8		
10,000	120	Glass	2,000	140.	1.4	540.	5.4
			2,500	490.	4.9	710.	7.1
			3,000	470.	4.7	710.	7.1
			3,500	760.	7.6	800.	8.0
	200	Glass	2,000	650.	6.5		
			3,500	990.	9.9		
	200	Teflon	2,000	75.	0.8		
			2,500	120.	1.2		
			3,000	170.	1.7		
			3,500	210.	2.1		

TABLE XVI

CENTRIFUGAL FOAM BREAKER CAPACITIES

Gas Spargers: extra-coarse fritted glass disks
Centrifuge Bowl: 4 in. in diameter, 4 in. high

Column Diameter (in.)	Solution Concentrations		Screen Mesh (per inch)	Centrifuge (rpm)	Foam Capacity (cc/min)
	Trepolate F-95 (ppm)	NaOH (N)			
6	250	0.01	120	1,515	3,500.
				1,670	4,000.
				2,000	10,000.
24	200	0.002	100	2,300	16,000.
				2,700	24,000.
			200	3,200	16,000.
				3,800	24,000.
	400	0.01	200	3,400	16,000.

by the results for foam from the 24-in.-diam column with extra-coarse-porosity fritted glass disks as gas spargers (Table XVI). Apparently the pressure causing flow through the screen increases with the foam density and the centrifugal field. The 200-mesh screen would be expected to offer more resistance to flow than the 100-mesh screen does. The initial bowl (about 4-5/8 in. in diameter and 6 in. high) was limited to less than 1600 rpm because of poor balancing and had a low capacity.

The percentage of uncondensed foam was decreased, and the results were much more reproducible when the edges of the screen were sealed to the perforated bowl wall with paraffin. Although the screens were carefully cut to fit the bowls, apparently small gaps permitted foam to escape without passing through the screen when the paraffin seals were not used. The tabulated results (Table XV) are those obtained from the use of the paraffin seals.

Since plastic walls seemed to improve the operation of small laboratory centrifuges used as foam breakers (30), a Teflon sheet was used to line the 6-in.-ID glass pipe around the centrifuge bowl for one series of tests (Table XV). For conditions where the glass wall gave uncondensed foam volumes larger than one percent of the feed foam volume, the Teflon sheet lining gave large reductions in the amount of uncondensed foam. The effect of the Teflon was not noticeable at conditions where the glass wall gave less than one percent of uncondensed foam.

Sonic Foam Breakers. The generation of intense sound and its

application to destroy foams has been described in technical literature (4, 9, 10). Several mechanisms are involved. Intensities of 143 to 155 decibels were effective, with a unidirectional radiation pressure effect predominant for frequencies above 2000 cps and acoustic pressure and bubble resonance phenomena important at low frequencies. Air-operated sound generators of several types were used, and foam was destroyed at rates of 0.20 to 0.36 cfm of foam per cubic feet per minute of operating air supplied at 40 to 60 psi (10).

Two air-operated whistles were purchased (Teknika, Inc. of Hartford 5, Conn.) and used for foam condensation. The first unit was a Teknika Airjet Sonic Defoamer recommended for destroying foam over a 6- to 24-in.-diam area. An air supply to deliver up to 15 scfm at 40 psig was specified to produce "highly intense sound at a frequency of 12,000 cps. This unit was used as the foam breaker for all the runs with Sr^{89} tracer. The unit was operated inside a 6-in.-ID Pyrex pipe vented to the "hot" off-gas system.

This unit condensed the foam for all flow rates used (0 to 12 liters/min, spinneret, and extra-coarse fritted-glass gas spargers). The foam came to within an inch of the whistle for some of the higher flow rates, and small scraps of foam were entrained out with the operating air. The foam from the fritted glass was more difficult to condense than foam at the same volume flow rates from the spinnerets. Water or dilute acid discharged at 10 ml/min immediately below the whistle seem to cause more efficient foam breakage. This discharge of acid was necessary during runs with Sr^{89} in order to obtain reproducible

condensed-foam rates and gross-beta material balances. Evaporation of water from this added stream was 2.8 to 3.5 g/min. This evaporation rate was greater than the condensed foam rate for some conditions, and the sonic foam breaker completely evaporated the water in the foam for some initial tests.

The second unit was described as a Sonic Vortex Transducer of increased efficiency, requiring 10 scfm of operating air at 40 psig. This unit, purchased as a package in a 6-in.-diam stainless steel tank, was tested with foam from extra-coarse fritted glass gas spargers in the 24-in.-diam column. The capacity was about 24 liters/min for foam from 250 ppm Trepolate F-95, 0.01 N NaOH solution, and 20 liters/min for foam from 500 ppm Trepolate F-95, 0.01 N NaOH solution.

Separation of the foam breaker and operating air from the foam by thin (0.001 to 0.002 in.) rubber or aluminum sheets was tested. The foam rose to the sheet surface (1/2 to 2 in. below the whistle) at flow rates where it would have been condensed at much lower positions had the sheets been absent. Most of the foam condensed near the sheets; some foam passed through the vent hole located at the sheet level. Thin plastic membranes are reported to decrease the sound outputs as much as 50% (10).

If sonic foam breakers were used for low-level waste decontamination, the cost of the operating air would be significant. The foam volume would be about 1000 ft^3 per 1000 gal of waste. Thus the operating air would be about 2×10^4 ft^3 per 1000 gal. Since the cost of

40-psig air would be about 1¢ per 1000 ft^3, the foam breaker air operating cost would be about 20¢ per 1000 gal.

CHAPTER VII

HTU_x MEASUREMENTS FOR A STRIPPING COLUMN

Values of the heights of transfer units for the stripping of Sr^{89} from aqueous solutions of dodecylbenzenesulfonate by a foam were measured experimentally. The results show the effects of column design and operating conditions on the efficiency of countercurrent contact. The explanation of these experimental values is partly based on observations of the foam through the glass column walls. The conditions were: the gas sparger, the liquid distributor, the gas and liquid flow rates, and the column length.

The effects of the conditions are shown by tabulations of HTU_x values selected from the detailed data in Appendix G. Conditions that show all factors constant except the one of immediate interest are compared whenever possible. The intention for most experimental runs was to select flow rates to give the phase flow ratio, $(\alpha V + E)/(L + E)$, values of 1.1 to 1.4. Values less than 1 permit pinching at the feed point. The HTU_x values selected are from runs with the phase flow ratio greater than 1 wherever possible since the values for ratios less than 1 are much less certain. The surface area flow rate and thus the surface concentration at the feed point are less accurately known than the other concentrations used to establish the operating line. Many of the earlier runs were with low phase ratios since the value of α was initially overestimated.

VII-1 Effect of Gas Sparger on HTU_x Values

The size of the gas bubbles and the uniformity of the size are

determined by the gas sparger, as discussed in Section VI-1; these two variables in turn effect the HTU_x values observed. Four spargers (Table VIII) were used for HTU_x determinations, and the foam from two other spargers was observed to be visibly inferior.

The lowest HTU_x values of about 1 cm were obtained with either spinneret A (50-μ-diam-holes) or spinneret B (80-μ-diam-holes) for liquid flow rates of up to 100 gal/ft^2·hr (Table XVII). The HTU_x values for the extra-coarse (EC) fritted glass gas spargers were all larger than 2 cm. The two spinnerets and the EC fritted glass spargers gave approximately equal HTU_x values for flow rates over 120 gal/ft^2·hr or for the less effective liquid distributors. The HTU_x for Micrometallic porosity D stainless steel spargers were higher than the values for either the spinneret or the EC fritted glass at the same low flow rates.

These HTU_x values and the observed behavior in the countercurrent foam column confirm the following explanation. When spinneret B and a good liquid distributor were used at liquid flow rates of 60 gal/ft^2·hr or less, good plug countercurrent flow of foam and liquid were obtained to give HTU_x values of about 1 cm, with very little back-mixing or channeling. Slightly more channeling and back-mixing were visible when spinneret A was used, and their effects on HTU_x values approximately cancelled out any decrease in HTU_x values from the decreased bubble diameter, compared with spinneret B. Appreciably more channeling and back mixing was observed when the EC fritted-glass spargers were used, and HTU_x values corresponding to plug countercurrent flow

TABLE XVII

EFFECT OF GAS SPARGER ON FOAM COLUMN HTU_x VALUES

Liquid Feed Distributor	Liquid Feed Rate, $L + E$ (cc/min)	Phase Flow Ratio, $\frac{\alpha V + E}{L + E}$ (cm^{-1})	Column Length, Z (cm)	Gas Sparger	HTU_x (cm)	Run No.
C	750	0.96	27	Spinneret A	1.7	17A
		1.08		Spinneret B	0.5	30A
	825	0.98		Spinneret B	1.5	33B
	900	0.92		EC fritted glass	2.5	21B
C	1000	0.89	27	Spinneret A	1.4	17E
	1100	0.92		Spinneret A	< 0.5	22B
		1.17		Spinneret B	1.8	30B
		2.43		EC fritted glass	5.7	36B
C	1450	0.77	27	Spinneret A	< 0.5	22A
		1.13		Spinneret B	1.8	30C
		1.29		EC fritted glass	2.3	24A
C	1450	0.62	85	Spinneret A	20.	63C
	1250	1.03	58	Spinneret B	1.5	31B
	1800	1.48	50	EC fritted glass	4.0	35C
D	1110	0.92	27	Spinneret A	1.5	23B
	1430	1.17		EC fritted glass	2.9	24B
E	1450	0.96	27	Spinneret A	5.0	27A
		1.17		EC fritted glass	7.1	26B
E	1700	1.38	27	Spinneret A	4.2	28B
	2400	0.99	19	EC fritted glass	3.1	26A
F	1100	1.01	85	Spinneret A	1.1	54B
	1200	1.06		Spinneret A	2.4	55B
	1300	1.06		Spinneret A	3.1	47B
	1100	2.73		EC fritted glass	10.	44C
	1800	2.28		EC fritted glass	5.8	44B
G	1250	1.08	27	Spinneret A	19.	29C
	1100	1.17		Spinneret B	19.	32C
G	1250	1.08	52	Spinneret A	1.5	29A
	1100	1.17	57	Spinneret B	2.2	32A
B	450	1.16	60	Spinneret A	2.2	14C
C	400		85	EC fritted glass	6.3	64A
A	452	1.73	45	Micrometallic D	4.7	13E
	250	2.23		Micrometallic D	5.6	13A

were never measured experimentally. Channeling and back mixing were prevalent for all spargers at high liquid flow rates, and the effects of liquid distribution were more important than those from the spargers used. The foam from the Micrometallic D sparger was much less uniform than that from any of the other three spargers, and it was difficult to maintain countercurrent flow without large voids for the low gas and liquid rates used.

The most important property of the gas sparger with respect to HTU_x values was the ability to give a uniform bubble size. Any lack of uniformity makes the foam less stable and favors the growth of large bubbles and the loss of surface area in an exponential manner. The larger surface area per volume of foam should give smaller HTU_x values for smaller bubble diameters, but this decrease was never realized due to increased channeling and back-mixing for the spargers which gave smaller bubbles. The foam density decreases as the bubble diameter increases; density differences can cause unequal linear foam velocities or actual inversion of volumes of foam when regions of differring bubble size are present in a column. The need for uniform bubble sizes increases as the column length or diameter increase. Since decreases in bubble uniformity are self-catalytic, the longer residence times in longer columns require more stable foams. The channeling effects caused by differences in foam density are more important in larger columns where the wall effects and the pressure drop due to foam flow are smaller.

VII-2 Effect of Liquid Feed Distributors on HTU_x Values

Eight liquid feed distributors were made (Table XII), of which six were used for HTU_x determinations (Table XVIII). The experimentally measured HTU_x values confirm the visually observed effects described in Section VI-II. If the liquid is uniformly distributed and introduced at low velocities into a uniform foam, the tendency to channel is minimized and is not excessive for liquid flows as high as 160 gal/ft^2·hr. The observed HTU_x values increased for either poor distribution or excessive velocities of the feed liquid.

The C spider distributor with 0.240-cm-ID capillaries gave the lowest HTU_x values, in agreement with the best visually observed performance. It gave a relatively uniform distribution of liquid throughout the flow range optimum for the 6-in.-diam column. The effects of the high inlet liquid velocity were noticeable for the B spider even at the relatively low total liquid flow rate of 500 cc/min. The effects of poor liquid distribution are apparent from the HTU_x values for the D and F distributors at flows below 1100 cc/min and for the E distributors for all flows tested (Table XVIII). As the liquid flow rate is increased over 1100 cc/min, the HTU_x values for the C distributor increase due to high exit velocities, while those for the F and and D distributors decrease due to more uniform distribution of the liquid. The poor distribution by the E (weir type) distributor at all flows up to 4000 cc/min (Table XIV) is the reason for the higher HTU_x values for this distributor. These effects are more clearly shown by a tabulation, with flow rates as the primary independent variable (Table

TABLE XVIII

EFFECT OF LIQUID FEED DISTRIBUTOR ON FOAM COLUMN HTU_x VALUES

Gas Sparger	Liquid Feed Rate, L + E (cc/min)	Phase Flow Ratio, $\frac{\alpha V + E}{L + E}$ (cm^{-1})	Column Length, Z (cm)	Liquid Feed Distrib.	HTU_x (cm)	Liquid Inlet Velocity (cm/sec)	Run No.
Spinneret A	500	1.06	28	B	5.0	63	16C
		1.21	27	C	2.8	26	17C
		1.10		D	8.2	7	23C
	500	1.16	60	B	2.2	63	14C
		1.43	85	C	small	26	63A
	1000	0.89	27	C	1.4	53	17E
	1100	0.92		C	< 0.5	58	22B
		0.92		D	1.5	15	23B
		0.94	29	E	14.	18	25B
	1250	1.08	27	G	19.	21	29C
	1450	0.77	27	C	< 0.5	76	22A
		0.77		D	1.5	19	23A
		0.96		E	5.0	24	27A
	1250	1.08		G	19.	21	29C
	1700	1.65	50	E	7.0	28	28A
	1300	1.06	85	F	3.1	28	47B
	1700	1.65	52	G	18.	28	29B
Spinneret B	1100	1.17	27	C	1.8	58	30B
				F	4.0	23	33A
				G	19.0	18	32C
	1450	1.13	27	C	1.8	76	30C
				F	2.1	31	33C
	1250	1.03	58	C	1.5	66	31B
	1100	1.17	57	G	2.2	18	32A
EC fritted glass	900	0.92	27	C	2.5	47.	21B
	750	1.25		D	5.2	10.	24C
	1430	1.17	27	D	2.9	19.	24B
				E	7.1	24.	26B

TABLE XIX

EFFECT OF GAS FLOW RATE OR PHASE FLOW RATIO ON FOAM COLUMN HTU_x VALUES

Gas Sparger	Liquid Feed Distr.	Liquid Feed Rate, L + E (cc/min)	Column Length, Z (cm)	Gas Flow Rate, V/A (cc/min)	Phase Flow Ratio, $\frac{\alpha V + E}{L + E}$ (cm^{-1})	HTU_x (cm)	Run No.
Spinneret A	B	450	60	900	1.16	2.2	14C
				1,260	1.47	4.9	14B
	B	500	10	640	0.77	5.9	15B
			14	870	1.06	4.8	16B
	B		20	640	0.77	8.3	15C
			28	870	1.06	5.0	16C
	C	1,000	27	1,770	0.89	1.4	17E
		1,100	27	2,180	0.92	< 0.5	22B
	E	1,100	29	2,400	0.94	14.	25B
		1,000	27	4,500	1.40	5.6	27B
	E	1,460	27	4,500	0.96	5.0	27A
		1,700	27	10,000	1.38	4.2	28B
	F	900	85	2,700	1.17	3.1	47C
		1,200		4,100	1.06	2.4	55B
		1,300		4,800	1.06	3.1	47B
EC fritted glass	D	750	27	960	1.25	5.2	24C
				1,130	1.47	5.1	24D
	D	1,430	27	1,860	1.17	2.9	24B
				2,180	1.29	2.3	24A
	F	1,100	85	1,900	1.50	10.	44C
				4,000	2.41	10.	44A

XX), rather than by the tabulation with the distributors as the variable (Table XVIII).

The single tube, distributor G, showed a very interesting effect (Table XXI). Channeling was very pronounced for about 1 ft below this nozzle, with only 1-1/2 transfer units for 27-cm column lengths. For the 1100 or 1250 cc/min flow rates, the bottom half of the 52- to 57-cm columns apparently gave very good countercurrent contact, with about 1-cm HTU_x values. A single run at a 1700 cc/min flow rate only gave 2.9 transfer units. These results show that the foam causes a uniform distribution of liquid at low liquid flow rates (less than 100 gal/$ft^2 \cdot hr$) and that the liquid distribution in large columns might be partly effected by allowing an extra length of countercurrent flow.

VII-3 The Effects of Foam Flow Rates on HTU_x Values

Increasing the gas flow rates or increasing $(\alpha)(V/L)$ decreased the HTU_x values (Table XIX). This is consistent with the more uniform plug flow of foam observed visually for increased gas flow rates. The foam density and the liquid holdup time increase as the gas rate is increased. The range of gas rates for which comparison of HTU_x values is possible is small because of the decreasing accuracy of the HTU_x determinations as $(\alpha)(V/L)$ decreases below 1 or increases above 1.5.

VII-4 The Effects of Liquid Feed Rates on HTU_x Values

The effects of liquid rates on HTU_x values is a complex combination of effects from channeling, from liquid feed distribution difference and from liquid holdup times, and these can only be partially

TABLE XX

EFFECT OF LIQUID FEED RATE ON FOAM COLUMN HTU_x VALUES

Gas Sparger	Liquid Feed Distrib.	Phase Flow Ratio, $\frac{\alpha V + E}{L + E}$ (cm^{-1})	Column Length, Z (cm)	Liquid Flow Rate (cc/min)	HTU_x (cm)	Run No.
Spinneret A	C	1.21	27	500	2.8	17C
		1.10		500	1.4	22C
		0.96		750	1.7	17A
		0.89		1000	1.4	17E
		0.92		1100	< 0.5	22B,22D
		0.77		1450	< 0.5	22A
	D	1.10	27	500	8.2	23C
		0.92		1100	1.5	23B
		0.77		1450	1.5	23A
	E	1.40	12	1000	4.0	27C
		1.38	13	1700	3.7	28C
		0.71	13	2000	2.1	25C
	E	1.40	27	1000	5.6	27B
		1.38		1700	4.2	28B
	F	1.85	85	600	9	54A
		1.30		800	~ 5	55A
		1.17		900	3.1	47C
		1.01		1100	1.1	54B
		1.06		1200	~ 2.4	55B
		1.06		1300	3.1	47B
	G	1.08	52	1250	1.5	29A
		1.65		1700	18.	29B
Spinneret B	C	1.08	27	750	0.5	30A
		1.17		1100	1.8	30B
		1.13		1450	1.8	30C
		1.06	23	2000	0.5	31D
	F	0.98	27	825	1.5	33B
		1.17		1100	4.0	33A
		1.13		1450	2.1	33C
		1.18		1800	2.5	33D

TABLE XX (continued)

Gas Sparger	Liquid Feed Distrib.	Phase Flow Ratio, $\frac{\alpha V + E}{L + E}$ (cm^{-1})	Column Length, Z (cm)	Liquid Flow Rate	HTU_x (cm)	Run No.
	G	1.17	57	1100	2.2	32A
		1.06	54	2000	1.1	32B
EC fritted glass	C	3.56	50	750	7.1,6.6	35A,36A
		2.42		1100	6.0,5.7	35B,36B
		1.48		1800	4.0,5.5	35C,36C
	D	1.25	27	750	5.2	24C
		1.29		1430	2.3	24A
	E	1.17	27	1430	7.1	26B
		0.99	19	2400	3.1	26A
	F	2.73	85	1100	10.	44C
		2.28		1800	5.8	44B

TABLE XXI

EFFECT OF COLUMN LENGTH ON FOAM COLUMN HTU_x VALUES

Gas Sparger	Liquid Feed Distrib.	Liquid Feed Rate, L + E (cc/min)	Phase Flow Ratio, $\frac{\alpha V + E}{L + E}$ (cm^{-1})	Column Length, Z (cm)	HTU_x (cm)	Run No.
Spinneret A	B	500	0.77	10	5.9	15B
			1.06	14	4.8	16B
			1.06	28	5.0	16C
			1.33	60	5.5	14A
	C	500	1.10	27	1.4	22C
			0.81	85	small	63A
		1450	0.77	27	< 0.5	22A
			1.10	85	20.	63C
	E	1000	1.40	12	4.0	27C
				27	5.6	27B
		1460	0.96	13.5	5.0	27D
				27	5.0	27A
		1700	1.38	13	3.7	28C
			1.38	27	4.2	28B
			1.65	50	7.0	28A
	G	1250	1.08	27	19.	29C
				52	1.5	29A
Spinneret B	C	1100	1.17	27	1.8	30B
				59	3.3	31A
		1450	1.13	27	1.8	30C
		1250	1.03	58	1.5	31B
	G	1100	1.17	27	19.	32C
				57	2.2	32A
EC fritted glass	C	900	0.92	27	2.5	21B
		1100	2.42	50	6.0	35B
	F	1100	2.41	85	10.	44A
	E	2400	0.98	12	3.0	26C
			0.99	19	3.1	26A

separated from the effects of foam flow rates. Visual observations and HTU_x results indicated that channeling was not excessive for liquid flows of up to 160 gal/ft·hr if the liquid was uniformly distributed at low velocities into a uniform foam. These conditions were met for the spinneret gas spargers for the F spider for flows over 900 cc/min and for the C spider at all flows. Increasing gas flow rates gave significant decreases in HTU_x values for otherwise constant conditions. These two effects probably account for most of the variations from liquid flow rate variations (Table XX). From visual observation of the columns, it is believed that increased channeling and increased HTU_x values are probably unavoidable no matter how good the liquid distribution for flows over 2000 cc/min or 160 gal/ft^2·hr. Flooding at about 200 gal/ft^2·hr was indicated by the drainage model (Figure 5). Due to the flow rates possible with the gravity feed systems as installed, and the poor performance (poor distribution or excessive foam breaking) of all of the feed distributors for flows over 2000 cc/min, none of the runs show high HTU_x values due to high liquid rates, independent of all other factors. The only conditions that might have shown this would have been the F distributor and the B spinneret at 2200-2400 cc/min liquid flow; this latter condition was not tested because of the channeling observed for lower flows for runs 33C and 33D (Table XX).

VII-5 The Effects of Column Length on HTU_x Values

The experimental results for the effect of column length (Table XXI) show the following:

1. There is little variation in HTU_x with column length for countercurrent lengths of 10 to 28 cm.
2. If the liquid distribution is not uniform at the feed point, there may be a length of inefficient countercurrent contact just below the feed point in which the foam acts to distribute the liquid. Then efficient contact with low HTU_x values may be obtained below this region. This is clearly shown for the single-tube liquid feed distributor G (Table XVIII).
3. The HTU_x values for 50-, 60-, or 85-cm countercurrent lengths are determined with poor accuracy; measurement of more than 8 to 10 transfer units is difficult. The HTU_x for these long columns (compared with 27-cm lengths at similar conditions) are larger for about two-thirds of the determinations and smaller for about a third.

The main costs of a foam column would be in end sections and accessory equipment; increasing the countercurrent section length requires only tank walls. Therefore, whether the conservative design value should be 5 cm or 10 cm per transfer unit is probably of little economic importance.

VII-6. Diffusion, HTU_x Values, and Adsorption Rates

If the mass transfer is diffusion controlled, as indicated by the low Reynolds number of the liquid between foam bubbles, the heights of transfer units could be estimated from liquid diffusivities. The effects of gross turbulence, that is, channeling, will be to increase

HTU_x values above those predicted from diffusion. The rates of adsorption on newly created bubbles can also be estimated by use of diffusion coefficients (see Chapter II).

For foam separation, we may assume that the mass transfer is diffusion controlled, with all the resistance in the liquid phase. (While a concentration gradient across a monomolecular layer does not appear possible, a film penetration or geometric effect could result in a film resistance.) The height of a transfer unit, HTU_x, is given by (15):

$$HTU_x = \frac{L'}{k_x aS} = \frac{L'\ell}{DaS} . \qquad (103)$$

From a simplified configuration for diffusion (see Section IV-5), the HTU_x values for these foam separation studies would be given by:

$$HTU_x = 3500\ Ld^2 ; \qquad (104)$$

$$\text{maximum value} = (3500)(0.2)(0.1)^2 = 7 \text{ cm} ,$$

$$\text{minimum value} = (3500)(0.02)(0.04)^2 = 0.1 \text{ cm} .$$

Using the conditions that gave the least channeling in the foam column:

$$HTU_x = (3500)(0.05)(0.10)^2 = 1.7 \text{ cm}.$$

This appears to confirm that the smallest HTU_x values obtained were approximately what would be expected for diffusion-controlled mass transfer in the liquid.

None of the measurements made were directly concerned with adsorption rates, but some interesting conclusions are possible. From the foam-density measurements for countercurrent flow, the liquid and

surface holdup times were always in excess of 2 sec per transfer unit. This time is larger than the times required to approach the equilibrium concentrations of surfactant on the surface, as indicated by either the theoretical or experimental adsorption models in the literature (see Chapter II). A second interesting result is shown by the pressure-drop-versus-flow-rate curves for the spinnerets (Figure 26). At all measurable flow rates, the pressure drop is the sum of the orifice frictional losses and the pressure necessary to overcome the surface tension of pure water. Only at flows of a few cubic centimeters per minute does the pressure drop show the low surface tension expected for dodecylbenzenesulfonate solution. The pressure drops for the spinneret with 50-μ-diam holes levels off at about 64 cm H_2O at low flow rates for discharge into either demineralized water or 300 ppm Trepolate F-95 in 10^{-3} M NaOH (Figure 26). At very low flow rates (below the 500 cc/min measurable by the rotameters used), the pressure drop for the DBS solution drops to 42 cm H_2O. The capillary pressures from the surface tensions would be:

$$h = 2\alpha/r\rho g \ .$$

$$\text{For pure } H_2O,\ h = \frac{(2)(73)(2)}{(980)(0.005)(1)} = 60 \text{ cm} .$$

$$\text{For } 7 \times 10^{-4} \text{ M DBS},\ h = \frac{(2)(42)(2)}{(980)(0.005)(1)} = 35 \text{ cm}.$$

The same effect was observed for the spinneret with 80-μ-diam holes, but not for the porous metal or glass spargers--probably because of their wide range of effective pore sizes. The flow rates corresponding to the low-pressure drop and surface tension would be on the order of

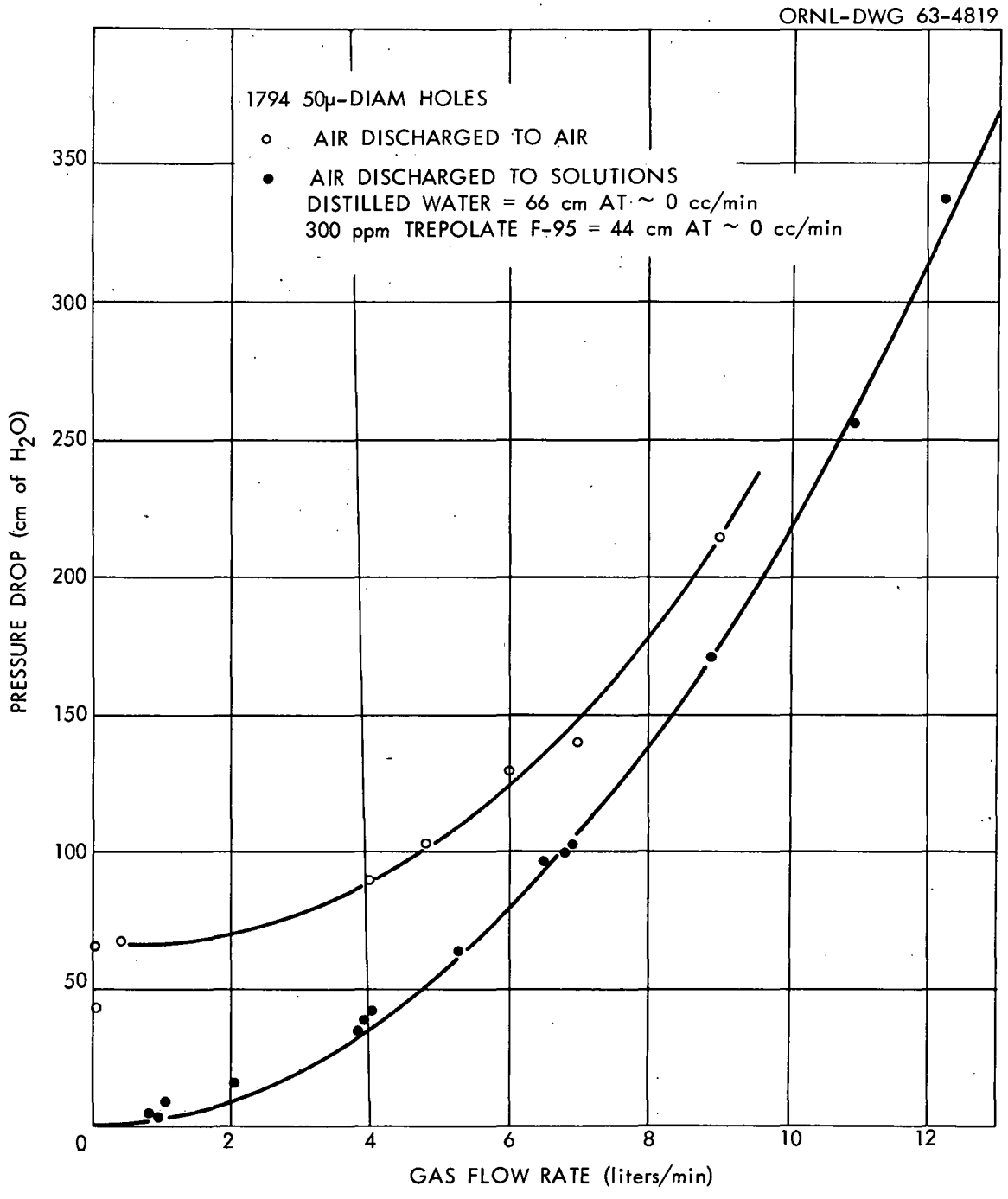

Figure 26. Pressure Drops for Air Flow through A Spinneret with 50-μ-diam Holes.

one bubble per hole per second. Actually when a bubble starts to form at a hole, it grows and releases in a fraction of a second. This indicates that adsorption occurs in less than a second, since the growth would be otherwise limited by adsorption. The 500-cc/min gas rate is about 50 bubbles per hole per second, and apparently adsorption to the surface is small in a fiftieth of a second.

CHAPTER VIII

APPLICATION OF FOAM SEPARATION COLUMNS TO LOW-LEVEL RADIOACTIVE WASTE

The initial application considered for foam separation columns was decontamination of Oak Ridge National Laboratory (ORNL) low-level waste (LLW), and brief engineering calculations and experiments were made to indicate the practicality of this approach. The calcium and magnesium content of this low-level waste determine the process flowsheet required and control the minimum costs and waste volumes possible. These engineering studies of low-level-waste decontamination were concerned with the interference of the calcium and magnesium, with minimizing the amount of surfactant required, and with evaluation of the process economics.

VIII-1 Interference from Nonradioactive Cations

The process flowsheet and the results for the application of foam separation to decontamination of ORNL low-level waste are largely determined by the nonradioactive calcium and magnesium present. This waste is essentially process water of about 30 ppm Ca^{2+}, 7 ppm Mg^{2+}, 7 ppm Na^{+}, and 100 ppm HCO_3^{-}, plus very low and variable concentrations of other solutes including detergents, chemical reagents, and radioactive Sr^{90} and Cs^{137}. Typical compositions of ORNL process water (Table XXII) and of the LLW radioactivity (Table XXIII) have been reported (8,11,12,34).

Removal of the calcium and magnesium by precipitation followed

TABLE XXII

COMPOSITIONS OF ORNL TAP WATER AND LOW-LEVEL-WASTE (LLW)

Constituent	Concentrations (ppm)		
	Typical Tap Water (34)	Tap Water (8)	LLW Water (8)
Total hardness	-	87	94
Dissolved CO_2	-	1.8	10.6
Total solids	-	84.2	183.
Uranium	-	< 0.003	0.01
PO_4	-	< 0.02	3.3
HCO_3^-	100	-	-
CO_3^{2-}	< 0.5	-	-
Ca^{2+}	27	-	-
Mg^{2+}	7	-	-
Na^+	7	3.	30.
F^-	-	1.	7.
Cl^-	1.5	1.1	4.9

TABLE XXIII

AVERAGED RADIOCHEMICAL ANALYSES OF ORNL LOW-LEVEL WASTE SAMPLES OVER AN EIGHT-MONTH PERIOD

Constituent and/or Type of Radioactivity	Equivalent Activities[a] Units	Amount	Percent of MPC_w[b,c]
Gross beta	counts min^{-1} ml^{-1}	36.2	-
Gross alpha	counts min^{-1} ml^{-1}	88.5	-
Sr^{90} beta	dis min^{-1} ml^{-1}	86.4	3891.
Co^{60}	dis min^{-1} ml^{-1}	130.2	12
Ru^{106}	dis min^{-1} ml^{-1}	7.7	4
TRE[d]	counts min^{-1} ml^{-1}	9.3	14
Cs^{137}	dis min^{-1} ml^{-1}	54.4	12
$Zr\text{-}Nb^{95}$	counts min^{-1} ml^{-1}	< 2.3	-

[a] From ORNL-3349 (12), Table 2.2.

[b] From ORNL-3349 (12), Table 2.3.

[c] Maximum permissible concentration for water based on continuous occupational exposure for a 168-hr week.

[d] Total rare earths.

by foam separation appears to be the only practical procedure for LLW decontamination by foam separation. A compound which formed a surface-active complex of strontium in preference to calcium or magnesium would give the best process, but no significant selectivity was found for any of the compounds tested in laboratory studies. Removal of all the calcium, magnesium, and strontium by foam separation would require excessive amounts of surfactant and surface per volume of liquid. The use of EDTA (ethylenediaminetetracetic acid) to preferentially complex calcium in a non-surface-active form was tested in laboratory studies (34). This procedure did not appear promising since the Ca^{2+} was approximately 85% complexed, and the cost of the EDTA necessary was prohibitive. The magnesium can be precipitated as $Mg(OH)_2$, and the calcium as $CaCO_3$ or $Ca_3(PO_4)_2$. The costs of NaOH, Na_2CO_3 or Na_3PO_4, and flocculating agents such as ferric compounds would be 15¢ to 40¢ per 1000 gal, depending on the flowsheets used.

The addition of 5×10^{-3} M NaOH and 5×10^{-3} M Na_2CO_3 to process water plus Sr^{89} resulted in the precipitation of $CaCO_3$ and $Mg(OH)_2$. When this slurry was used as foam column feed for run 38, strontium decontamination factors (DF's) were 81 to 162 (Table XXIV). This result shows that the removal of a precipitated solid by the foam concurrent with separation of a surface-active complex is possible. The smaller DF's, compared with those for runs with a demineralized water feed, would be expected since the presence of soluble calcium and magnesium reduces Γ/c for strontium.

The remaining three runs were made with 10 ppm of FAB added to

TABLE XXIV

DECONTAMINATION OF SIMULATED LOW-LEVEL WASTE IN THE 6-IN.-DIAM FOAM COLUMN

Surfactant: Dodecylbenzenesulfonate added to liquid pot as Trepolate F-95
Feed: Process water with following sequence of additions with mixing: Fab (when used); Sr^{89} tracer; precipitating reagents as one concentrated, mixed solution
Column conditions: EC sintered glass gas spargers, C or F liquid feed distributors, 10.5-in.-ID drainage section

Quantity	Symbol	Units	Run Numbers											
			38A	38B	38C	39A	39B	39C	40A	40B	40C	41A	41B	41C
FAB added to feed	--	ppm	0	0	0	10	10	10	10	10	10	10	10	10
NaOH added to feed	--	10^{-3} M	5	5	5	5	5	5	4	4	4	5	5	5
Na_2CO_3 added to feed	--	10^{-3} M	5	5	5	5	5	5	0	0	0	5	5	5
PO_4^{3-} as Na_3PO_4	--	ppm	0	0	0	0	0	0	50	50	50	0	0	0
Precipitated $CaCO_3$ as slurry	--	10^{-3} M	0	0	0	0	0	0	0	0	0	5	5	5
Time from reagent addition to run	--	hr	24	25	26	3	4	5	3	4	5	3	4	5
Liquid rate in	$L + E_p$	cc/min	750	1,100	1,800	750	1,800	1,800	750	1,100	1,800	750	1,100	1,800
Gas rate	V/A_p	cc/min	4,100	4,100	4,100	4,100	4,100	5,800	4,100	4,100	4,100	5,700	4,100	4,100
Condensed foam rate	E_p	cc/min	16	17	19	18	19	47	16	15	23	30	13	20
Net liquid rate	L_p	cc/min	730	1,080	1,780	730	1,780	1,750	730	1,085	1,780	720	1,090	1,780
Surfactant concentration out (calculated)	--	ppm Trepolate	270	270	270	270	270	270	270	270	400	270	270	400
Countercurrent length	Z	cm	50	50	50	50	50	50	86	86	86	86	86	86
Surface area rate	V	10^5 cm^2/min	4.4	4.6	4.8	5.2	5.2	7.2	4.9	5.3	5.1	5.7	5.1	4.6
Surface/liquid ratio	V/L	cm^2/cc	600	430	270	710	290	410	670	480	290	790	470	260
Gross beta in liquid feed	x_2	counts min^{-1} cc^{-1}	9,200	9,200	9,200	9,200	9,200	9,200	8,200	8,200	8,200	8,800	8,800	8,800
Gross beta in liquid out	x_b (also x_1*)	counts min^{-1} cc^{-1}	57	89	114	4,960	4,600	3,600	4,100	4,600	3,500	6,700	7,500	7,400
Gross beta in condensed foam	$y_2V + x_2*E_p$	10^3 counts min^{-1} min^{-1}	6,760	10,150	15,400	1,700	4,200	7,000	2,670	2,800	2,000	1,300	1,000	1,300
Gross beta material balance	--	%	98	101	95	78	77	82	93	87	57	95	95	92
Decontamination factor	$DF = x_2/x_b$	dimensionless	162	103	81	1.9	2	2.6	2	1.8	2.3	1.3	1.2	1.2
Volume reduction	L/E_p	dimensionless	47	59	95	42	95	38	47	73	78	25	85	90

process water to simulate the detergent and total phosphate content of the low level waste. (FAB is one widely used detergent at ORNL.) While visible precipitation occurred within a minute after the addition of the NaOH and Na_2CO_3 to process water for run-38 feed, the addition of the same reagents to process water plus 10 ppm of FAB did not give any visible precipitation within 30 min. Decontamination factors in the foam column for the slurry feed containing FAB were less than 3 (run 39, Table XXIV). The precipitation and loss of Sr^{89} from solution continued in the samples of column effluent. The same low DF's with precipitation in the column effluent occurred when 50 ppm of PO_4^{3-} plus 4×10^{-3} N NaOH (run 40) or 5×10^{-3} N NaOH, 5×10^{-3} M Na_2CO_3 and 5×10^{-3} M precipitated $CaCO_3$ as a seed slurry (run 41) were used to precipitate the calcium and magnesium. From these results, it appears that the foam column could handle precipitated $CaCO_3$ and $Mg(OH)_2$ concurrently with the foam separation of strontium. However, the precipitation of the calcium and magnesium by simple mixing of the low-level waste with reagent solutions was too slow to permit practical holdup times for a full-scale waste-treatment plant.

The chemistry of these kinetic and supersaturation effects for the precipitation of $CaCO_3$ in LLW were extensively investigated as part of the foam separation laboratory studies (7,31). Commercial detergents such as FAB and Turco 4234, and the polyphosphates which are used as builders in commercial detergents, inhibited the precipitation of $CaCO_3$ (31). The best results were obtained by the addition of 5×10^{-3} M NaOH, 5×10^{-3} M Na_2CO_3, and 2 to 5 ppm of ferric ion to the ORNL LLW as

it was fed to a single-chamber agitated-bed contactor. These conditions seemed to minimize the deleterious effects of the varying LLW contaminants on the precipitation. The bed of precipitate materials appeared to provide surfaces on seed crystals to start the precipitation and reduced the supersaturation effects which otherwise occurred. The bed effluents were 2.1 to 4.5 ppm total hardness, expressed as $CaCO_3$ (7).

Two runs were made with process water plus Sr^{89} to simulate low-level waste in the 6-in.-diam foam column in which the slurries were precipitated by the addition of 4×10^{-3} N NaOH, 50 ppm of PO_4^{3-} as Na_3PO_4 solution, and 10 ppm of Fe^{3+} as $FeCl_3$ solution were fed to the foam column. For the second run, 10 ppm of FAB commercial detergent were added prior to the precipitation to simulate low-level-waste impurities.

Decontamination factors for strontium for these runs were 19 to 52, without any consistent variation from the addition of 10 ppm of FAB (Table XXV). When the same precipitation conditions were used in beakers and samples were taken through fine filter paper, the strontium decontamination factors were about 7 in 10 min and about 10 in 2 or 68 hr. The decontamination factors for the precipitation of $Ca_3(PO_4)_2$ were probably controlled by the incomplete flotation of the precipitate. For the runs without the ferric ion as a flocculant (run 40A, 40B, 40C, Table XXIV), the effluent was very hazy, and the DF's were only 1.8 to 2.3. The effluent was slightly hazy at times for the runs with the flocculant; the DF's would have been limited to 20 to 50 if 2 to 5%

TABLE XXV

DECONTAMINATION OF SYNTHETIC LOW-LEVEL WASTE IN A 6-IN.-DIAM-FOAM COLUMN

Surfactant: Dodecylbenzenesulfonate added as Trepolate F-95 to the column liquid pot
Feed: Process water for run 51, process water plus 10 ppm FAB for run 52 plus chemicals as listed
Column Conditions: 85-cm countercurrent length, F liquid distributor, 10.5-in.-diam drainage section, EC fritted glass gas spargers
Zero time: Start of feed at conditions listed

Quantity	Symbol	Units	Run Number 51A	51B	51C	52A	52B	52C
Time of addition of $4 \cdot 10^{-3}$ M NaOH and 50 ppm $PO_4^{\equiv}$	--	min	-20	-120	-200	-15	-115	-195
Time of addition of 10 ppm Fe^{+3} as $FeCl_3$ solution	--	min	-15	-115	-195	-10	-110	-190
Liquid rate in	$L + E_p$	cc/min	600	1100[a]	600[a]	600	1100	600
Condensed foam rate	E_p	cc/min	18	40[a]	21[a]	20	33	10
Net liquid rate	L_p	cc/min	580	1060	580	580	1070	590
Surfactant concentration out	--	ppm	220	310	220	230	360	230
Gas rate	V/A	cc/min	4100	4600	4100	4100	4100	4100
Surface rate	V	10^5 cm^2/min	4.8	4.8	4.8	4.8	4.8	4.8
Surface.liquid ratio	V/L	cm^2/cc	830	450	830	830	450	810
Gross beta in liquid feed	x_2	counts min^{-1} cc^{-1}	8200	8200[a]	8200[b]	9300	9300	9300[b]
Gross beta in liquid out	x_B (also x_1*)	counts min^{-1} cc^{-1}	410	300[a]	290[a,b]	400	500	180[b]
Gross beta in condensed foam	$y_2V + x_2^* E_p$	10^3 counts min^{-1}	2700	5800[a]	1600[a,b]	4600	5500	1200[b]
Gross beta material balance	--	min^{-1} %	60	68[a]	37[a,b]	87	59	23[b]
Decontamination factor	DF	dimensionless	20	27	28	23	19	52
Volume reduction	VR	dimensionless	33	28	29	29	31	59

[a]An accumulation of nonmoving foam and solids started in the foam breaker during run 51B and increased until the end of run 51. This partially explains the lower volume reductions and material balances.

[b]The liquid level in the feed tank dropped below the agitator level during 51 C and 52C. This results in a short period of high concentration of solids in the feed to the column followed by a relatively low slurry concentration.

of the precipitated solids had not been removed.

Several undesirable effects of the precipitated solid on foam column operation were noted. Visible areas of foam downflow at the wall were slightly more numerous, much more persistent, and existed over longer lengths of column. The volumes of condensed foam for these slurry feed runs were two to three times the volumes for solid-free runs at similar conditions. During run 51B, an accumulation of stationary foam and solids started in half of the 10.5-in.-ID drainage section. This accumulation increased until only half of the drainage section showed visible flow of foam by the end of run 51C. When the foam collapsed after the column was shut down, gram quantities of solids as agglomerates up to 1/4 in. across fell to the bottom of the column. The volume reductions practical when the calcium and magnesium precipitates are fed to the foam column are probably only about a tenth of the maximum volume reductions practical if nearly all the precipitates are removed as a pretreatment.

Two periods of high solids concentration probably account for the poor material balances of runs 51 and 52 (Table XXV). The analyses are for steady-state operation after an initial period to allow the column to come to steady state. The feed tank is a conical-bottom drum, with an agitator near the conical-cylindrical intersection. The feed leaves through the bottom of the cone. Some solids settle in spite of the gentle agitation, and this results in a high solids concentration during the unsteady-state part of runs 51A or 52A. When the liquid level drops below the agitator level, the remaining solids tend

to settle out and give a short period of high solids concentration during the non-steady-state parts of runs 51C or 52C. Thus the liquid feed has a below-average concentration of precipitated solids during the steady-state parts of 51A, 51B, 52A, and 52B and a low concentration of precipitated solids during the steady-state parts of 51C and 52C.

Decontamination of Clarifier Effluent. Several runs were made in order to determine strontium decontamination factors in the 6-in.-diam foam column for low-level waste that had been passed through the laboratory-scale clarifier to precipitate calcium and magnesium. This clarifier can reduce the hardness from about 100 ppm to 2 to 4 ppm (as $CaCO_3$) (7). While 100-ppm hardness would require an excessive amount of surfactant and surface per volume of liquid, good decontamination for strontium, calcium, and magnesium should be practical for hardnesses of 2 to 4 ppm.

Effluent from the 9-in.-diam clarifier as operated on low-level waste in Building 2528 (7) was used for foam column feed after the addition of Sr^{89} and dodecylbenzenesulfonate. The clarifier effluent was collected during 24-hr periods of operation with intermittent attention and appeared to be free of either suspended or settled solids. The foam column conditions and procedures used were similar to those previously used to obtain low HTU_x values except the surface/liquid volume ratio was increased to favor high decontamination.

Decontamination factors for strontium were 24 or greater for one countercurrent run (Table XXVI) and two batch runs to determine (Γ/c)

TABLE XXVI

EXPERIMENTAL DATA AND CALCULATIONS FROM CONTINUOUS COUNTERCURRENT STRIPPING OF STRONTIUM FROM LOW-LEVEL-WASTE CLARIFIER EFFLUENT

Gas sparger: EC porosity fritted glass
Strontium distribution coefficient: $1.7 \cdot 10^{-3}$ cm

Quantity	Symbol	Units	Run Number 57A	57B
Liquid feed distributor	--	--	F	F
Countercurrent length	Z	cm	85	85
Liquid feed rate	$L + E_p$	cc/min	400	800
Condensed foam rate	E_p	g/min	9	12
Net liquid rate	L	cc/min	390	790
Gas rate	V/a	cc/min	4000	4000
Bubble diameter (area average)	$D/\sqrt{n}$	mm	--	--
Surface area rate	V	10^5 cm^2/min	4.8	4.8
Surfactant rate in condensed foam	--	mg/min	--	--
Surfactant concentration in effluent liquid	--	ppm	190	190
Phase flow ratio	$(\alpha V + E)/(L + E)$	dimensionless	2.06	1.03
Gross beta in liquid feed	x_2	counts min^{-1} cc^{-1}	3400	3400
Gross beta in effluent liquid	X_B (also X_1*)	counts min^{-1} cc^{-1}	140	240 to 1100
Gross beta in condensed foam	$y_2V + X_2{}^*E_p$	10^3 counts min^{-1} min^{-1}	1310	2100
Gross beta material balance	--	%	101	90 to 120
Decontamination factor	$DF = X_2/X_B$	dimensionless	24	3-15
Volume reduction	$VR = (L + E)/E_p$	dimensionless	45	65

for strontium (Table XXVII). The same lot of clarifier effluent was used for batch run 56 and the continuous countercurrent runs, 56A and 56B. The variable effluent concentrations of 56B might be explained by the effects of small flow variations since $(\Gamma/c)_{Sr}\, V \simeq L$. The conditions of 56A should have provided for more than 10 transfer units and a strontium decontamination factor greater than 300.

The strontium decontamination factors for the other continuous countercurrent runs were low, being 2 to 4 (Table XXVIII). Since previous results showed that a large number of transfer units (more than 10) are obtained for this column, these low decontamination factors must be the result of "pinching" of the operating and equilibrium lines at the feed point. The surface and liquid must be close to equilibrium at this point, and the distribution coefficient for strontium, $(\Gamma/c)_{Sr}$, can be calculated from material balances:

$$\left(\frac{\Gamma}{c}\right)_{Sr} = \left(1 - \frac{x_B}{x_2}\right)\frac{L}{V} \text{ or } \left(\frac{\Gamma}{c}\right)_{Sr} = \frac{[Vy_P + E_P x_2^*]}{Vx_2} - \frac{E_P}{V}, \qquad (128)$$

where

x_2 = the feed liquid concentration,

x_B = the effluent liquid concentration,

L = the net liquid flow down the column,

V = the surface flow up the column,

E_P = the volume flow rate of condensed foam,

$[Vy_P + E_P x_2^*]$ = the solute (i.e., Sr^{89}) effluent rate as condensed foam.

TABLE XXVII

DETERMINATION OF Γ/c FOR STRONTIUM BY BATCH RUNS
ON LOW-LEVEL-WASTE CLARIFIER EFFLUENT

Gas Sparger: A spinneret with 50-μ holes
Strontium Concentration: 5 mc of Sr^{89} tracer only
Gross beta half-lives in solution: From Figure 27

Quantity	Units	Run Number 49	56A	56B
Trepolate F-95 concentration	ppm	330	330	~ 220
Gas rate, V/a	cc/min	2,100	2,100	4,800
Surface area rate, V	10^5 cm^2/min	1.8	1.8	2.5
Liquid volume in column	cc	14,800	9,900	9,200
Gross beta half-life in liquid, $t_{\frac{1}{2}}$	min	37	22	16
$\frac{\Gamma}{c} = \left(\frac{0.693}{t_{\frac{1}{2}}}\right)\left(\frac{\text{volume}}{V}\right)$	10^{-3} cm	1.5	1.7	1.6
Gross beta half-life of cond. foam rate, $t_{\frac{1}{2}}$	min	42	--	--
$\frac{\Gamma}{c} = \left(\frac{0.693}{t_{\frac{1}{2}}}\right)\left(\frac{\text{volume}}{V}\right)$	10^{-3} cm	1.4	--	--
Maximum gross-beta DF	dimensionless	27	42 for whole run	

TABLE XXVIII

DETERMINATION OF (Γ/c) FOR STRONTIUM BY CONTINUOUS COUNTERCURRENT RUNS WITH "PINCHING" AT THE FEED POINT

Quantity	Symbol	Units	Run Numbers 45A	45B	45C	46	53A	53B
Strontium concentration	--	10^{-6} M	tracer	tracer	tracer	tracer	tracer	tracer
NaOH concentration added	--	M	0.001	0.001	0.001	none	none	none
Effluent Trepolate F-95 concentration	--	ppm	260	260	260	260	380	220
Gas sparger used	--	--	A Spin	A Spin	A Spin	EC glass	EC glass	EC glass
Countercurrent column length	z	cm	85	85	85	85	85	85
Estimated number of transfer units[a]	N_x	dimensionless	20	20	20	8	8	8
Liquid feed rate[b]	$L + E_p$	cc/min	900	900	1,200	600	600	600
Condensed foam rate	E_p	cc/min	7	3	10	19	16	8
Net liquid rate	L	cc/min	890	900	1,190	580	585	590
Gas rate	V/a	cc/min	4,700	2,900	5,700	4,000	4,000	4,000
Surface area rate	V	10^5 cm^2/min	2.5	2.0	2.8	4.8	4.8	4.8
Gross beta in liquid feed	x_2	counts min^{-1} ml^{-1}	9,400	9,400	9,400	11,500	11,500	11,500
Gross beta in effluent liquid	x_B	counts min^{-1} ml^{-1}	5,400	5,950	5,600	2,800	3,350	5,100
Gross beta in condensed foam	$y_2V + x_2 * E_p$	10^3 counts min^{-1} min^{-1}	5,200	3,450	6,500	5,300	3,600	3,300
Gross beta material balance	--	%	118	104	117	100	81	87
Γ/c for strontium from x_2 and x_B	$(\Gamma/c)_{Sr}$	10^{-3} cm	1.5	1.7	1.7	0.9	0.9	0.7
Γ/c for strontium from x_2 and $[Vy_2 + x_2 * E_p]$	$(\Gamma/c)_{Sr}$	10^{-3} cm	2.2	1.8	2.4	0.9	0.6	0.6
Decontamination factor	$DF = x_2/x_B$	dimensionless	1.7	1.6	1.7	4.1	3.5	2.3

[a] Number of transfer units for similar conditions with demineralized water.

[b] Feed Solution: LLW clarifier effluent (as collected in Building 2528).

Distribution coefficients estimated by this procedure vary from (0.6--1.8) x 10^{-3} cm (Table XXVII). This variation is probably due to a variation in the calcium and magnesium concentrations in the clarifier effluent. Analyses of calcium, magnesium, and total hardness at these concentrations in the presence of 0.01 N sodium and variable low-level-waste impurity concentrations is difficult. Analyses reported for these effluents are shown along with the runs for which they were used (Table XXIX). Except for batch C, the clarifier effluents were partly collected during periods of unattended operation and short periods of poor operation could have occurred without detection.

The strontium distribution coefficients of (1.4--1.7) x 10^{-3} cm determined by batch tests with clarifier effluent (Figure 27, Table XXVII) agreed with that from continuous countercurrent runs (Table XXX). Batch charges were foamed and the distribution coefficient calculated from the slope of the concentration-vs-time curve by assuming one theoretical stage. These values agreed with those reported for about 5 ppm Ca^{2+} in laboratory studies.

These results indicate strontium distribution coefficients (1.4--2) x 10^{-3} for the effluent of the clarifier as usually operated on low-level waste. This coefficient did not vary as the strontium was removed during two batch foamings. The decontamination of strontium was much less for a continuous countercurrent run than would be expected for the $(\Gamma/c)_{Sr}$ and the conditions used. This result could be explained by the existence of a strontium complex of low surface activity which is slowly converted to the dodecylbenzenesulfonate

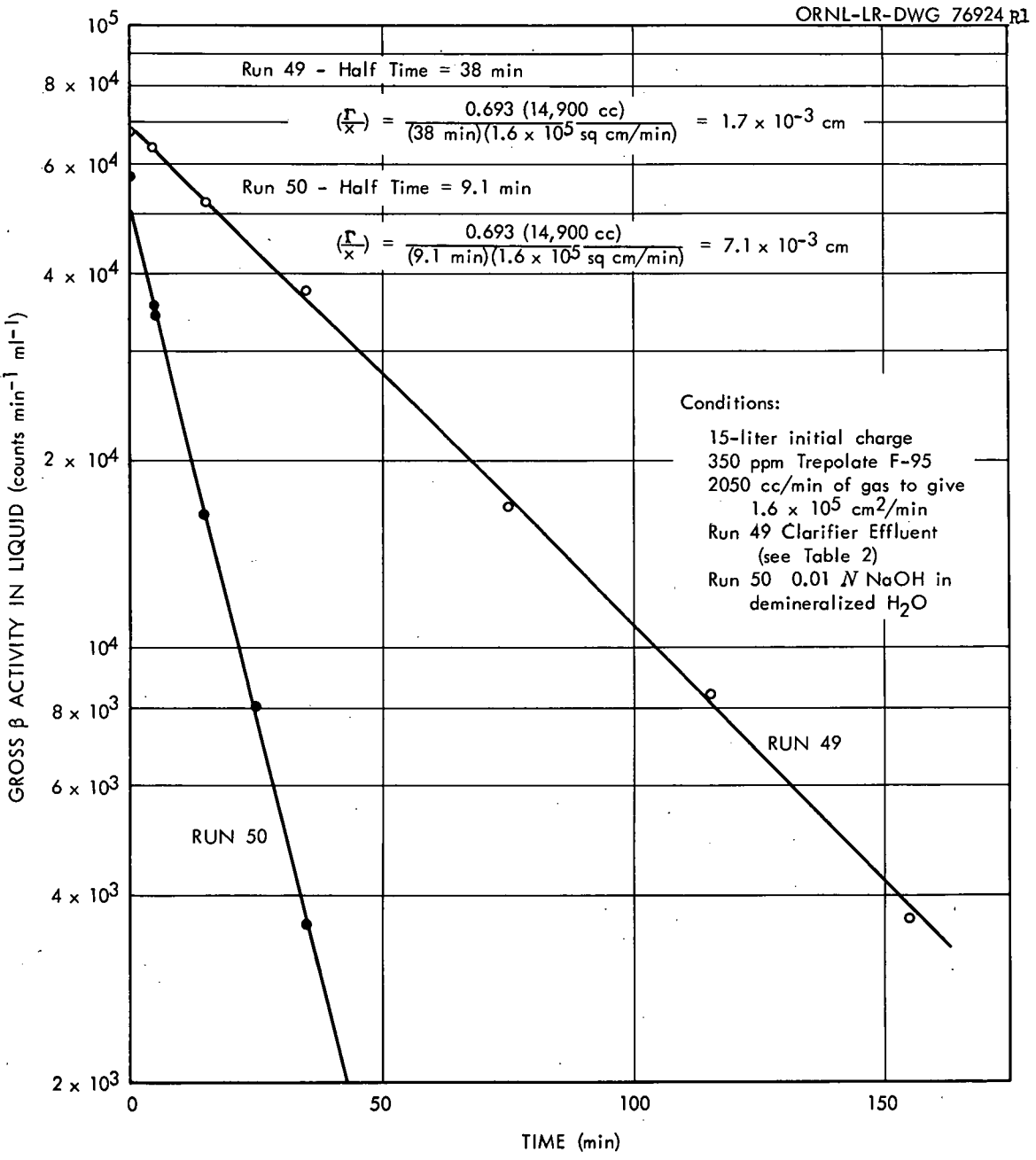

Figure 27. Batch Determinations of $(\Gamma/x)_{SR}$ for 350-ppm Trepolate F-95.

TABLE XXIX

CONSTITUENTS OF CLARIFIER EFFLUENTS

Drum Designation	When Collected	Volume (liters)	Concentrations of Constituents		
			ppm Ca	ppm Mg	ppm Total Hardness as $CaCO_3$
A	9-20-62 and 9-21-62	150	--	--	--
B	9-20-62 and 9-21-62	150	--	--	--
C	10-17-62	20	--	--	--
D	10-17-62 and 10-18-62	125	1, 1	< 1, 7	--
E	10-17-62 and 10-18-62	150	1, 1	8, 4	
Run No.	Feed Used				
45	Drum A and half of drum B	215	--	--	--
46	Half of drum B	80	< 1, < 1	< 5, < 5	9.6
49	Drum C	15	--	--	--
53	Drum D	125	1, 1	< 1, 7	--
56	Drum E	10	1, 1	8,4	--
57	Drum E	168	1, 1	8, 4	--

complex of strontium or by a high saturation of the surface and a slow exchange due to the high sodium concentrations in solution. Either of these causes would explain the lower strontium distribution coefficients for clarifier effluent, compared with that expected from the effluent calcium concentrations.

VIII-2 Recovery of Surfactant

The recovery of surfactant from the effluent from the foam column was briefly investigated. For low-level waste decontamination by foam separation, the cost of the surfactant is significant, and high surfactant concentrations in decontaminated waste to be discharged are objectionable. In the countercurrent column, the surfactant concentration must be high enough to give a stable foam without appreciable loss of surface area through the countercurrent region. Unstable foams may be produced at much lower concentrations. In practice, the foam separation column effluent could be foamed in a pot with high superficial foam velocity and little drainage. The condensed foam from this pot could be returned to the foam separation column liquid pot, and the liquid effluent could be at a much lower surfactant concentration than that practical for the countercurrent column.

The low-level waste treated with sodium hydroxide and other reagents to precipitate calcium and magnesium could probably be stripped to about 5 ppm dodecylbenzenesulfonate (DBS). Concentrations were determined by ultraviolet absorption for Trepolate F-95 (about 90% NaDBS or 85% DBS) and NaOH or $NaHCO_3$ in demineralized water (Table XXX). The minimum final concentrations decreased from 21 to 24 ppm at

TABLE XXX

STRIPPING OF TREPOLATE F-95

Conditions: 10 to 13 liters of solution charged to a 6-in.-ID column and foamed at 4 liters/min until discharge of foam to the foam breaker became negligible; about 1 ft of 6-in.-diam drainage section above liquid surface

Added Salt		Trepolate F-95 Concentrations (ppm)			
Formula	Concentration (M)	Starting	Appearance of Voids	Sporadic Foam Discharge	Final Concentration
$NaHCO_3$	0.001	100	35	27	24
$NaHCO_3$	0.001	40	--	--	21
NaOH[a]	0.01	21	21	--	12
NaOH	0.01	45	--	8	7
NaOH	0.02	40	12	5	4.3

[a] NaOH added to solution from previous test.

0.001 M Na^+ to 4.3 ppm at 0.02 M Na^+. Foam separation columns should be operated with concentrations above those listed for the appearance of voids, but the recovery system could probably discharge liquid near the concentrations listed for sporadic foam discharge. Other impurities would probably effect the stability of the foam; therefore, the exact minimum concentrations possible for any particular system would have to be determined by experiments.

With the about 1 ft of drainage height and 22 cm/min superficial foam velocity used, the condensed foam was 200 to 500 ppm Trepolate for all liquid concentrations. The foam density decreased as the liquid concentration decreased. Higher concentrations could be obtained by providing more drainage, but the minimum liquid concentration possible would increase slightly. The surfactant concentrations necessary for the countercurrent column could be easily maintained by recycle of the condensed foam from the recovery system.

Recycle of the liquid countercurrent to the foam through a "spider" feed distributor was tested for one run after the foam discharge became sporadic. This liquid recycle did not increase the discharge of foam and actually broke the foam and prevented any discharge at high recycle rates.

A three-stage continuous surfactant recovery system (Figure 28) was operated to verify the dependability of calculations and the advantages of multistage recovery. Liquid flowed in series through the three 2-in.-diam stages. The air flow was in parallel, one-third to each stage, and the foam streams were combined and condensed in a

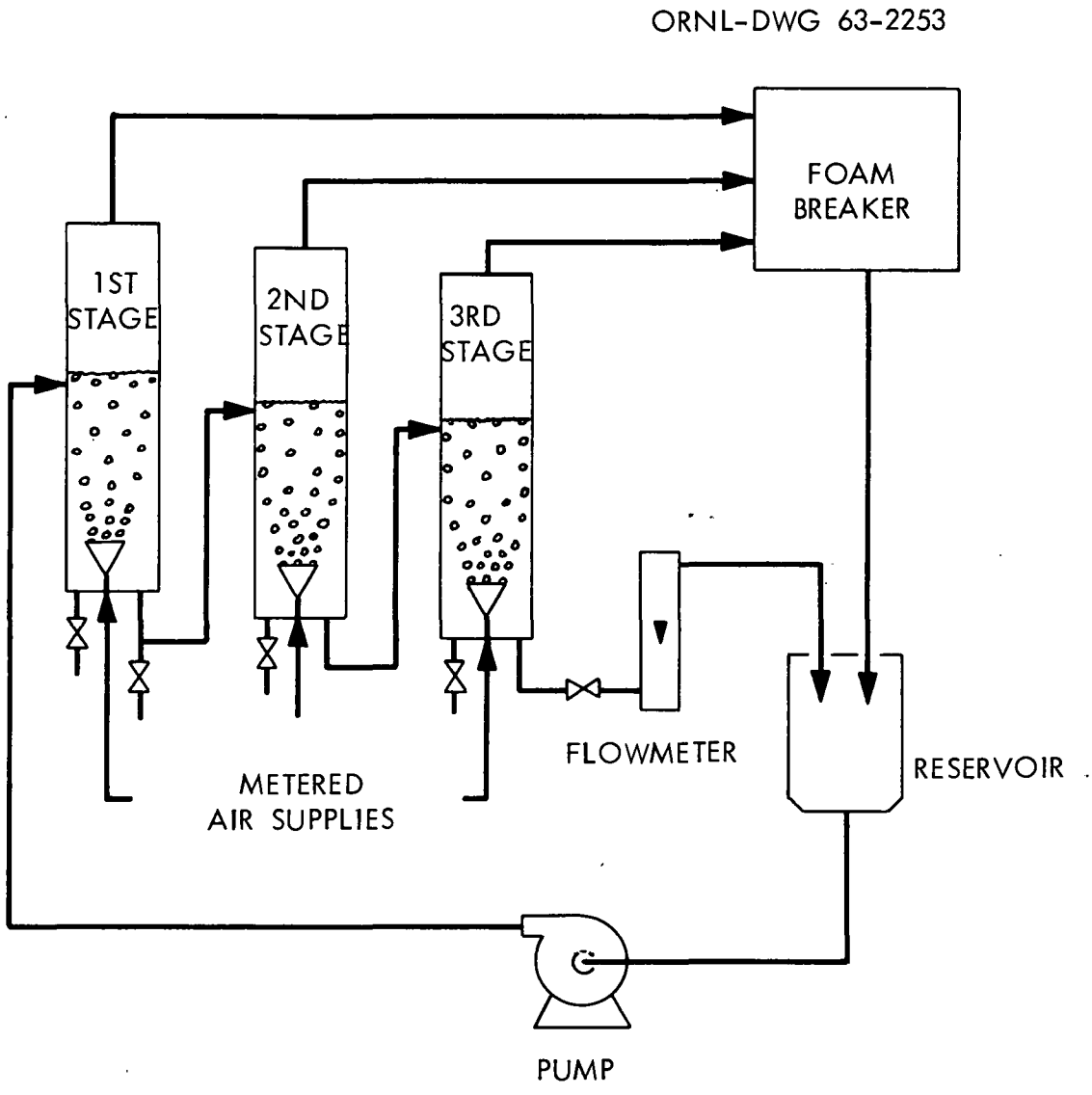

Figure 28. Multistage Surfactant Recovery Test Apparatus.

single centrifugal foam breaker. The air rate and liquid rate were set at selected values, then the pump rate and the vertical positions of the stages were adjusted to maintain the desired liquid levels. The initial surfactant concentrations were usually in the ratios 1:1:0.5:0.2 for the reservoir, first stage, second stage, and third stage, respectively. About 2 hr were allowed to reach equilibrium. The condensed foam rate was measured and the condensed foam and each stage were sampled.

The observed concentrations agree well with those calculated for $(\Gamma/c)_{DBS}$ equal to $7 \cdot 10^{-4}$ cm (Table XXXI). The flow rates and the value of $(\Gamma/c)_{DBS}$ were used to calculate the ratios of the concentrations in each stage to those in the reservoir. The fractions of the total condensed foam from each stage was assumed from observations of the foam flows. The calculated concentrations tabulated are from these ratios, with the total amount in agreement with the total amount indicated by analyses. For example, test-C samples showed 99, 55, 17, and 158 ppm of Trepolate F-95 in the first stage, second stage, third stage, and condensed foam, respectively. For a volume of 1 liter per stage and in the reservoir, these analyses show 308 mg present, while 338 were added to the system (rough volume measurements). The calculated concentration ratios, assuming theoretical stages, are: 1.0: 0.75:0.45:0.16 for the reservoir, first stage, second stage, and third stage solutions. If 308 mg is present, these ratios indicate concentrations of 98, 58, 21, and 150 ppm for the first stage, second stage, third stage, and condensed form solutions.

TABLE XXXI

MULTISTAGE SURFACTANT RECOVERY TESTS

Volumes: 1 liter each stage and liquid reservoir

Quantity	Units	Test A	Test B	Test C	Test D	Test E
Liquid effluent, third stage	cc/min	75	75	50	25	75
Gas rate per stage	cc/min	730	730	1400	1400	1000
Surface rate per stage	10^5 cm^2/min	1.1	1.1	1.6	1.6	1.35
Initial conc., first stage	ppm	250	125	125	125	125
second stage	ppm	125	63	63	63	63
third stage	ppm	50	25	25	25	25
reservoir	ppm	50	125	125	125	125
Total initial amount	mg	475	338	338	338	338
Condensed foam rate	g/min	60[a]	40	285	230	165
Measured conc., first stage	ppm	141	103	99	106	111
Measured conc., second stage	ppm	92	32	55	46	79
Measured conc., third stage	ppm	61	14	17	6	34
Measured conc., cond. foam	ppm	350[a]	340	158	125	171
Reservoir concentration	ppm	190	128	137	114	128
Total final amount	mg	484	277	308	272	352
Calculated conc., first stage	ppm	140	80	98	88	105
Calculated conc., second stage	ppm	81	43	58	45	67
Calculated conc., third stage	ppm	44	21	21	11	35
Calculated conc., cond. foam	ppm	435	343	150	139	196
Assumed cond. foam flow split[b]		50-30-20	60-35-5	60-35-5	60-35-5	50-30-20

[a]Estimated, not measured.

[b]Percent of total volume from each stage, based on appearance.

VIII-3 Economic Considerations

For the flowsheet recommended for low-level waste decontamination, the costs of the precipitation to remove Ca^{2+} and Mg^{2+} would equal or exceed the costs of the foam separation portion of the process. Chemicals costs per thousand gallons would be about:

5×10^{-3} M NaOH	5¢
5×10^{-3} M Na_2CO_3	10¢
5 ppm Fe^{3+}	1¢
50 ppm dodecylbenzenesulfonate	15¢

For a moderate size plant (10^5 to 10^6 gal/day), it is probable that the costs would be about a third for the chemicals listed above, a third for the equipment and waste disposal amortization, and a third for the operating and maintenance costs. This cost of about $0.90 per 1000 gal would decrease if the plant size were increased, but costs below $0.50 per 1000 gal are unlikely without flowsheet changes.

The principle alternatives to foam separation as LLW decontamination processes are ion exchanges processes, with distillation as a second but less likely possibility. The ion exchange processes also lack selectivity for strontium and must remove nearly all the calcium and magnesium if a good strontium decontamination factor is to be obtained. One ion exchange flowsheet calls for the use of the same precipitation of $CaCO_3$ and $Mg(OH)_2$ proposed as a preliminary to foam separation. If this is done, the chemical and equipment costs are very similar, and the choice between processes would probably be based on ease of scaleup and operating dependability and simplicity.

The costs for distillation might be estimated from figures for the recovery of potable water from sea water. While the starting low-level waste is much less concentrated than sea water, the soluble salts would have to be highly concentrated, while the sea water is discharged after only a small amount of concentration. It appears that either ion exchange or foam separation should be cheaper than distillation for LLW decontamination.

CHAPTER IX

CONCLUSIONS

The experimental results confirm that the drainage of solution between foam bubbles is principally through the Plateau borders between bubbles. This is shown by a comparison of theoretical equations with experimental data for four different foam drainage situations. The relationship between the independent variables (the superficial liquid velocity, the superficial gas velocity, the foam bubble diameter, the fractional volume of liquid in the foam, the time, and the configuration) are in excellent agreement with the form of the theoretical equations. The experimental coefficients differ by a factor of two or less from the theoretical ones using the solution properties; this is good, considering the approximations required for the derivations. By using these equations, the flow rates and drainage conditions required for countercurrent foam separation columns may be calculated.

Mass transfer in the liquid to the foam surface is diffusion controlled. Heights of transfer units (based on the liquid phase) were about 1 cm for the best conditions of uniform foams, liquid flows of 100 gal/ft^2·hr or less, and uniform liquid feed distribution with low inlet velocities. The most important property of the gas spargers used to form foams with respect to obtaining low HTU_x values was the ability to provide a uniform bubble size. There was little variation in HTU_x values for countercurrent column lengths of 10 to 28 cm. The chief effects of liquid and foam flow rates and of liquid feed distributors

on HTU_x values were due to their effects on the amount of channeling. It appeared that liquid feed distribution in large columns might be partly effected by allowing an extra length of countercurrent flow.

According to the operation of 6- and 24-in.-diam foam columns, the operation of large columns with a large number of stages or transfer units appears practical. The most stable and uniform foams were produced by spinnerets, as used in the rayon industry. Good distribution of the liquid feed was obtained by using orifices or capillary tubes to split the flow into equal streams which were introduced separately over the column cross section. Drainage to give foams having a density of less than 1 mg/cc was possible with continuous foam flow in either vertical sections of enlarged diameter or in sections with horizontal flow of foam. Foam was condensed during flow through an orifice, with air-operated sonic whistles, with screen-lined centrifugal foam breakers, or with cyclones.

Decontamination of Oak Ridge National Laboratory low-level waste by foam separation to remove strontium would require the removal of calcium and magnesium by precipitation as a preliminary step. Good decontamination of strontium would be possible, and only about 5 ppm dodecylbenzenesulfonate surfactant would remain in the effluent if a surfactant stripping step were included. The costs of the precipitation step would equal or exceed the cost of the foam separation part of the process; the total costs would be $0.50 to $1.00 per 1000 gal.

THIS PAGE

WAS INTENTIONALLY

LEFT BLANK

BIBLIOGRAPHY

1. Adamson, A. W., Physical Chemistry of Surfaces, pp 73-90, New York, Interscience (1960).

2. _____, Physical Chemistry of Surfaces, Chapter IX, New York, Interscience (1960).

3. _____, Physical Chemistry of Surfaces, pp 464-93, New York, Interscience (1960).

4. Anonymous, "Defoaming by Sound Waves Explained," Chem. Eng. Progr., 57, No. 11, pp 169-70 (November 1961).

5. Bikerman, J. J., Foams: Theory and Industrial Applications, New York, Reinhold (1953).

6. _____, Contributions to the Thermodynamics of Surfaces, published by the author, Cambridge 39, Mass. (1961).

7. Blanco, R. E., and Parker, F. L., Waste Treatment and Disposal Quarterly Progress Report August—October, 1962, ORNL-TM-482 (Mar. 25, 1963).

8. _____ and Struxness, E. G., Waste Treatment and Disposal Progress Report for April—May, 1962, ORNL-TM-376 (Nov. 5, 1962).

9. Boucher, R. M. G., "Ultrasonics in Processing," Chem. Eng., No. 20, pp 83-100 (Oct. 2, 1961).

10. _____ and Weiner, A. L., "Sonic Defoaming—Its Present Status," Food Processing (October 1962).

11. Brooksbank, R. E., Low Level Waste Treatment Pilot Plant—Run HR-2 Summary, ORNL-CF-61-12-32 (Dec. 21, 1961).

12. _____, Browder, F. N., Holcomb, R. R., and Whitson, W. R., Low-Radioactivity-Level Waste Treatment, Part II. Pilot Plant Demonstration of the Removal of Activity from Low-Level Process Wastes by a Scavenging-Precipitation Ion-Exchange Process, ORNL-3349 (1963).

13. Chang, Richard C., Schoen, Herbert M., and Grove, C. S., Jr., "Bubble Size and Bubble Size Determination," Ind. Eng. Chem., 48, pp 2035-9 (1956).

14. Davies, J. T., and Rideal, E. K., Interfacial Phenomena, pp 165-196, New York, Academic Press (1961).

15. Foust, Alan S., Wenzel, Leonard A., et al., Principles of Unit Operations, Chapter 16, New York, John Wiley and Sons, Inc., (1960).

16. Gibbs, J. W., The Collected Works of J. Willard Gibbs, p. 219, Vol. I, New York, Longmans, Green and Company (1931).

17. Guggenheim, E. A., "The Thermodynamics of Interfaces in Systems of Several Components," Trans. Faraday Soc., 36, pp 397-412 (1940).

18. _____, and Adams, N. K., "The Thermodynamics of Adsorption at the Surface of Solutions," Proc. Roy. Soc., A-139, pp 218-36, London (1933).

19. Hoel, Paul G., Introduction to Mathematical Statistics, 2nd ed., pp 163-72, New York, John Wiley and Sons (1954).

20. Jacobi, W. M., Woodcock, K. E., and Grove, C. S., Jr., "Theoretical Investigation of Foam Drainage," Ind. and Eng. Chem., 48, No. 11, pp 2046-51 (1956).

21. Kevorkian, Victor, and Gaden, Elmer L., Jr., "Froth-frothate Concentration Relations in Foam Fractionation," A.I.Ch.E.J., 3, No. 2, pp 180-82 (1957).

22. Leva, Max, Fluidization, Chapter 3, New York, McGraw Hill Book Company, Inc. (1959).

23. Maier, Charles G., Producing Small Bubbles of Gas in Liquids by Submerged Orifices, pp 62-95, U. S. Bureau of Mines Bulletin 260 (1927).

24. Miles, Gilbert D., Shedlovsky, Leo, and Ross, John, "Foam Drainage," J. Phys. Chem., 49, 93-107 (1945).

25. Perry, John H., Chemical Engineer's Handbook, 3rd ed., pp 548-55, New York, McGraw-Hill Book Company, Inc. (1950).

26. Plateau, J., Mém. Acad. Roy. Sci. Belgique, 23, 2nd series (1849) and 33, 5th and 6th series (1861).

27. Posner, A. M., and Alexander, A. E., "The Kinetics of Adsorption from Solution to the Air/Water Interface," J. Colloid Sci., 8, pp 575-92 (1953).

28. Rubin, Eliezer, Foam Separation of Metals, Ph.D. Thesis, Columbia University (1962).

29. _____, Schonfeld, Ernest, Everett, Richard, Jr., The Removal of Metallic Ions by Foaming Agents and Suspensions: Laboratory and Engineering Studies, U. S. At. Energy Comm., RAI-104, Radiation Applications, Inc., New York (Oct. 4, 1962).

30. Schonfeld, Ernest, Oak Ridge National Laboratory, personal communication (April, 1961).

31. _____, Sanford, R., Mazzella, G., Ghosh, D., and Mook, S., The Removal of Strontium and Cesium from Nuclear Waste Solutions by Foam Separation—Final Report, U. S. At. Energy Comm., NYO-9577 (July 29, 1962).

32. Sherwood, T. K., and Pigford, R. L., Adsorption and Extraction, 2nd ed., p 21, New York, McGraw Hill Book Company, Inc. (1952).

33. Ward, A. F. H., and Tordai, L., "Time Dependence of Boundary Tensions of Solutions I. The Role of Diffusion in Time-Effects," J. Chem. Phys., 14, pp 453-61 (1946).

34. Weinstock, J. J. et al., Foam Separation, U. S. At. Energy Comm., RAI-100, Radiation Applications, Inc., New York (Oct. 1, 1961).

35. Wilke, C. R., "Estimation of Liquid Diffusion Coefficients," Chem. Eng. Progr., 45, pp 218-24 (1949).

THIS PAGE

WAS INTENTIONALLY

LEFT BLANK

APPENDIXES

Detailed descriptions of apparatus and procedures, detailed experimental data, and sample calculations are included in these appendixes to complete the description of the work done. The tabulations and descriptions in the body of the report are limited to those necessary to demonstrate and prove results and conclusions.

APPENDIX A

ESTIMATION OF k FOR $\epsilon = k\epsilon_{PB}$

The definition of k is given by Equation 30 in which it is introduced:

$$\epsilon = k\epsilon_{PB} = nk(1 - \epsilon)\frac{\pi\delta^2}{4} \quad . \tag{30}$$

The values of n, δ, and k must be mutually consistent, but it is not possible to show that any one value of k is the only correct value. Some of the considerations from which the value of k = 1.5 were selected will be presented in this appendix.

An intuitive approach is to consider the geometry for $k = \epsilon/\epsilon_{PB}$. All three terms are dimensionless; ϵ is the volume fraction of liquid in the foam and ϵ_{PB} is a fractional cross section available for liquid flow. If all the liquid contributes to the drainage flow, that is, is present in vertical channels, then k would be one. It is obvious that k must be greater than one in a real foam. For a cubical lattice with two-thirds of the flow channels horizontal and one-third vertical, k would be three. These two extreme configurations indicate that k would be between one and three. From inspection of more complex and more representative configurations, it is felt that k would be closer to to one than to three.

Packed Bed Equations. The hydraulic configuration for drainage flow of liquid between stationary foam bubbles is similar to that for flow of a fluid through packed beds of solids. The differences between

the foam-liquid system and the normal packed-bed system do not invalidate the packed-bed hydraulic models. The fact that the fluid has a higher density than the bed particles (or air bubbles) is not an important difference. The fluid pressure drop and fluid-to-particle density differences can be defined in agreement with the models without difficulty. The literature on packed beds considers either gases or liquids as the fluid. The most significant difference between the systems is the property of foam bubbles to alter in shape and give very low "void" volumes. The foam densities divided by the liquid density of 1 g/cc would give the equivalent of the "void" volume in packed beds. The foam densities were estimated to be as low as 0.001 g/cc from the drainage model; experimental observations indicate values of 0.001 to 0.4 g/cc, while packed beds of solids normally have void volumes of 0.2 to 0.6. Because of this ability of foam bubbles to alter their shape, the hydraulic diameter of the flow channels would be different at low void volumes than the hydraulic diameters for the channels in a packed bed of solids. However, the packed-bed correlations have been experimentally verified at void volumes of 0.3 or higher. Therefore a value of k may be estimated by requiring that the packed-bed correlation and the foam drainage model predict the same fluid flow rate at $\epsilon = 0.30$.

A derivation for an easily understood model is given by Leva (22). The equations derived have been verified experimentally. Substituting the values for the DBS solution for the fluid properties in Leva's equation (3.-5) (22) gives:

$$L_o = 670 \frac{d^2 \epsilon^3}{1 - \epsilon} \quad . \tag{129}$$

Substituting $\epsilon = 0.30$ gives $L_o = 26\ d^2$. For the same values of ϵ, Equation 60 gives $L_o = 140\ d^2/k^2$. Solving these equations for k gives $k = 1.6$. The value of k depends on the value of ϵ at which the two equations are compared. However, the foam drainage equation is not valid for high values of ϵ while the packed-bed equations have not been verified for low values of ϵ. Values of ϵ near 0.3 are the only ones where a comparison is justified.

Integration for a Random Orientation of Plateau Border. The value of k as defined by Equation 30 may be calculated for a random orientation of Plateau borders using an integration.

$$k = \frac{\epsilon}{\epsilon_{PB}} = \epsilon \left[n(1 - \epsilon) \frac{\pi \delta^2}{4} \right]^{-1} \tag{30a}$$

In order to do this, the bubbles will be represented as randomly oriented dodecahedrons for the purpose of estimating the lengths of Plateau border and number of Plateau borders per unit volume. Perfect dodecahedrons cannot be fitted together without voids, but they are probably a good approximation of the bubble shapes in dry foam.

Consider bubbles in the form of dodecahedrons of "bubble diameter" of d equal to the perpendicular distance between faces and edges of 0.45 d. The Plateau borders are then represented by 10 capillaries of equivalent diameter, δ, and length, 0.45 d, per bubble. The bubble volume is $7.66\ (0.45\ d)^3$ or $0.70\ d^3$. If only the liquid in Plateau borders is considered,

$$\epsilon = \frac{\frac{\pi\delta^2}{4}(10)(0.45\ d)}{0.70\ d^3} = 5.04\ \frac{\delta^2}{d^2} \quad . \tag{130}$$

The number of Plateau borders per cm^3 is $10/0.70\ d^3 = 14.2/d^3$.

Calculate n, the number of Plateau borders which intersect a unit area of horizontal plane, as follows where ℓ is the height of foam column considered. The number of Plateau borders is $14.2\ \ell/d^3$. The probability of angle θ is cos θ. The vertical projection for a particular angle, θ, is 0.45 d sin θ and the probability of intersecting the specified plane is $(0.45\ d \sin \theta)/\ell$. Then the number which intersects the horizontal plane is:

$$n = \int_o^{\pi/2} \frac{14.2\ \ell}{d^3} \cos\theta \left(\frac{0.45\ d \sin\theta}{\ell}\right) d\theta \quad , \tag{131}$$

$$n = \left(\frac{14.2}{d^2}\right)(0.45)\left(\frac{\sin^2\theta}{2}\right)\Bigg]_o^{\pi/2} = \frac{3.2}{d^2} \quad . \tag{132}$$

Substituting in Equation 30a and approximating $(1 - \epsilon)$ by one:

$$k = \left(5.04\ \frac{\delta^2}{d^2}\right)\left(\frac{4\ d^2}{(3.2)\pi\delta^2}\right) = 2.0 \quad . \tag{133}$$

Empirical Evaluation. The value of k could be considered an unknown constant to be determined from the experimental foam drainage data. From Equation 58, cT(0) is proportional to k^{-1}. The empirical values of cT(0) in Table III would agree best with k = 1.45. From Equation 60, $\epsilon^2 d^2/L_o$ is proportional to k^2. My experimental values in Table IVa would agree with k = 1.6 while the data of Jacobi in Table 46,

with an assumed value of d, would agree with k = 1.1. Similarly, the data of Table V would agree best with k = 1.4. The data of Table VI for horizontal drainage would agree best with k = 1.6. The vertical drainage correlation is particularly sensitive to the value of k since ϵ_p is proportional to k - 1 (see Equation 66). However, the data shown by Figures 8, 9, 10, and 11 are affected by foam collapse and bubble growth at the low superficial gas velocities. Using the values for high gas velocities only, the indicated values of k would be about 1.4, 1.4, 1.5, and 1.4 for Figures 8, 9, 10, and 11, respectively.

APPENDIX B

SOLUTION TO DIFFERENTIAL DRAINAGE EQUATIONS BY SEPARATION OF VARIABLES

In this appendix, a solution of Equation 42 for a stationary bed of foam and of a corresponding equation for the model of Jacobi (20) will be developed:

$$\frac{\partial L_o}{\partial z} = - \frac{\partial \epsilon}{\partial t} = \frac{\rho g}{32\mu} \frac{8\epsilon}{\pi n k^2} \frac{\partial \epsilon}{\partial z} \quad . \tag{42}$$

If the variables are separable, we can write:

$$\epsilon(t,z) = T(t)\ Z(z) \ , \tag{43}$$

$$\frac{\partial \epsilon}{\partial t} = Z(z) \frac{dT}{dt} \ , \tag{134}$$

$$\frac{\partial \epsilon}{\partial z} = T(t) \frac{dZ}{dz} \quad . \tag{135}$$

Substituting Equations 43, 134, and 135 in Equation 42:

$$- Z(z) \frac{dT}{dt} = \left(\frac{\rho g}{32\mu}\right)\left(\frac{4}{\pi n k^2}\right) 2\ T(t)\ Z(z)T(t) \frac{dZ}{dz} \ , \tag{136}$$

Rearranging to separate the variables and using c for a constant:

$$- \frac{1}{T^2(t)} \frac{dT}{dt} = \frac{\rho g}{32\mu} \frac{4}{\pi n k^2} 2 \frac{dZ}{dz} = c \quad . \tag{44}$$

Integrating between limits of T and T(0), t and t_o, Z and Z(0) and z and z_o:

$$\int_{T(0)}^{T(t)} - \frac{1}{T^2(t)} dT = \int_{t}^{t_o} c\,dt \ , \tag{137}$$

$$T(t) = \left[c(t - t_o) + \frac{1}{T(0)}\right]^{-1} \ , \tag{45}$$

$$\int_{Z(0)}^{Z(z)} dZ = \left[2 \frac{\rho g}{32\mu} \left(\frac{4}{\pi n k^2}\right)\right]^{-1} \int_{z_o}^{z} c\,dz \quad , \tag{138}$$

$$Z(z) = Z(0) + c\left[2\left(\frac{\rho g}{32\mu}\right)\left(\frac{4}{\pi n k^2}\right)\right]^{-1} (z - z_o) \quad . \tag{46}$$

Substituting into Equation 43 and 32 and simple algebraic rearrangement leads to Equations 47 and 48 previously given.

The same type of solution can be obtained from the model of Jacobi (20). Substituting the nomenclature of this report for that of Jacobi (ϵ for ℓ, L for R and W for V) and noting that k and c are constants, but not equal quantities, the equations are:

$$L_o = \frac{\rho g}{12\mu} k^{3'} S \epsilon^3 \quad , \tag{139}$$

$$\frac{\partial \epsilon}{\partial t} = \frac{\rho g}{12\mu} k^{3'} S \; 3 \; \epsilon^2 \frac{\partial \epsilon}{\partial z} \quad , \tag{140}$$

$$\epsilon(t,z) = \left[\frac{2/3\,(z - z_o) + \frac{Z^2(0)}{c}}{2\,\frac{\rho g}{12\mu} k^{3'} S (t - t_o) + \frac{1}{cT^2(0)}}\right] \quad , \tag{141}$$

$$\epsilon(t,z_o) = \frac{\epsilon(t_o,z_o)}{\left[2\,\frac{\rho g}{12\mu}\,(k^{3'} S)\; cT^2(0)(t - t_o) + 1\right]^{1/2}} \quad , \tag{142}$$

$$L_o(t,z_o) = \frac{L_o(t_o,z_o)}{\left[2\,\frac{\rho g}{12\mu}\,(k^{3'} S)\; cT^2(0)(t - t_o) + 1\right]^{3/2}} \quad , \tag{143}$$

$$W(t,Z_o) = \frac{2\,L_o(t_o z_o)}{2cT^2(0)\;\frac{\rho g}{12\mu}\,(k^{3'} S)} \left\{1 - \frac{1}{\left[2\,\frac{\rho g}{12\mu} k^{3'} S c T^2(0)(t - t_o) + 1\right]^{1/2}}\right\} \quad . \tag{144}$$

Rearranging Equation 139 to put it in a form equivalent to Equation 60 gives:

$$\frac{\epsilon^3 d^2}{L_o} = \frac{12\mu}{\rho g} \frac{d^2}{k^3 S'} \quad . \tag{105}$$

For Jacobi's model, d^2/k^3S' is dimensionless since k is defined by:

$$k = \frac{2\tau}{\epsilon} \quad , \tag{145}$$

and S' is the liquid film length per sq cm of cross section. Definitions consistent with Jacobi's model and with previous calculations are $\epsilon = \tau a = 6\tau/d$ and S' = perimeter/area to give:

$$k = \frac{2\tau}{\epsilon} = \frac{2\tau d}{6\tau} = \frac{d}{3} \quad , \tag{146}$$

$$S' = \frac{1}{2}(\pi d)\left(\frac{\pi d^2}{4}\right)^{-1} = \frac{2}{d} \quad . \tag{147}$$

Substituting:

$$\frac{d^2}{k^3 S'} = \frac{d^2 3^3 d}{d^3 2} = 13.5 \quad . \tag{148}$$

APPENDIX C

DESCRIPTION OF FOAM COLUMN SYSTEM

Two 6-in.-ID foam column systems and one 24-in.-ID column were used for the experiments. The gas spargers, liquid distributors, and foam breakers were described in detail in the discussions of experimental development of these components. The columns themselves were simply vertical cylinders. Therefore, the descriptions of the three systems will consist mainly of some schematic diagrams and a few principal dimensions.

The experimental runs with strontium tracer were in a column assembled from 6-in.-diam Pyrex glass pipe and mounted inside a shielded radiochemical cell (Figures 29 and 30). The feed tanks were located on the top cell level so that liquid flowed by gravity, with the liquid level of the column controlled by a jackleg. Flows were controlled manually by needle valves, with rotameters as flow indicators. The sonic foam breaker was connected to a hot off-gas line and vented to the atmosphere. The result was a low vacuum in the foam breaker at all times and from -2 to 24 in. of water pressure in the foam column, depending on the foam rate and the shape of the drainage section. The feed distributor was located by tightening a 1/2-in. tubing fitting on the feed tube after it had been inserted to the desired location. The drainage section was simply the length of 6-in.-diam column above the feed distributor for most of the runs to determine HTU_x values. A 10.5-in.-ID enlargement of 27 liters volume was used for runs 34 to 65,

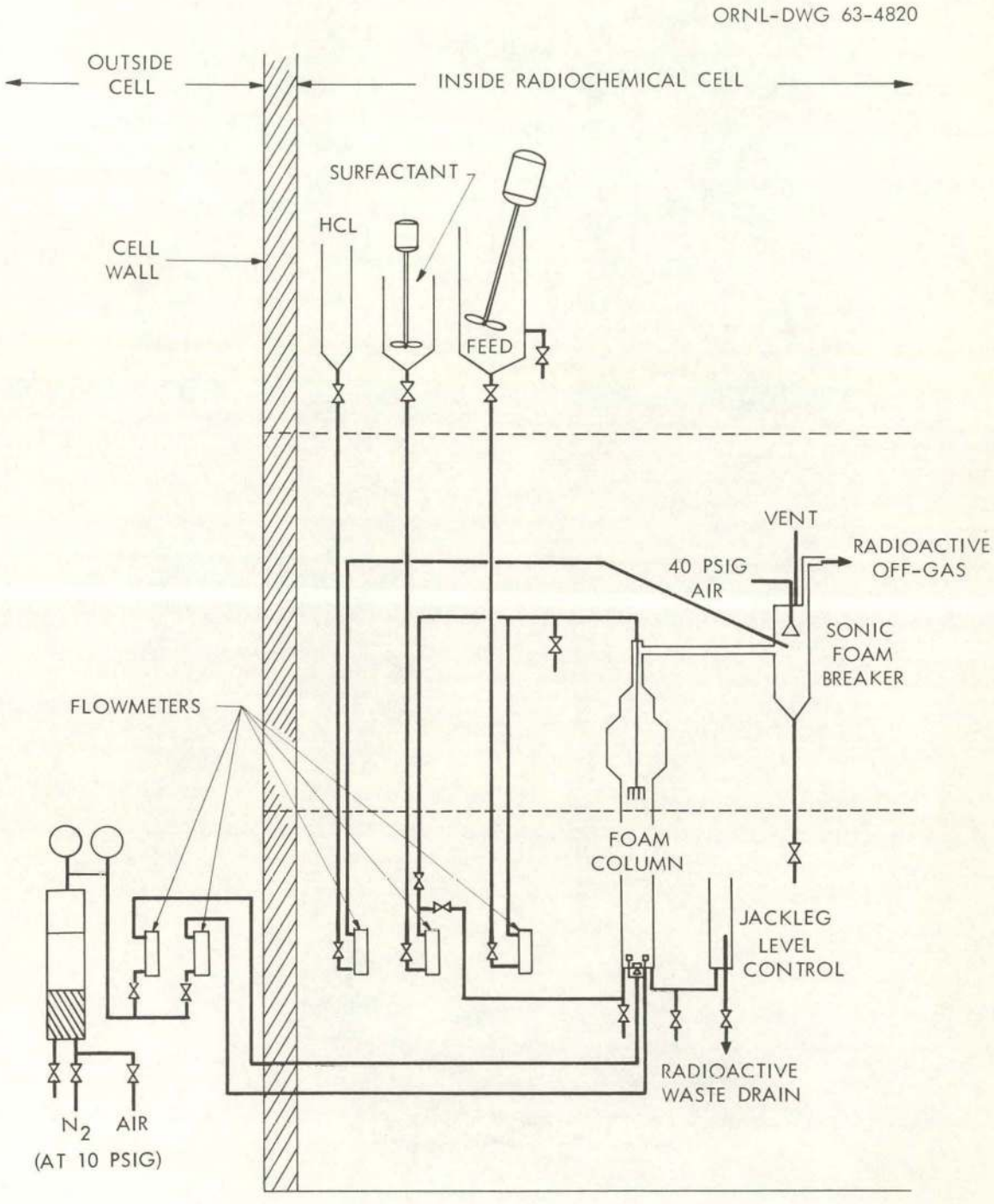

Figure 29. A 6-in.-diam Foam Column System as Used for HTU_x Measurements.

ORNL-PHOTO 58383

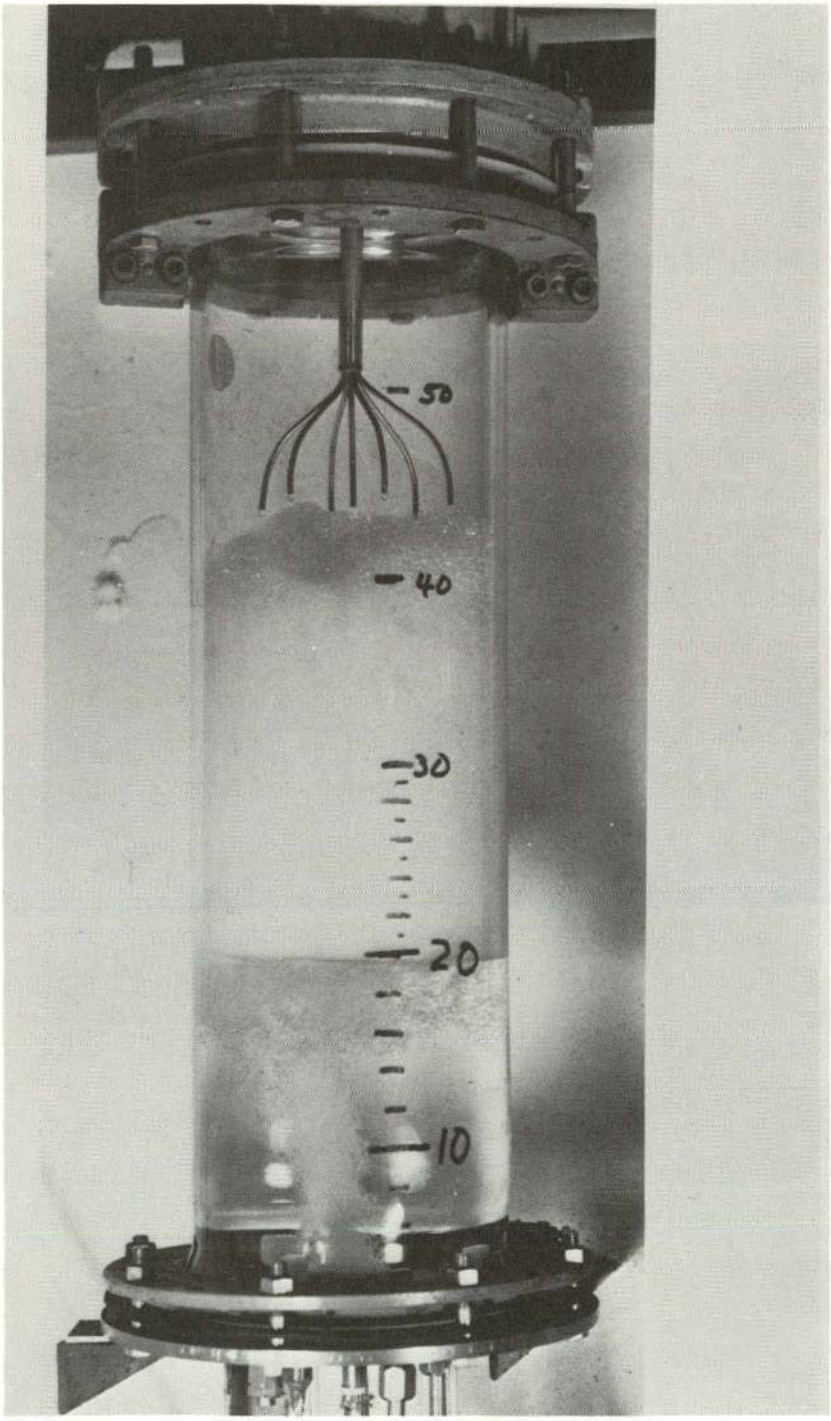

Figure 30. The 6-in.-diam Column Bottom and Feed Distributor C as Used for HTU Determinations.

which included most of the runs with real or simulated low-level waste. The nitrogen or air was scrubbed with 1 N NaOH in a packed column and then metered to the gas spargers.

A second, simpler, 6-in.-diam glass column system was used for tests without Sr^{85} tracer. Numerous alterations were made for tests of components such as the cyclone, orifice, and centrifugal foam breakers, the horizontal drainage section, and several gas spargers. This system was normally run with batch charges of feed and recycle of the condensed foam and the discharged liquid to give time steady-state operation without the need of a feed system. A finger pump was used to recycle condensed foam from the cyclone or orifice foam breakers.

The hydraulic behavior of a large column and the performance of components were determined by using a 24-in.-ID column with a 48-in.-long Plexiglas cylinder as the column body (Figure 25). Countercurrent foam-liquid flow was obtained by pumping liquid from the column to a feed flow splitter. Three extra-coarse-porosity fritted-glass disks of 125 mm diameter were used as gas spargers. Sonic, centrifugal, and orifice foam breakers were tested with this system.

APPENDIX D

PROCEDURES FOR OPERATING THE COLUMN

The general procedures used during runs to measure HTU_x values are typical of those used for other experiments. Specific details on variations important to particular experimental data were noted when the data were presented and used. The commonly accepted procedures for safe handling of chemicals were used at all times. The accepted methods for handling less than 10 mc of a radioactive tracer were used where applicable.

Concentrated solutions were prepared by simple mixing, plus heat if necessary, and then diluted to the desired feed concentrations. For the usual HTU_x determinations, the concentrated solutions were:

1. 55.0 g Trepolate F-95 surfactant
   200 cc of 1 N NaOH
   0.1048 g of $Sr(OH)_2 \cdot xH_2O$
   About 15 liters of demineralized water
2. Sr^{89} tracer diluted to 0.1 mc/ml
3. Concentrated hydrochloric acid

About 150 liters of demineralized water was put into the feed drum. The surfactant and tracer solutions [(1) and (2) above] were added with agitation. Demineralized water was added to give a 200-liter total volume and stirring continued with a plastic cover over the tank to reduce the absorption of carbon dioxide from the air. The feed was sampled from the tank and from the feed line near the column during the

run. The concentrated hydrochloric was added to demineralized water to give about 0.05 N HCl for the foam breaker purge.

The column was filled with foam, and acceptable operation was verified with nonradioactive solution before tracer feed was started. The feed distributor was set at the desired level, and the feed system was operated with demineralized water before the solutions were added to the feed tank. An initial charge of about 6 liters of Trepolate F-95 (0.5 g/liter) and 0.002 N NaOH was added to the column through the jackleg or by feeding in demineralized water and solution from the surfactant feed tank. The feed gas pressure in the sodium hydroxide scrub column was set at about 9 psig by adjusting a pressure regulator. The gas rate was set manually by a needle valve and a rotameter. The dilute hydrochloric acid and the operating air to the sonic foam breaker were started. Radioactive feed and a run timer were started after the foam reached the foam breaker. The jackleg drain valve was opened and the jackleg adjusted to maintain 20 to 22 cm of liquid in the column. The flow rates and the feed-nozzle position were changed between runs without stopping column operation. Normally, three or four sets of conditions were run with one 200-liter batch of feed.

Periodically, the effluent liquid stream was sampled, and the accumulated condensed foam was drained, weighed, and bottled as a sample. The gross-beta analyses appeared to approach equilibrium after throughputs of about five column volumes of liquid and foam; normally, only samples after this unsteady-state period were analyzed. A 200- to 400-cc purge of the effluent liquid sample line was drawn before taking the 50-ml samples.

APPENDIX E

ANALYTICAL METHODS

Analyses were by the Oak Ridge National Laboratory Analytical Chemistry Division, using their standard procedures. Gross-beta determinations of less than 50 cpm/cc were determined at the low-level radiochemical laboratory. The conversions for comparisons to the regular gross-beta analyses were checked by diluted samples of known concentration. The regular gross-beta samples were analyzed at about 11% geometry. The analyses and the attainment of time steady state were verified by using the average of two or three analyses in sequence.

Corrections were required for radioactive decay and for the Sr-Y^{90} impurities in the Sr^{89} tracer. The Sr^{89} tracer was the Sr^{89}-P, carrier free, as received in 1 N HCl solution from the Oak Ridge National Laboratory Isotopes Sales Department. The Sr^{90} activity was normally 2 to 5% of the total tracer activity; three shipments were 5 to 8% Sr^{90}. Because of the long half-life of Sr^{90}, the half-life used for radioactive-decay corrections was 52 days instead of the 50.4 days for Sr^{89}. The Y^{90} had a lower distribution coefficient than the strontium and thus tended to limit the initial transfer of gross beta activity. All the gross-beta counts tabulated are for at least two weeks' decay after the runs (more than five half-lives for Y^{90}). For the runs with high decontamination factors, longer decay periods were used, or the decay over the two weeks was used to correct for the residual Y^{90} radioactivity.

The dodecylbenzenesulfonate concentrations were determined from the ultraviolet adsorption peak at 2230 A or 223 mμ. All samples were diluted to the 3 to 30-ppm range, and samples of known concentrations were run with each set of analyses. Dilutions with hydrochloric acid were used when possible; nitrate, carbonate, and other complexes contribute significantly to adsorption at the 2230-A wavelength.

APPENDIX F

GAS VOLUME RATE CORRECTIONS

Corrections to the gas volumes as indicated by rotameters were made as follows in order to obtain the volume of foam bubbles in the column. The pressures in the foam-filled sections of the column were between atmospheric and 3 in. (water gauge) for most runs, with higher pressures of up to 10 in. (water gauge) for gas flows of 6000 to 10,000 cc/min.

The corrections to rotameter readings are conveniently divided into factors as follows:

$$\frac{G}{G_{std}} = k_T \, k_M \, k_{P1} \, k_{P2} \, , \tag{145}$$

where

G_{std} is the full-scale capacity in standard volume units at 70°F (manufacturers rating),

G is the full-scale capacity in volume units at the foam conditions,

k_T is the temperature correction,

k_M is the average gas molecular weight correction,

k_{P1} is the correction from standard pressure to column pressure,

k_{P2} is the correction for metering at the rotameter pressure as compared to the column pressure.

For the calibration with a wet test meter, $k_M \simeq$ and $k_{P2} = 1$, so that the full-scale capacity should be: $G_{std} \, k_T \, k_{P1}$.

The individual correction factors are evaluated as follows: All measurements were at room temperature or about 70°F, so $k_T = 530/492 = 1.08$ to convert standard volumes to volumes at room temperature. Since k_M is proportional to the square root of the ratio of densities, k_M is 1.02 for nitrogen, while the effect of saturation with water vapor is negligible. Since G_{std} is in terms of volume at standard pressure, the effect of 0 to 10 in. of water above the atmospheric pressure is that $k_{P1} = \sqrt{\text{pressure ratio}} \simeq 1.01$. Similarly, the effect 20 to 27 cm of solution and 40 to 200 cm of water pressure drop through the sparger would give: $k_{P2} = \sqrt{\text{pressure ratio}} \simeq 1.03$ to 1.11.

Thus the capacities shown by the wet test gas meter should be 1.09 times the manufacturers rated capacities at 70°F. Calibrations gave 1.05 to 1.09. The volumes of the gas in foam bubbles should range from 1.04 to 1.12 times the wet-test gas-meter calibrations, depending on the gas-sparger pressure drops. The above corrections were applied with the experimentally determined gas-sparger pressure drops to determine the gas volume rate corrections for each sparger.

APPENDIX G

TABULATED CONDITIONS AND DATA

More detailed experimental data than those used in the discussions of results are tabulated in this Appendix. Table XXXII is the drainage data which is discussed in sections V-1 and V-2. Table XXXIII is a listing of the experimental conditions used for countercurrent runs. Tables XXXIV through XXXVII are the experimental determinations of values of Γ/x for strontium. Tables XXXVIII through XLIII are the detailed data for the HTU_x determinations discussed in Chapter VII. Throughout these tables, the experimental equipment is designated by letters or abbreviations which refer to more detailed descriptions of the gas spargers in Section VI-1 and Table VIII and of the feed distributors in Section VI-2 and Table XII. The nomenclature is that listed in the body of the report. The calculation of HTU_x values is described in section IV-3.

TABLE XXXII

LIQUID HOLDUP AND DRAINAGE DATA FOR COUNTERCURRENT LIQUID-FOAM FLOW

Solution: 275 ppm Trepolate F-95 and 0.002 *M*NaOH in demineralized water.
Column: 132-cm length of 6 in.-ID glass pipe topped by a 12 in. length of 10.5 in.-ID drainage section

Quantity	Units	Test Identification												
		A	B	C	D	E	F	G	H	I	J	K	L	M
a. Spinnerette A as Gas Sparger, Feed Distributor "C" at 130 cm with Respect to Scale														
Liquid flow	cc/min	1100	1100	1100	1100	1100	1100	1450	500	2060	1970	500	500	1770
Gas flow	cc/min	4100	2900	5700	10100	1400	2900	2900	2900	2900	5700	1400	730	10100
Interface, 0 min	cm	19.5	28.5	20.3	21.1	20.2	20.2	21.4	20.3	26.7	22.3	23.4	19.1	20.0
Interface, 1/4 min	cm	22.0	31.0	22.6	24.0	21.9	22.0	24.0	21.4	30.1	26.2	24.3	20.0	24.0
Interface, 1/2 min	cm	24.0	33.0	25.1	26.6	23.6	24.0	26.6	22.4	33.9	30.4	25.1	20.8	28.2
Interface, 1 min	cm	29.0	37.2	29.7	30.1	27.2	28.0	32.0	24.4	40.2	36.0	26.9	22.4	31.2
Interface, 2 min	cm	33.3	41.5	33.0	32.1	32.3	33.0	37.0	28.4	44.6	38.8	30.7	24.5	32.5
Interface, 3 min	cm	35.0	43.1	34.2	32.8	34.3	34.7	38.6	30.4	46.1	39.8	33.0	25.9	33.1
Interface, 4 min	cm	35.7	43.8	34.9	33.0	35.2	35.6	39.4	31.3	46.8	40.3	34.2	26.8	33.5
Interface, 5 min	cm	36.1	44.3	35.3	33.1	35.9	36.2	40.0	31.9	47.4	40.7	34.9	27.5	33.7
Interface, 6 min	cm	36.6	44.7	35.7	33.2	36.4	36.5	40.4	32.3	47.8	41.0	35.3	27.8	33.8
Interface, 7 min	cm	37.0	44.9	35.9	33.3	36.7	36.8	40.7	32.6	48.1	41.3	35.7	28.1	33.9
					33.5 (41 min)									
b. Extra Coarse Fritted Glass Cylinders as Gas Spargers, Feed Distributor "C" at 130 cm with Respect to Scale														
Liquid flow	cc/min	1100	1100	1100	1100	1100	500	1450	500	2040	1870	500	1100	1700
Gas flow	cc/min	3950	2750	5500	9250	1360	730	2750	2750	2750	5500	1360	730	9250
Interface, 0 min	cm	18.2	19.6	19.0	18.8	20.7	18.2	20.2	17.9	22.5	18.9	15.2	17.7	21.5
Interface, 1/4 min	cm	21.1	22.4	23.1	24.1	22.6	19.1	23.5	19.5	26.4	24.1	16.3	19.5	27.9
Interface, 1/2 min	cm	24.1	25.2	27.1	29.4	24.6	20.1	26.8	21.4	30.5	28.9	17.4	21.3	33.8
Interface, 1 min	cm	30.3	30.7	34.8	38.4	28.9	22.0	33.4	25.0	38.4	37.5	19.6	24.9	41.8
Interface, 1-1/2 min	cm	35.9	36.0	40.4	43.1	33.2	23.9	39.1	28.5	44.3	42.8	21.6	28.6	46.1
Interface, 2 min	cm	39.5	40.0	43.9	45.8	37.1	25.8	42.8	31.8	48.1	46.0	23.9	32.3	48.6
Interface, 3 min	cm	43.5	44.6	47.8	48.9	41.9	29.6	46.9	36.4	52.4	49.4	28.3	37.4	51.4
Interface, 4 min	cm	45.8	47.2	50.1	50.9	44.6	32.5	49.2	39.0	54.8	51.5	31.4	40.3	53.1
Interface, 5 min	cm	47.4	48.9	51.7	52.2	46.2	34.4	50.6	40.7	56.3	52.8	33.5	42.1	54.3
Interface, 6 min	cm	48.6	50.1	52.8	53.2	47.4	35.7	51.7	42.0	57.4	53.8	35.1	43.3	55.2
Interface, 7 min	cm	49.5	51.1	53.8	54.0	48.3	36.7	52.5	43.0	58.3	54.7	36.2	44.3	55.9
							41.8 (45 min)							

TABLE XXXIII

FOAM COLUMN RUN CONDITIONS

Surfactant: Trepolate F-95 for run 4 and all subsequent runs; this material is about 380 g/moles of the sodium salt of dodecylbenzene-sulfonate (NaDBS); sodium lauryl sulfate was used for runs 0 to 3

Strontium tracer: Sr^{89} as received from the Oak Ridge National Laboratory Isotopes Sales Department, item Sr^{89}-P for all runs except no tracer for 0 to 4, and 37

Sparge gas: Prepurified nitrogen in cylinders; scrubbed with 1 *M* NaOH at 9 psig prior to metering for run 10 and all subsequent runs; compressed air was used for runs 0 to 9

Foam breaker: A sonic Airjet Defoamer as purchased from Teknika, Inc., and operated on 40 psig inlet air pressure for run 11 and subsequent runs; a cyclone foam breaker for runs 0 to 10

Run Identification		Equipment Designations			Sr Feed Concentration: 10^{-6} *M* $Sr(OH)_2$	Purpose and Remarks
No.	Date	Sparger	Liquid Distributor	Counter-current Length (cm)		
0	5-19-61	E MM	Ring	~50	0	Test of mechanical operation
1	6-16-61	E MM	Ring	~50	0	Test of mechanical operation and observation of channeling
2	6-21-61	E MM	Ring	~50	0	Test of mechanical operation and observation of channeling
3	6-23-61	E MM	A	48	0	Run 2 repeated with new liquid distributor
4	7-24-61	D MM	A	48	20	Test of run 5 conditions without tracer
5	8-7-61	D MM	A	48	2	To determine HTU_x for exchange of active and inactive Sr
6	8-16-61	D MM	A	48	8	Same as run 6 with higher Sr and DBS concentrations
7	8-24-61	D MM	None		9	Batch run to determine (Γ/c) for Sr
8	9-6-61	D MM	A	48	500	Very high Sr concentration to see if Sr/DBS mole ratio >0.5
9	9-13-61	D MM	None		Tracer only	Batch run to determine Γ/c for Sr at low Sr concentration
10	9-26-61	D MM	None		500	Same as run 8 with scrubbed N_2 as sparge gas to avoid CO_2
11	10-13-61	D MM	None		50	To determine (Γ/c) for Sr with *N* Sr equal to *N* DBS
12	10-16-61	D MM	None		250	Same as run 11 with higher Sr and DBS concentrations
13	10-27-61	D MM	A	61	2.0;3.8	To determine HTU_x for exchange of active and inactive Sr
14	11-14-61	A Spin.	B	61	2.5;4.7	Run 13 repeated with different sparger and liquid distributor

TABLE XXXIII (CONTINUED)

Run Identification No.	Run Identification Date	Equipment Designations: Sparger	Equipment Designations: Liquid Distributor	Equipment Designations: Counter-current Length (cm)	Sr Feed Concentration: 10^{-6} *M* $Sr(OH)_2$	Purpose and Remarks
15	12-14-61	A Spin.	B	0–20	2	To determine HTU_x for stripping of Sr
16	12-21-61	A Spin.	B	0–27	2	Same as run 15 with higher gas rates
17	1-11-62	A Spin.	C	0–27	2	Same as run 16 with new liquid distributor, higher flow rates
18	1-18-62	A Spin.	None		2	To determine (Γ/c) for Sr
19	1-18-62	A Spin.	None		2	Same as run 18 with a higher gas rate
20	1-19-62	EC glass	None		2	Same as run 18 with extra coarse fritted glass gas spargers
21	1-23-62	EC glass	C	27	2	Same as run 17 with extra coarse fritted glass gas spargers
22	3-19-62	A Spin.	C	26.5	2	Same as run 17 as a check and with higher flow rates
23	3-21-62	A Spin.	D	26.5	2	Same as run 22 with new liquid distributor
24	3-23-62	EC glass	D	26.5	2	Same as run 21 with new liquid distributor
25	4-17-62	A Spin.	E	13,27	2	Same as run 22 with new liquid distributor
26	5-3-62	EC glass	E	13,27	2	Same as run 21 with new liquid distributor
27	5-10-62	A Spin.	E	13,27	2	Repeat of run 25 with better flow ratios
28	5-22-62	A Spin.	E	13,27,50	2	Same as run 27 with higher flow rates
29	5-24-62	A Spin.	G	27,50	2	Same as runs 27 and 28 with new liquid distributor
30	5-29-62	B Spin.	C	0–28	2	To test B spinneret gas sparger at best conditions for A spinneret
31	6-14-62	B Spin.	C	0–57	2	To test B spinneret gas sparger at higher gas flow rates
32	6-21-62	B Spin.	G	0–57	2	To check run 29 results
33	6-28-62	B Spin.	F	27	2	To test "F" liquid distributor
34	7-17-62	B Spin.	C	55	1	To combine high Sr DF and high VR using new drainage section
35	7-26-62	EC glass	C	50	2	Same as run 34 with extra coarse fritted glass gas spargers
36	7-31-62	EC glass	C	50	2	To check effect of adding surfactant to liquid pot only
37	8-7-62	EC glass	C	50	None	Run with process water plus NaOH and Na_2CO_3; no tracer
38	8-10-62	EC glass	C	50	Tracer	To determine Sr DF for process water after precipitation of $CaCO_3$ and $Mg(OH)_2$
39	8-16-62	EC glass	C	50	Tracer	Same as run 38 with 10 ppm FAB added prior to precipitation

TABLE XXXIII (CONTINUED)

Run Identification No.	Run Identification Date	Equipment Designations: Sparger	Equipment Designations: Liquid Distributor	Equipment Designations: Counter-current Length (cm)	Sr Feed Concentration: 10^{-6} *M* $Sr(OH)_2$	Purpose and Remarks
40	8-23-62	EC glass	F	85	2	To determine Sr DF for process water +10 ppm FAB after precipitation of $Ca_3(PO_4)_2$ and $Mg(OH)_2$
41	8-30-62	EC glass	F	85	2	Same as run 39 with $5 \cdot 10^{-3}$ *M* $CaCO_3$ slurry added prior to precipitation
42	9-5-62	A Spin.	F	85	2	To determine Sr DF for long column, addition of surfactant to liquid pot only
43	9-11-62	A Spin.	F	85	1	To determine Sr DF for long column
44	9-18-62	EC glass	F	85	1	Same as 43, EC glass gas spargers
45	9-27-62	A Spin.	F	85	Tracer	To determine Sr DF and VR for LLW clarifier effluent
46	10-4-62	EC glass	F	85	Tracer	To repeat run 45 with higher V/L ratios
47	10-9-62	A Spin.	F	85	2	To check HTU_x and Γ/c for Sr in a long column
48	10-11-62	A Spin.	F	85	2	Same as run 47 for a lower surfactant concentration
49	10-19-62	A Spin.	None		Tracer	Batch run to determine (Γ/c) for Sr in LLW clarifier effluent
50	10-24-62	A Spin.	None		Tracer	Same as run 49 except demineralized water
51	10-26-62	EC glass	F	85	Tracer	To determine Sr DF for process water after precipitation by $PO_4^{\equiv}$, OH^-, and Fe^{+3}
52	11-9-62	EC glass	F	85	Tracer	Same as run 52 with 10 ppm FAB added prior to precipitation
53	11-19-62	EC glass	F	85	Tracer	To determine Sr DF and VR for LLW clarifier effluent
54	11-28-62	EC glass	F	85	Tracer	To collect effluent for rerun
55	12-3-62	A Spin.	F	85		To determine Sr DF for rerun of effluent
56	12-19-62	A Spin.	None		Tracer	Batch run to determine Γ/c for Sr in a LLW clarifier effluent
57	1-5-63	EC glass	F	85	Tracer	To determine Sr DF and VR for same LLW clarifier effluent used for run 56 feed
58	1-9-63	A Spin.	F	85	10	To collect effluent for rerun, H_2O demineralizer exhausted
59	1-11-63	A Spin.	F	85		To determine Sr DF for rerun of effluent
60	1-18-63	A Spin.	F	85	10	To determine Γ/c for Sr by pinching at the feed point
61	1-21-63	A Spin.	F	85	5	To collect effluent for rerun
62	1-23-63	A Spin.	F	85		To determine Sr DF for rerun of effluent
63	2-4-63	A Spin.	C	85	2	To determine HTU_x for a long column
64	2-13-63	EC glass	C	85	2	To determine effect of $2 \cdot 10^{-5}$ *M* $Ca^{++} + Mg^{++}$ and 3 ppm FAB on Sr DF

TABLE XXXIV

DETERMINATION OF Γ/c FOR STRONTIUM BY CONTINUOUS RUNS WITH ZERO COUNTERCURRENT LENGTH

	Symbol	Units	Run Numbers										
			15A	16A	17D	21A	23D	24E	25D	26D	27E	28D	32D
Gas Sparger used			A Spin.	A Spin.	A Spin.	EC glass	A Spin.	EC glass	A Spin.	EC glass	A Spin.	A Spin.	B Spin.
Liquid feed rate	$L + E_p$	cc/min	500	500	500	900	1110	1430	2000	2400	1460	1700	1100
Condensed foam rate	E_p	cc/min	~1	~1	~2	~2	11	38	23	100	30	92	30
Net Liquid rate	L	cc/min	500	500	500	900	1100	1390	1975	2300	1430	1610	1070
Gas rate	V/a	cc/min	640	870	1020	830	2180	2220	4400	3080	4400	10100	4500
Bubble diameter	d	mm	0.57	0.54	0.56	0.32			1.3	0.41	1.2	1.5	1.2
Surface area rate	V	10^5sq cm/min	0.7	0.9	1.0	1.5	1.8	3.3	2.4	4.2	2.4	4.1	2.3
Surfactant rate in condensed foam		mg/min	6.1	~8	6.7	5.5	14.3	26.0	19.4	48.3	25.1	51.5	27
Surfactant concentration in effluent liquid		ppm	265	417	262	272	267	260	253	269	~260	~260	~260
Gross β in liquid feed	X_2	cpm/cc	5700	4700	5000	4120	3900	3380	2680	3700	3350	2800	3600
Gross β in effluent liquid	x_B	cpm/cc	3160	2700	2540	2310	2400	1750	1800	1820	1950	1270	2050
Gross β in condensed foam	$y_2V + X_2^*E_p$	10^3 cpm/min	1110	1230	1360	1340	1900	2850	2100	4700	2500	2630	2450
Gross β in material balance		%	94	110	105	92	106	109	105	100	108	98	117
Γ/c for Sr from x_2 and x_B	$(\Gamma/c)_{Sr}$	10^{-3} cm	5.8	4.1	4.9	4.7	3.9	4.1	4.1	5.9	4.4	5.0	3.6
Γ/c for Sr from x_2 and $y_2V + x_2^* E_p$	$(\Gamma/c)_{Sr}$	10^{-3} cm	5.0	5.1	5.4	3.9	4.4	4.8	4.9	5.9	5.4	4.9	5.1

TABLE XXXV

DETERMINATION OF Γ/c FOR STRONTIUM BY BATCH RUNS WITH NO LIQUID FEED

	Symbol	Units	Run Numbers									
			18	19	20	50	10	11	12	49	56A	56B
Solution before reagent additions			Demineralized Water							LLW clarifier effluent[a]		
Gas sparger used			A Spin.	A Spin.	EC glass	A Spin.	D MM	D MM	D MM	A Spin.	A Spin.	A Spin.
Sr concentration		10^{-6} *M*	2	2	2	Tracer	500	50	250	Tracer	Tracer	Tracer
Surfactant concentration		ppm	260	260	260	330	180	90	450	330	330	~220
NaOH concentration		*M*	0.001	0.001	0.001	0.01	0.001	0.001	0.001	~0.004	~0.004	~0.004
Gas rate	V/a	cc/min	860	2230	840	2100	3320	3320	3320	2100	2100	4800
Surface area rate	V	10^5 sq cm/min	0.9	1.8	1.7	1.8	~2.0	~2.0	~2.0	1.8	1.8	2.5
Liquid volume in column		cc	7900	7900	7800	14,600	5900	6900	6900	14,800	9900	9200
Gross β half life in liquid	$t_{½}$	min	17	5	4	9	32	6	8	37	22	16
Gross β half life of condensed foam	$t_{½}$	min	21		6			9		42		
Sr distribution coefficients from liquid concentration	$(\Gamma/c)_{Sr}$	10^{-3} cm	3.6	6.1	7.9	6.3	0.6	4.0	3.0	1.5	1.7	1.6
Sr distribution coefficients from foam concentration	$(\Gamma/c)_{Sr}$	10^{-3} cm	2.9		5.3			2.7		1.4		

[a]Produced in Low Level Waste Pilot Plant, Building 2508.

TABLE XXXVI

DETERMINATION OF Γ/c FOR STRONTIUM BY CONTINUOUS RUNS WITH PINCHING AT THE FEED POINT FOR $Sr(OH)_2$ AND NaOH IN DEMINERALIZED WATER

	Symbol	Units	Run Numbers										
			21C	25A	17B	63B	60A	60B	61A	61B	64B	64C	62A
Feed solution (before reagent additions)			Demineralized H_2O										
Surfactant concentration at pinch point		ppm	270	270	270	270	300	300	200	200	270	270	180
Strontium concentration		10^{-6} *M*	2	2	2	2	10	10	5	5	2	2	3
NaOH concentration		*M*	0.001	0.001	0.001	0.001	0.010	0.010	0.005	0.005	0.020	0.020	0.005
Total Na concentration		*M*	0.001	0.001	0.001	0.001	0.010	0.010	0.005	0.005	0.020	0.020	0.005
Total Ca + Mg + Sr		10^{-6} *M*	2	2	2	2	10	10	5	5	22[a]	22[a]	3
Gas sparger used			EC glass	A Spin.	A Spin.	A Spin.	A Spin.	A Spin.	A Spin.	A Spin.	EC glass	EC glass	A Spin.
Countercurrent column length	z	cm	27	28	27	85	85	85	85	85	85	85	85
Estimated number of transfer units	N_x	Dimensionless											
Liquid feed rate	$L + E_p$	cc/min	1250	2000	1250	1000	1930	1300	1000	600	800	1100	1000
Condensed foam rate	E_p	cc/min	~3	21	16	~1	~2	~2	6	3	16	3	4
Net liquid rate	L	cc/min	1250	1980	1230	1000	1930	1300	995	600	785	1100	995
Gas rate	V/a	cc/min	830	4400	2300	3200	2100	2100	4100	2900	4000	2300	4100
Surface area rate	V	10^5 sq cm/min	1.5	2.4	1.8	2.1	1.7	1.7	2.3	1.95	4.8	3.3	2.3
Gross β in liquid feed	x_2	cpm/cc	4120	2680	5000	3000	3000	3000	13,500	13,500	7700	7700	3200
Gross β in effluent liquid	x_B	cpm/cc	850	480	225	1000	2370	2150	5600	3500	3000	5300	500
Gross β in condensed foam	$y_2V + x_2^*E_p$	10^3 cpm/min	3200	4650	5300	1900	770	750	6900	5100	3600	2420	3000
Gross β material balance		%	83	105	108	97	92	91	93	89	97	97	110
Γ/c for strontium from x_2 and x_B	$(\Gamma/c)_{Sr}$	10^{-3} cm	6.6	6.8	6.5	3.2	2.4	2.2	2.5	2.3	1.0	1.0	3.6
Γ/c for strontium from x_2 and $(Vy_2 + x_2^*E_p)$	$(\Gamma/c)_{Sr}$	10^{-3} cm	5.2	7.1	5.8	3.0	1.5	1.5	2.2	1.9	1.0	1.0	4.1

[a]Two volume percent process water used with demineralized water to give about $20 \cdot 10^{-6}$ *M* Ca + Mg for runs 64B and 64C; 3 ppm of FAB also added.

TABLE XXXVII

DETERMINATION OF Γ/c FOR STRONTIUM IN CLARIFIER EFFLUENT [LOW-LEVEL WASTE (LLW) FEED] BY CONTINUOUS COUNTERCURRENT RUNS WITH PINCHING AT THE FEED POINT

Quantity	Symbol	Units	Run Numbers					
			45A	45B	45C	46	53A	53B
Feed Solution (before reagent additions)			LLW Clarifier Effluent (as collected in Bldg. 2528)					
Strontium concentration		$10^{-6}M$	Tracer	Tracer	Tracer	Tracer	Tracer	Tracer
NaOH concentration added		M	0.001	0.001	0.001	None	None	None
Effluent Trepolate F-95 concentration		ppm	260	260	260	260	380	220
Gas sparger used			A Spin.	A Spin.	A Spin.	EC glass	EC glass	EC glass
Countercurrent column length	z	cm	85	85	85	85	85	85
Estimated number of transfer units[a]	N_t	Dimensionless	20	20	20	8	8	8
Liquid feed rate	$L + E_p$	cc/min	900	900	1200	600	600	600
Condensed foam rate	E_p	cc/min	7	13	10	19	16	8
Net liquid rate	L	cc/min	890	900	1190	580	585	590
Gas rate	V/a	cc/min	4700	2900	5700	4000	4000	4000
Surface area rate	V	10^5 sq cm/min	2.5	2.0	2.8	4.8	4.8	4.8
Gross β in liquid feed	x_2	cpm/cc	9400	9400	9400	11,500	11,500	11,500
Gross β in effluent liquid	x_B	cpm/cc	5400	5950	5600	2800	3350	5100
Gross β in condensed foam	$y_2V + x_2^*E_p$	10^3 cpm/min	5200	3450	6500	5300	3600	3300
Gross β material balance		%	118	104	117	100	81	87
Γ/c for strontium from x_2 and x_B	$(\Gamma/c)_{Sr}$	10^{-3} cm	1.5	1.7	1.7	0.9	0.9	0.7
Γ/c for strontium from x_2 and $(Vy_2 + x_2^*E_p)$	$(\Gamma/c)_{Sr}$	10^{-3} cm	2.2	1.8	2.4	0.9	0.6	0.6
Decontamination factor	$DF = x_2/x_B$	Dimensionless	1.7	1.6	1.7	4.1	3.5	2.3

[a]Number of transfer units for similar conditions with demineralized water.

TABLE XXXVIII

EXPERIMENTAL DATA AND CALCULATIONS FOR HTU_x DETERMINATIONS WITH SPINNERET "A" AS THE GAS SPARGER

Strontium distribution coefficient: 5.5×10^{-3} cm

Quantity	Symbol	Units	Run Number									
			14A	14B	14C	15B	15C	16B	16C	17A	17C	17E
Liquid feed distributor	(See Table XII)		B	B	B	B	B	B	B	C	C	C
Countercurrent length	z	cm	60	60	60	10	20	14	28	27	27	27
Liquid feed rate	$L + E_p$	cc/min	500	450	450	500	500	500	500	750	500	1000
Condensed foam rate	E_p	g/min	5	6	~2	~1	~2	~2	~2	5	~2	12
Net liquid rate	L	cc/min	495	495	450	500	500	500	500	745	500	990
Gas rate	V/a	cc/min	1260	1260	900	640	640	870	870	1380	1040	1770
Bubble diameter (surface area average)	d_s	mm				0.57	0.57	0.54	0.54	0.58	0.56	0.57
Surface area rate	V	10^5 sq cm/min	1.2	1.2	0.95	0.7	0.7	0.95	0.95	1.3	1.1	1.6
Surfactant rate in condensed foam		mg/min		7.7	6.6	6.1	8.1		9.5	9.5	7.3	14.9
Surfactant concentration in effluent liquid		ppm	242	250	247	258	261	400	395	264	260	259
Phase flow ratio	$(\alpha V + E)/(L + E)$	Dimensionless	1.33	1.47	1.16	0.77	0.77	1.06	1.06	0.96	1.21	0.89
Gross β in liquid feed	x_2	cpm/cc	5500	6100	6100	5700	5700	4700	4700	5000	5000	5000
Gross β in effluent liquid	x_B (also x_1^*)	cpm/cc	8.5	7.4	8.4	2010	1900	630	440	204	104	154
Gross β in condensed foam	$y_2V + x_2^*E_p$	10^3 cpm/min	1820	2200	2620	1815	1960	1490	1950	3300	2230	4100
Gross β material balance		%	67	81	96	99	102	77	92	92	91	83
Liquid gross β for equilibrium with y_2	x_2^*	cpm/cc	2740	3310	5020	4700	5080	2800	3760	4590	3680	4600
Liquid gross β entering liquid pot	x_1	cpm/cc	19	18	18	3560	3370	1300	910	400	230	290
Liquid gross β concentration change	$x_2 - x_1$	cpm/cc	5480	6080	6080	2140	2330	3400	3790	4600	4770	4710
Log mean liquid concentration difference	$(x - x^*)_{ln\ mean}$	cpm/cc	498	500	227	1260	980	1180	675	289	505	245
Number of transfer units	N_x		11.0	12.2	26.8	1.7	2.4	2.9	5.6	15.9	9.5	19.3
Height of a transfer unit	HTU_x	cm	5.5	4.9	2.2	5.9	8.3	4.8	5.0	1.7	2.8	1.4
Decontamination factor	$DF = x_2/x_B$	Dimensionless	650	830	730	3.1	3.0	7.5	11.0	24	48	32
Volume reduction	$VR = (L + E)/E_p$	Dimensionless	100	75	~200	~500	~300	~250	~250	150	~250	80

TABLE XXXVIII (CONTINUED)

Strontium distribution coefficient: 5.5×10^{-3} cm

Quantity	Symbol	Units	Run Number														
			22A	22B	22C	22D	23A	23B	23C	25B	25C	27A	27B	27C	27D	28A	28B	28C
Liquid feed distributor	(See Table XII)		C	C	C	C	D	D	D	E	E	E	E	E	E	E	E	E
Countercurrent length	z	cm	27	27	27	27	27	27	27	29	13	27	27	12	13.5	50	27	13
Liquid feed rate	$L + E_p$	cc/min	1450	1110	500	1110	1450	1110	500	1100	2000	1460	1000	1000	1460	1700	1700	1700
Condensed foam rate	E_p	g/min	20	14	~2	14	15	9	2	11	28	30	30	30	30	160	92	86
Net liquid rate	L	cc/min	1430	1100	500	1100	1435	1100	500	1090	1970	1430	970	970	1430	1540	1610	1610
Gas rate	V/a	cc/min	2830	2180	960	2180	2830	2180	960	2400	4500	4500	4500	4500	4500	12,200	10,000	10,000
Bubble diameter (surface area average)	d_s	mm	0.7	0.65	0.6	0.65				0.9	1.0					1.65	1.55	1.55
Surface area rate	V	10^5 sq cm/min	2.0	1.8	1.0	1.8	2.0	1.8	1.0	1.85	2.5	2.5	2.5	2.5	2.5	4.8	4.1	4.1
Surfactant rate in condensed foam		mg/min	17.4	14.8	3.85	15.9	13.9	11.8	5.9	15.8	21.9		22.4		20.0	70	47	53
Surfactant concentration in effluent liquid		ppm	262	264	260	264	262	267	265	246	253	~260	~260	~260	~260	~260	~260	~260
Phase flow ratio	$(\alpha V + E)/(L + E)$	Dimensionless	0.77	0.92	1.10	0.92	0.77	0.92	1.10	0.94	0.71	0.96	1.40	1.40	0.96	1.65	1.38	1.38
Gross β in liquid feed	x_2	cpm/cc	3600	3600	3600	3600	3900	3900	3900	2680	2680	3350	3350	3350	3350	2800	2800	2800
Gross β in effluent liquid	x_B (also x_1^*)	cpm/cc	180	17.8	4.1	18.7	200	54	510	650	590	490	195	390	625	55	115	280
Gross β in condensed foam	$y_2 V + x_2^* E_p$	10^3 cpm/min	4400	3600	1450	3850	4060	3320	1450	2000	3550	4100	3080	2880	3140	4950	4640	4300
Gross β material balance		%	92	91	81	97	77	78	87	92	88	98	98	97	83	106	101	100
Liquid gross β for equilibrium with y_2	x_2^*	cpm/cc	3930	3540	2620	3790	3650	3320	2630	1940	2520	2920	2190	2050	2230	1770	1980	1850
Liquid gross β entering liquid pot	x_1	cpm/cc	320	34	8.60	35.5	350	102	1070	1250	1000	950	463	925	1115	140	268	640
Liquid gross β concentration change	$x_2 - x_1$	cpm/cc	3280	3570	3590	3560	3550	3800	2830	1430	1680	2400	2890	2425	2235	2660	2530	2160
Log mean liquid concentration difference	$(x - x^*)_{\ln \text{ mean}}$	cpm/cc		33	181		200	213	865	670	270	440	610	820	820	378	397	620
Number of transfer units	N_x		Large	108	19.8	Large	17.8	17.8	3.3	2.1	6.2	5.4	4.8	3.0	2.7	7.1	6.4	3.5
Height of a transfer unit	HTU_x	cm	Small	0.3	1.4	Small	1.5	1.5	8.2	14	2.1	5.0	5.6	4.0	5.0	7.0	4.2	3.7
Decontamination factor	$DF = x_2/x_B$	Dimensionless	20	200	880	190	20	72	8	4.1	4.5	7	17	9	5	51	24	10
Volume reduction	$VR = (L + E)/E_p$	Dimensionless	70	80	~250	80	100	120	~250	100	70	50	35	35	50	11	18	20

TABLE XXXIX

EXPERIMENTAL DATA AND CALCULATIONS FOR HTU_x DETERMINATIONS WITH SPINNERET "A" AS THE GAS SPARGER

Strontium distribution coefficient: 5.5×10^{-3} cm

Quantity	Symbol	Units	Run Number									
			29A	29B	29C	29D	47B	47C	54A	54B	55A	55B
Liquid feed distributor	(See Table XII)		G	G	G	G	F	F	F	F	F	F
Countercurrent length	z	cm	52	52	27	27	85	85	85	85	85	85
Liquid feed rate	$L + E_p$	cc/min	1250	1700	1250	850	1300	900	600	1100	800	1200
Condensed foam rate	E_p	g/min	25	160	30	8	5	2	7	8	~2	4
Net liquid rate	L	cc/min	1225	1540	1220	840	1295	900	595	1090	800	1200
Gas rate	V/a	cc/min	4100	12,200	4100	1650	4800	2700	3200	3200	2800	4100
Bubble diameter (surface area average)	d_s	mm	0.95	1.65	0.9	0.65						
Surface area rate	V	10^5 sq cm/min	2.3	4.8	2.3	1.5	2.5	1.9	2.0	2.0	1.9	2.3
Surfactant rate in condensed foam		mg/min	23.2	70	22.8	11.2						
Surfactant concentration in effluent liquid		ppm	~260	~260	~260	~260	260	260	260	260	250	250
Phase flow ratio	$(\alpha V + E)/(L + E)$	Dimensionless	1.08	1.65	1.08	0.98	1.06	1.17	1.85	1.01	1.30	1.06
Gross β in liquid feed	X_2	cpm/cc	2550	2550	2550	2550	4700	4700	7300	7300	~1100	~800
Gross β in effluent liquid	X_B (also X_1^*)	cpm/cc	12	190	700	770	12	11	17	35	6	7
Gross β in condensed foam	$y_2 V + X_2^* E_p$	10^3 cpm/min	3120	4060	2320	1590	5500	4200	3900	7900	900	950
Gross β in material balance		%	99	100	100	103	89	99	89	99		
Liquid gross β for equilibrium with y_2	X_2^*	cpm/cc	2320	1450	1720	1910	4000	4000	3520	7110	860	750
Liquid gross β entering liquid pot	X_1	cpm/cc	25	485	1440	1520	25	24	48	70	14	14.5
Liquid gross β concentration change	$X_2 - X_1$	cpm/cc	2525	2065	1110	1030	4675	4675	7250	7230	~1090	~790
Log mean liquid concentration difference	$(X - X^*)_{ln\ mean}$	cpm/cc	75	610	780	690	172	172	782	92	68	22
Number of transfer units	N_x		34	2.9	1.4	1.5	27.2	27.2	9.3	79	~16	~36
Height of a transfer unit	HTU_x	cm	1.5	18	19	18	3.1	3.1	9	1.1	~5	~2.4
Decontamination factor	$DF = X_2/X_B$	Dimensionless	210	13	3.7	3.3	390	430	430	210	~200	~100
Volume reduction	$VR = (L + E)/E_p$	Dimensionless	50	11	42	100	260	~500	90	140	~400	300

TABLE XL

EXPERIMENTAL DATA AND CALCULATIONS FOR HTU_x DETERMINATIONS WITH SPINNERET "B" AS THE GAS SPARGER

Strontium distribution coefficient: 5.5×10^{-3} cm

Quantity	Symbol	Units	Run Number												
			30A	30B	30C	31A	31B	31D	32A	32B	32C	33A	33B	33C	33D
Liquid feed distributor	(See Table XII)		C	C	C	C	C	C	G	G	G	F	F	F	F
Countercurrent length	Z	cm	27	27	27	59	58	23	57	54	27	27	27	27	27
Liquid feed rate	$L + E_p$	cc/min	750	1100	1450	1100	1250	2000	1100	2010	1100	1100	825	1450	1800
Condensed foam rate	E_p	g/min	12	25	42	27	28	82	29	84	30	27	15	48	84
Net liquid rate	L	cc/min	740	1075	1410	1070	1220	1920	1070	1925	1070	1070	810	1400	1715
Gas rate	V/a	cc/min	2800	4500	6700	4500	4500	11,300	4500	11,300	4500	4500	2800	6700	11,300
Bubble diameter (area average)	$D/\sqrt{n}$	mm	1.08	1.17	1.16	1.25	1.25	2.20	1.25	2.20	1.25	1.50	1.30	1.55	2.20
Surface area rate	V	10^5 sq cm/min	1.45	2.3	2.9	2.3	2.3	3.7	2.3	3.7	2.3	2.3	1.45	2.9	3.7
Surfactant rate in condensed foam		mg/min	14.5	22.0	31.9	25		57	27	60		28	16.8	43	67
Surfactant concentration in effluent liquid		ppm	260	260	260	260	260	260	260	255	260	260	260	260	250
Phase flow ratio	$(\alpha V + E)/(L + E)$	Dimensionless	1.08	1.17	1.13	1.17	1.03	1.06	1.17	1.06	1.17	1.17	0.98	1.13	1.18
Gross β in liquid feed	X_2	cpm/cc	3850	3850	3850	4600	4600	4600	3650	3650	3650	4250	4250	4250	4250
Gross β in effluent liquid	X_B (also X_1^*)	cpm/cc	13	51	26	9.2	13.2	82	8	75	980	240	148	160	130
Gross β in condensed foam	$y_2V + X_2^*E_p$	10^3 cpm/min	2980	4100	4800	4350	5400	9600	3960	7600	3360	4200	3200	6200	7400
Gross β material balance		%	103	98	87	86	94	106	99	105	110	96	95	103	100
Liquid gross β for equilibrium with y_2	X_2^*	cpm/cc	3680	3190	2940	3380	4190	4530	3060	3580	2600	3260	3950	3780	3500
Liquid gross β entering liquid pot	X_1	cpm/cc	27	109	55	19.7	26.5	165	17	151	2100	514	291	336	277
Liquid gross β concentration change	$X_2 - X_1$	cpm/cc	3820	3740	3795	4580	4570	4430	3630	3500	1550	3730	3960	3910	3970
Log mean liquid concentration difference	$(X - X^*)_{ln\ mean}$	cpm/cc	63	246	255	254	117	77	139	73	1080	555	218	299	370
Number of transfer units	N_x		60	15.2	14.9	18.0	39	57	26.1	48	1.4	6.8	18.2	13.1	10.7
Height of a transfer unit	HTU_x	cm	0.5	1.8	1.8	3.3	1.5	0.5	2.2	1.1	19	4.0	1.5	2.1	2.5
Decontamination factor	$DF = X_2/X_B$	Dimensionless	296	76	148	500	350	56	460	49	3.7	18	29	27	33
Volume reduction	$VR = (L + E)/E_p$	Dimensionless	58	44	35	41	45	24	38	24	37	41	55	30	21

TABLE XLI

EXPERIMENTAL DATA AND CALCULATIONS FOR HTU_x DETERMINATIONS WITH EC (EXTRA-COARSE FRITTED) GLASS GAS SPARGERS

Strontium distribution coefficient: 5.5×10^{-3} cm except that it was about 7×10^{-3} cm for run 36C and 10^{-2} cm for runs 44 because of lower surfactant concentration

Quantity	Symbol	Units	Run Numbers																
			21B	24A	24B	24C	24D	26A	26B	26C	35A	35B	35C	36A	36B	36C	44A	44B	44C
Liquid feed distributor	(See Table XII)		C	D	D	D	D	E	E	E	C	C	C	C	C	C	F	F	F
Countercurrent length	z	cm	27	27	27	27	27	19	27	12	50	50	50	50	50	50	85	85	85
Liquid feed rate	$L + E_p$	cc/min	900	1430	1430	750	750	2400	1430	2400	750	1100	1800	750	1100	1800	1100	1800	1100
Condensed foam rate	E_p	g/min	~3	45	27	2	3	110	30	90	26	27	28	30	31	27	15	7	~1.5
Net liquid rate	L	cc/min	900	1385	1400	750	750	2290	1400	2310	725	1070	1770	720	1070	1770	1085	1790	1100
Gas rate	V/a	cc/min	830	2180	1860	960	1130	3060	1860	3060	4000	4000	4000	4000	4000	4000	4000	3100	1900
Bubble diameter (area average)	$D/\sqrt{n}$	mm	0.32	0.38	0.35	0.30	0.30	0.41	0.33	0.39	0.50	0.50	0.50	0.50	0.50	0.50	0.56	0.57	
Surface area rate	V	10^5 sq cm/min	1.5	3.3	3.0	1.7	2.0	4.1	3.0	4.1	4.8	4.8	4.8	4.8	4.8	4.8	4.8	4.1	3.0
Surfactant rate in condensed foam		mg/min	11.6	32.2	21.1	6.2	5.6	50.5	24.8	46.1	69.8	74.4	79.2	20.7	16.4	12.0			
Surfactant concentration in effluent liquid		ppm	272	263	273	266	266	263	266	264	~200	~220	~240	~260	~260	~210	~260	~260	~260
Phase flow ratio	$(\alpha V + E)/(L + E)$	Dimensionless	0.92	1.29	1.17	1.25	1.47	0.99	1.17	0.98	3.56	2.42	1.48	3.56	2.43	1.88	2.41	1.26	1.50
Gross β in liquid feed	x_2	cpm/cc	4120	3380	3380	3380	3380	3700	3700	3700	7300	7300	7300	7150	7150	7150	6800	6800	6800
Gross β in effluent liquid	x_B (also x_1^*)	cpm/cc	350	63	125	185	130	390	460	640	116	14.1	25.6	8.8	10.5	23.6	25	33	25
Gross β in condensed foam	$y_2 V + x_2^* E_p$	10^3 cpm/min	3150	5030	4600	2080	2280	7400	4600	7200	5900	8200	13,000	6400	7960	12,500	9900	11,500	5000
Gross β material balance		%	93	107	99	88	93	95	97	98	108	103	99	119	102	98	132	95	68
Liquid gross β for equilibrium with y_2	x_2^*	cpm/cc	3800	2720	2740	2220	2070	3120	2740	3070	2220	3080	4870	2400	2980	3700	3720	5060	3030
Liquid gross β entering liquid pot	x_1	cpm/cc	670	143	260	415	320	760	990	1240	52	48	63	40	36	68	85	75	63
Liquid gross β concentration change	$x_2 - x_1$	cpm/cc	3450	3240	3110	2965	3060	2940	2710	2460	7250	7250	7240	7110	7110	7080	6715	6725	6740
Log mean liquid concentration difference	$(x - x^*)_{ln\ mean}$	cpm/cc	320	274	334	575	580	470	720	610	1040	870	575	940	815	780	760	455	815
Number of transfer units	N_x		10.8	11.8	9.3	5.2	5.3	6.2	3.8	4.0	7.0	8.3	12.5	7.6	8.7	9.1	8.8	14.8	8.3
Height of a transfer unit	HTU_x	cm	2.5	2.3	2.9	5.2	5.1	3.1	7.1	3.0	7.1	6.0	4.0	6.6	5.7	5.5	10	5.8	10
Decontamination factor	$DF = x_2/x_B$	Dimensionless	12	54	27	18	26	10	8	6	630	520	285	810	680	320	270	210	270
Volume reduction	$VR = (L + E)/E_p$	Dimensionless	300	32	53	400	300	22	48	27	29	41	64	25	35	67	74	260	~700

TABLE XLII

EXPERIMENTAL DATA AND CALCULATIONS FOR HTU_x DETERMINATIONS WITH A POROUS METAL SPARGER

Strontium distribution coefficient: 5.5×10^{-3} cm

Quantity	Symbol	Units	Run Numbers			
			13A	13B	13D	13E
Liquid feed distributor	(See Table XII)		A	A	A	A
Countercurrent length	z	cm	45	45	45	45
Liquid feed rate	$L + E_p$	cc/min	250	250	225	452
Condensed foam rate	E_p	g/min	8	14	8	14
Net liquid rate	L	cc/min	240	235	215	440
Gas rate	V/a	cc/min	1300	2300	1920	1920
Bubble diameter (Surface area average)	d_s	mm		0.93	0.85	
Surface area rate	V	10^5 sq cm/min	1.0	1.5	1.4	1.4
Surfactant rate in condensed foam		mg/min	4.2	2.7	2.7	11.8
Surfactant concentration in effluent liquid		ppm	210	191	209	228
Phase flow ratio	$(\alpha V + E)/(L + E)$	Dimensionless	2.23	3.35	3.46	1.73
Gross β in liquid feed	x_2	cpm/cc	1600	1600	1800	1800
Gross β in effluent liquid	x_B (also x_1^*)	cpm/cc	4.5	7.4	5.4	6.9
Gross β in condensed foam	$y_2 V + x_2^* E_p$	10^3 cpm/min	210	388	80	427
Gross β material balance		%	55	97	20	57
Liquid gross β for equilibrium with y_2	x_2^*	cpm/cc	715[a]	465[a]	513[a]	1030[a]
Liquid gross β entering liquid pot	x_1	cpm/cc	14.4	31.8	23.8	18.6
Liquid gross β concentration change	$x_2 - x_1$	cpm/cc	1585	1570	1775	1780
Log mean liquid concentration difference	$(x - x^*)_{\text{ln mean}}$	cpm/cc	195	290	300	185
Number of transfer units	N_x		8.1	5.4	5.9	9.6
Height of a transfer unit	HTU_x	cm	5.6	8.3	7.6	4.7
Decontamination factor	$DF = x_2/x_B$	Dimensionless	350	220	330	260
Volume reduction	$VR = (L + E)/E_p$	Dimensionless	31	18	27	32

[a] Values of x_2^* were calculated assuming 100% material balance to calculate values of $(\alpha V + E_p)x_2^*$.

TABLE XLIII

EXPERIMENTAL DATA AND CALCULATIONS FOR HTU_x OR STRONTIUM DF DETERMINATIONS WITH NONSTANDARD CONDITIONS

Quantity	Symbol	Units	Run Numbers												
			34	42A	42C	43A	43B	48A	48B	48C	62B	62C	64A	63A	63C
Liquid feed distributor		(See Table XII)	C	F	F	F	F	F	F	F	F	F	C	C	C
Countercurrent length	z	cm	55	86	86	86	86	85	85	85	85	85	85	85	85
Gas sparger used			Spin B	Spin A	Spin A	Spin A	Spin A	Spin A	Spin A	Spin A	Spin A	Spin A	EC glass	Spin A	Spin A
Liquid feed rate	$L + E_p$	cc/min	750	1100	900	1100	900	1700	1700	1100	600	600	400	500	1450
Condensed foam rate	E_p	g/min	9	~1	3	3	4	~1	~1	2	3	4	15	~0.5	~1
Net liquid rate	L	cc/min	740	1100	900	1100	895	1700	1700	1100	595	595	385	500	1450
Gas rate	V/a	cc/min	4600	3600	4700	3600	4700	2100	2500	2900	2900	4100	4000	1400	6100
Bubble diameter (area average)	$D/\sqrt{n}$	mm	1.30	1.13	1.33	1.30	1.15								
Surface area rate	V	10^5 sq cm/min	2.3	2.2	2.5	2.2	2.5	1.7	1.85	2.0	2.0	2.3	4.8	1.3	2.9
Surfactant rate in condensed foam		mg/min		11.3	8.3	9.7	14.4							8.6	30
Surfactant concentration in effluent liquid		ppm	130	400	450	130	130	130	130	130	180	180	260	260	260
Estimated strontium distribution coefficient	Γ/c	10^{-3} cm	10	4.5	4.5	10	10	10	10	10	3.8	3.8	1.0	3.1	3.1
Phase flow ratio	$(\alpha V + E)/(L + E)$	Dimensionless	3.1	0.90	1.26	2.00	2.78	1.00	1.09	1.82	1.27	1.46	1.24	0.81	0.62
Gross β in liquid feed	x_2	cpm/cc	24,500	7250	7250	6700	6700	4900	4900	4900	3200	3200	7700	3000	3000
Gross β in effluent liquid	x_B (also x_1^*)	cpm/cc	30	320	12	20	16	78	60	17	150	60	49	600	600
Gross β in condensed foam	$y_2V + x_2^*E_p$	10^3 cpm/min	17,700	6500	8000	5700	6100	4900	6100	5000	1610	2700	2940	1400	1620
Gross β material balance		%	96	86	123	77	102	60	74	93	91	144	97	113	58
Liquid gross β for equilibrium with y_2	x_2^*	cpm/cc	7700	6550	7080	2580	2440	2880	3300	2500	2120	3080	5930	3460	1800
Liquid gross β entering liquid pot	x_1	cpm/cc	121	610	27	60	60	156	125	48	340	148	108	1080	970
Liquid gross β concentration change	$x_2 - x_1$	cpm/cc	24,400	6640	7220	6640	6640	4740	4775	4850	2860	3050	7600	1920	2030
Log mean liquid concentration difference	$(x - x^*)_{ln\ mean}$	cpm/cc	3180	460	65	880	920	560	480	545	510	103	570	small	470
Number of transfer units	N_x		7.7	14.4	110	7.6	7.2	8.5	10.0	8.9	5.6	30	13.4	large	4.3
Height of a transfer unit	HTU_x	cm	7.1	6	0.8	11	12	10	8.5	9.6	15	2.8	6.3	small	20
Decontamination factor	$DF = x_2/x_B$	Dimensionless	820	23	600	350	420	60	80	290	21	52	157	5	5
Volume reduction	$VR = (L + E)/E_p$	Dimensionless	83	~1000	300	350	225	~1700	~1700	~500	200	150	27	~500	~1500

NOTATION

Symbol	Meaning
A	cross section area
a	specific surface area of foams; approximated by $6/d$ for dry foam and $6(1 - \epsilon)/d$ for wet foam
a_i	the thermodynamic property, called activity, of the i th component
c	a constant, the time dependence of drainage is a function of $cT(0)$ which has units of sec^{-1}
D	diffusion coefficient
$D/\sqrt{n}$	an average bubble diameter where n is the number of bubbles visible in a circle of diameter, D.
d	the diameter of foam bubbles
E	the flow rate per unit cross section area of liquid entrained with the foam
$E, E^S, E^\alpha, E^\beta$ or E^σ	the thermodynamic "internal energy"
g	the gravitational constant
HTU	the height of a transfer unit
h	the fraction of the total liquid head effective for causing flow in a capillary, $h = 1 - \epsilon$, cm/cm
k	a constant defined so $\epsilon = k\epsilon_{PB}$
$k_1, k_2, \ldots k_i$	constants
L	superficial net liquid velocity down the column
L_o	superficial liquid velocity with $v = 0$

Symbol	Meaning
ℓ	vertical length of the foam column section considered
N_x	number of transfer units based on the liquid phase
n	defined such that $n(1 - \epsilon)$ is the number of Plateau borders per sq cm of cross section area
n_i	number of moles of the ith component
P	pressure, ΔP is a pressure drop or pressure difference
R	radius of curvature of bubble walls
R'	gas constant
Re	Reynolds number
r	radius of a gas sparger or foam breaker orifice
S	thermodynamic "entropy"
T	absolute temperature
T(t)	defined by $\epsilon(t,z) = T(t)Z(z)$
t	time
u	average liquid velocity in Plateau border capillaries with respect to foam bubbles
V	superficial foam surface flow rate
$V', V^S, V^\alpha, V^\beta$ or V^σ	volume
v	superficial gas velocity; the foam bubble velocity is $v/(1 - \epsilon)$
W	the accumulated drained liquid with $W = 0$ at $t = t_o$
x, x_i	concentrations in the bulk liquid

Symbol	Meaning
x'	average concentration of the liquid entrained with the foam
y, y_i	surface concentration per unit area, i.e., surface excess as defined by the Gibbs model
$Z(z)$	Defined by $\epsilon(t,z) = T(t)Z(z)$
z	vertical position in the foam column increasing upward
α	equilibrium constant or y/x at equilibrium
Γ	surface excess per unit area as defined by Gibbs model
γ	interfacial tension
δ	equivalent diameter of Plateau border capillaries
ϵ	volume fraction of liquid in foam, cc/cc foam, density for a liquid density of one
ϵ_{PB}	a fractional cross section for liquid flow
μ	viscosity
μ_i	thermodynamic "chemical potential" of the ith component
π	mathematical constant = 3.14159 . . .
ρ	density
$\Delta\rho$	a density difference
σ	thickness of the interface for Gibbs model
τ	The film half-thickness; i.e. the product $a\tau$ is the liquid content of the films between bubbles exclusive of the Plateau borders
τ_{eq}	the equilibrium film half-thickness for persistent foams

Symbol	Meaning
Superscripts and Subscripts	
B	bottom exit liquid from a foam column
c	values in a region of countercurrent liquid-foam flow--independent of z
i	ith component
o	a value at zero time, zero position, or zero gas flow rate
p	top exit stream from a foam column
PB	Plateau border enclosed by three bubbles
S	excess quantity of a thermodynamic property associated with the existence of a surface
s	film between two bubbles
x	referred to solution or x phase
y	referred to surface or y phase
α	one phase of Gibbs model
β	one phase of Gibbs model
σ	whole interface including all variations from bulk phases in Gibbs model or thickness of surface layer for a Langmuir-type model

THIS PAGE

WAS INTENTIONALLY

LEFT BLANK

ORNL-3527
UC-4 – Chemistry
TID-4500 (41st ed.)

INTERNAL DISTRIBUTION

1. Biology Library
2-4. Central Research Library
5. Reactor Division Library
6-7. ORNL – Y-12 Technical Library Document Reference Section
8-42. Laboratory Records Department
43. Laboratory Records, ORNL R.C.
44. J. O. Blomeke
45. F. L. Culler
46. Wallace Davis, Jr.
47-66. D. E. Ferguson
67. D. A. Gardiner
68-73. P. A. Haas
74. J. Holmes
75. C. A. Horton
76. H. F. Johnson
77. J. S. Johnson
78. A. D. Kelmers
79. A. H. Kibbey
80. L. J. King
81. K. A. Kraus
82. C. E. Larson
83. H. G. MacPherson
84. E. C. Miller
85. J. T. Roberts
86. A. D. Ryon
87. E. Schonfeld
88. M. J. Skinner
89. A. M. Weinberg
90-91. M. E. Whatley
92. P. H. Emmett (consultant)
93. J. J. Katz (consultant)
94. C. W. J. Wende (consultant)
95. C. E. Winters (consultant)

EXTERNAL DISTRIBUTION

96. Research and Development Division, AEC, ORO
97-659. Given distribution as shown in TID-4500 (41st ed.) under Chemistry category (75 copies – CFSTI)